

Multiconfiguration self-consistent field methods for large molecules

Von der Fakultät Chemie der Universität Stuttgart
zur Erlangung der Würde eines Doktors der
Naturwissenschaften (Dr. rer. nat.) genehmigte Abhandlung

Vorgelegt von

David Amos Kreplin

aus Heidelberg

Hauptberichter: Prof. Dr. Hans-Joachim Werner

Mitberichter: Prof. Dr. Peter J. Knowles

Prüfungsvorsitzender: Prof. Dr. Joris van Slageren

Tag der mündlichen Prüfung: 15. Dezember 2020

Institut für Theoretische Chemie der Universität Stuttgart

2020

Zusammenfassung

Die Methoden der Elektronenstrukturtheorie ermöglichen eine ab-initio Beschreibung von chemischen Systemen. Eine sehr allgemeine Ansatz bietet hier die *multiconfiguration self-consistent field* (MCSCF) Methode, in welcher in der ersten Näherung der Wellenfunktion mehrere Elektronenkonfigurationen berücksichtigt werden. Dies ermöglicht eine qualitativ korrekte Beschreibung von Bindungsbrüchen, angeregten Zuständen oder Übergangsmetallkomplexen. In diesen oft stark korrelierten Fällen ist die Wellenfunktion von mehreren Elektronenkonfigurationen dominiert, sodass die weitverbreiteten Single-Referenz Methoden wie Dichtefunktionaltheorie oder Hartree-Fock für diese Systeme von Grund aus falsche Ergebnisse produzieren können.

Die Elektronenkonfigurationen der MCSCF Methode werden typischerweise durch eine "full configuration interaction" (full-CI) innerhalb einer Auswahl von aktiven Orbitalen erzeugt. Die MCSCF Wellenfunktion hängt somit sowohl von den Orbitalen als auch von den CI Koeffizienten ab. Eine anschließende Berechnung der dynamischen Korrelation ist ähnlich zu den Single-Referenz Methoden möglich, so wurden lokale störungstheoretische Methoden entwickelt, die auch Multi-Referenz Berechnungen mit mehr als hundert Atomen ermöglichen.

Im Rahmen dieser Dissertation wurden verschiedene MCSCF Methoden entwickelt, die eine zuverlässige MCSCF Optimierung ermöglichen und manche davon sind auf große Systeme anwendbar. Eine Herausforderung in der Optimierung ist hierbei, dass die MCSCF Wellenfunktion von zwei verschiedenen Variablentypen abhängt. Oftmals wird die Optimierung der Orbitale und der CI Koeffizienten getrennt und somit die Orbital-CI Kopplungen vernachlässigt, was eine lineare Konvergenz der Energie zur Folge hat. Dieses Vorgehen wird auch in der weitverbreiteten Werner-Meyer-Knowles (WMK) Methode angewandt, in der die Optimierung innerhalb einer Modellenergie durchgeführt wird. Durch die Modellenergie kann trotz der getrennten Optimierung eine schnelle quadratische Konvergenz erzielt werden. In stark gekoppelten Fällen können allerdings auch hier Konvergenzprobleme auftreten. Um dieses Problem zu lösen, wurde zunächst die explizite Orbital-CI Kopplung innerhalb der WMK Methode hergeleitet und implementiert. Dadurch kann zwar die langsame Konvergenz bei stark gekoppelten Fällen behoben werden, allerdings werden viele zusätzliche CI Berechnungen

benötigt. Eine weitere Lösung für das Problem wurde gefunden, indem die Orbital-CI Koppelung mit einer Quasi-Newton Methode approximiert wird. Dabei ist es möglich einen Konvergenzbeschleuniger aus der Quasi-Newton Methode abzuleiten, wodurch keine zusätzlichen CI Berechnungen notwendig sind, die Konvergenz aber trotzdem deutlich verbessert wird. Die verschiedenen Optimierungen in der WMK Methode werden anhand von Beispielen miteinander verglichen. Hier zeigte sich die Optimierung mit dem Konvergenzbeschleuniger selbst bei stark gekoppelten Fällen der explizit gekoppelten Optimierung überlegen.

Für große Moleküle ist die quadratische Optimierung ungeeignet, da hier die teuren Berechnungen der zweiten Ableitungen die Optimierung auf weniger als hundert Atome beschränken. Berechnungen für solche Systeme sind möglich, indem Approximationen für die zweiten Ableitungen eingeführt werden und dadurch auf die quadratische Konvergenz verzichtet wird. Ein Beispiel dafür ist die weitverbreitete Super-CI Methode von Roos, die auch im Rahmen dieser Arbeit innerhalb eines neuen MCSCF Programms implementiert wurde. Die Super-CI Methode wird in dieser Dissertation im Detail besprochen und eine Verbindung zur Störungstheorie aufgezeigt. Sie ermöglicht eine Optimierung von wesentlich größeren Systemen, ist jedoch anfälliger für Konvergenzprobleme.

Um dieses Problem zu beheben, entwickelten wir eine neue MCSCF Methode (SO-SCI), in der die quadratische Optimierung der aktiven Orbitale mit der Super-CI Methode kombiniert wird. Diese benötigt nur eine geringfügig höhere Rechenzeit pro Iteration als Super-CI, zeigt aber eine schnellere und stabilere Konvergenz. Der Konvergenzbeschleuniger sorgt auch hier für eine starke Verbesserung, sodass auch schwierige Systeme verlässlich optimiert werden können. Anhand von verschiedenen Beispielen wird gezeigt, dass die neu entwickelte SO-SCI Methode anderen MCSCF Methoden überlegen ist. Ein besonderer Schwerpunkt wurde auf eine effiziente Implementierung und eine gute Parallelisierung gelegt. Das größte Beispiel, das wir präsentieren, ist ein Nickelkomplex mit 231 Atomen und 5154 Basisfunktionen, dessen Optimierung eine Rechenzeit von weniger als 10 Stunden auf einer Workstation mit 20 Prozessoren benötigt. Darüber hinaus funktioniert die SO-SCI Methode auch sehr gut bei großen offenschaligen Systemen und zeigt sich hier der klassischen Hartree-Fock Methode überlegen.

Abstract

The methods of electronic structure theory allow an ab-initio description of chemical systems. Here, a very general approach is provided by the *multiconfiguration self-consistent field* (MCSCF) method in which multiple electron configurations are included in the first approximation of the wavefunction. This allows a qualitatively correct description of bond breaking, excited states or transition metal complexes. In these strongly correlated cases, the wavefunction is dominated by multiple electron configurations, and commonly used single-reference methods as for example density functional theory or Hartree-Fock can produce fundamentally wrong results.

The electron configurations of the MCSCF method are typically constructed by a full configuration interaction (full-CI) within a selection of active orbitals. Therefore, the MCSCF wavefunction depends on both the orbitals and the CI coefficients. A subsequent calculation of the dynamic correlation is possible by similar methods as in the single-reference case. Local post-MCSCF methods based on perturbation-theory have been developed which allow multireference calculations with more than hundred atoms.

In this dissertation, several MCSCF methods have been developed which allow a reliable MCSCF optimization, and some are also applicable to large molecules. A challenge in the optimization is the dependency of the MCSCF wavefunction on two different types of variables. Often, the optimization of the orbitals and the CI coefficients is separated, and the orbital-CI coupling is neglected which results in a linear convergence of the energy. This approach has also been employed in the commonly used Werner-Meyer-Knowles (WMK) method in which the optimization is shifted to a model energy. Due to the model energy, a fast quadratic convergence is possible despite the separated orbital-CI treatment. However, convergence problems are still observed in strongly coupled systems. We first derived and implemented the explicit orbital-CI coupling within the WMK method to find a solution to this problem. The explicit coupling solves the slow convergence in strongly coupled cases, but on the other hand requires numerous additional CI evaluations. Another solution was found by approximating the orbital-CI coupling by a quasi-Newton method. Here, it is possible to derive a convergence accelerator based on the quasi-Newton method, and no additional CI evaluations are

required while the convergence is substantially improved. The different optimization strategies in the WMK method are compared in multiple examples. Here, the optimization with the convergence accelerator outperforms the explicit coupled treatment even in strongly coupled scenarios.

In case of larger molecules, the quadratic optimization is unsuitable, since the expensive calculation of the second-order derivatives limits the application to systems with less than hundred atoms. A treatment of larger systems is possible by introducing approximations into the second-order derivatives which breaks the quadratic convergence. An example is the widely used Super-CI method of Roos which in this work is also implemented into a new MCSCF program. In this thesis, the Super-CI method is discussed in detail and a relationship to the perturbation theory is illustrated. The Super-CI method allows an optimization of larger systems but is also vulnerable to convergence issues.

To solve this problem, we developed a new MCSCF method (SO-SCI) in which the quadratic optimization of the active orbitals is combined with the Super-CI method. This requires a slightly higher iteration time as Super-CI, but shows a faster and more robust convergence. Here, the convergence accelerator also yields a strong improvement such that difficult systems can be reliably optimized. We particularly focused on an efficient and parallel implementation. The largest example that we present is a nickel complex with 231 atoms and 5154 basis functions, which requires a computation time of less than ten hours on a single workstation with 20 processors. Furthermore, the SO-SCI method shows an excellent performance for large open-shell systems and is superior to the classic Hartree-Fock optimization.

Contents

List of Abbreviations and Notations		VII
1 Introduction		1
2 Electronic structure theory		9
2.1 The Born-Oppenheimer approximation		9
2.2 The many-electron wavefunction		11
2.3 Second-quantization and the coupling coefficients		16
2.4 Basis functions and integral evaluation		19
2.4.1 Density fitting		21
3 MCSCF theory		23
3.1 MCSCF energy and density		24
3.2 Variational conditions and the Brillouin theorem		25
3.3 Restricted open-shell Hartree-Fock		29
3.4 Excited states		31
3.5 Coupled-perturbed MCSCF		32
3.6 Multi-reference perturbation theory		36
4 The numerical optimization of the MCSCF energy		41
4.1 The augmented Hessian method		43
4.2 The P-space Davidson method		44
4.3 The uncoupled optimization (UC-AH)		47
4.4 Z-vector equation solver for CP-MCSCF		48
5 Second-order MCSCF		51
5.1 The WMK method		52
5.1.1 Micro-iterations		55
5.1.2 Internal optimization		58

CONTENTS

5.2	Coupled optimization of the micro-iterations	59
5.2.1	Additional expansion vectors	64
5.2.2	Disadvantages of the explicit coupling	66
6	Quasi-Newton coupling	67
6.1	The L-BFGS optimization	68
6.2	L-BFGS convergence acceleration	70
7	First-order MCSCF	77
7.1	The Super-CI method	78
7.2	The SO-SCI method	83
7.2.1	Other wavefunction transformation approaches	86
7.2.2	Start with the WMK method	87
8	Benchmark calculations	89
8.1	Starting guesses	90
8.2	Aromatic systems	91
8.3	$[(\text{NH}_3)_3\text{Cu}]_2\text{O}_2^{2+}$ isomerization	94
8.4	Large transition metal clusters	99
8.4.1	Single-reference calculations	103
8.5	Rydberg orbitals	105
8.6	The Ni(NHC) catalyzed rearrangement	106
8.7	RASSCF calculations of Mg-porphyrin	113
8.8	Computational performance	116
9	Conclusion and Outlook	121
	Acknowledgements	123
	Bibliography	125
	Declaration of Authorship	151

List of Abbreviations and Notations

AH	Augmented Hessian
AO	Atomic orbital
AVAS	Automated Construction of Molecular Active Space from Atomic Valence Orbitals
BCH	Baker-Campbell-Hausdorff
BFGS	Broyden-Fletcher-Goldfarb-Shanno
CADPAC	Cambridge analytic derivation package
CAHF	Configuration-averaged Hartree-Fock
CAS	Complete active space
CASPT2	CAS perturbation theory
CASSCF	Complete active space self-consistent field
CF	Configuration function
CI	Configuration interaction
CP-MCSCF	Coupled-perturbed MCSCF
CPU	Central processing unit
CSF	Configuration state function
DF	Density fitting
DFT	Density-functional theory
DIIS	Direct inversion of the iterative subspace
DMRG	Density matrix renormalization group
FCIQMC	Full-CI quantum Monte Carlo
full-CI	Full configuration interaction
GAS	Generalized active space
GBT	Generalized Brillouin theorem
GPU	Graphics processing units
GTO	Gaussian type orbital
GUGA	Graphical unitary group approach
HF	Hartree-Fock

List of Abbreviations and Notations

L-BFGS	Limited-memory BFGS
LCAO	Linear combination of atomic orbitals
MCSCF	Multiconfiguration self-consistent field
MO	Molecular orbital
MRCC	Multireference coupled cluster
MRCI	Multireference CI
MRPT	Multireference perturbation theory
NEVPT2	N-electron valence state perturbation theory
NR	Newton-Raphson
PNO	Pair natural orbitals
QN	Quasi-Newton
RAS	Restricted active space
RASSCF	Restricted active space self-consistent field
RDM	Reduced density matrix
RHS	Right-hand side
ROHF	Restricted open-shell Hartree-Fock
WMK	Werner-Meyer-Knowles

Notations

Index notation (if not otherwise noted):

i, j :	Inactive / closed-shell orbitals
t, u, v, w :	Active orbitals
k, l :	Occupied orbitals (inactive and active)
a, b :	Virtual orbitals
p, q, r, s :	Any orbitals
α :	Reduced space vectors
μ, ν, ρ, σ :	Atomic orbitals
A, B :	Density fitting basis
n, m :	Electronically excited states

Throughout this work, multi dimensional expressions are written bold, for example entry r, s of matrix \mathbf{F} is written as $F_{rs} = [\mathbf{F}]_{rs}$. Operators are indicated by a hat: \hat{H} .

In equations, "leading to" is abbreviated by \rightarrow , and "contributes to" is denoted as \leftarrow .

1 | Introduction

The methods of quantum chemistry allow access to the world of molecules, where microscopical observations become increasingly difficult or downright impossible. In combination with experiments, these methods have supported the foundation of modern chemistry since their first developments nearly a century ago [3, 4]. Today, the predictive character becomes increasingly important in computer simulations to reduce expensive and difficult chemical experiments. This is possible since they are ab-initio methods which originate from quantum physics with only physical constants as parameters. However, well balanced approximations in the method development are required to enable calculations on today's computer hardware. This yields a whole catalog of different methods for various applications [5]. Widely-used are density-functional theory (DFT) methods [6, 7] which provide reasonably accurate results for relatively low computational costs [8]. However, predictive calculations usually require a higher accuracy for which coupled-cluster theory is the gold standard today [9]. A successful application of these methods requires that the wavefunction is dominated by a single electron configuration. Then, a first-principles solution can be obtained with a mean-field approximation as done in Kohn-Sham DFT or with the Hartree-Fock (HF) method yielding the molecular orbitals of the system. The neglected electron interaction is subsequently added by dynamical correlation methods in which contributions from excitations into non-occupied orbitals are included. Examples for these post-HF methods are the Møller-Plesset perturbation theory [10, 11], configuration interaction (CI) [12] or coupled cluster theory [9, 13].

The single-reference approach is not always justified, since the electronic wavefunction can be dominated by more than a single configuration. Examples for such systems are electronically excited states or molecules outside their equilibrium region as for example transition states. Furthermore, transition metal complexes often show a strong multireference character, since the degeneracy of the 3d orbitals is not necessarily lifted by the surrounding ligands. The multireference character of the wavefunction can cause a severe failure of the single-reference methods. A solution is the multiconfiguration self-consistent field (MCSCF) method [14] in which multiple electron configurations are included in the reference wavefunction. The dynamic correlation can be added by subsequent treatments as done in the single-reference case.

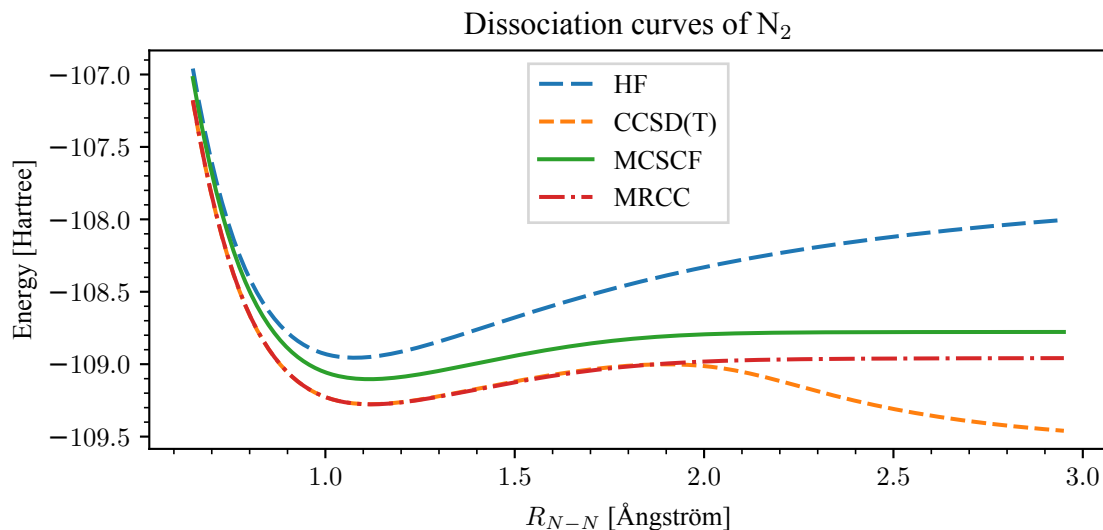


Figure 1.1: Dissociation curves of nitrogen with Hartree-Fock (HF), Coupled-cluster (CCSD(T)), MCSCF, and multireference coupled-cluster (MRCC). All calculations are done using the cc-pVDZ basis [15] and a full valence active space for the MCSCF and the MRCC.

A famous example for the breakdown of the single-reference theory is the dissociation of nitrogen [16]. Figure 1.1 displays the dissociation curves calculated with the single-reference HF and the subsequent coupled-cluster calculation with CCSD(T). The Hartree-Fock energy exhibits a wrong asymptotic behavior of the dissociation, since the single electron configuration also includes ionic contributions. The coupled-cluster method is able to compensate for this erroneous behavior at short distances, but visibly breaks down for distances greater than 1.9 Å. The MCSCF provides the correct dissociation, since all strongly contributing configurations are included in the first-principles wavefunction, and the bond breaking of the σ and the two π orbitals is correctly described. The missing dynamic correlation is calculated by the multireference coupled cluster (MRCC) program GeCCo of Köhn et al. [17–19].

The development of MCSCF methods dates back more than half a century, and various reviews are available in the literature [14, 20–23]. The main reason for this long period of development is a challenging numerical optimization due to the optimization of two different types of variables, the CI coefficients and the molecular orbitals. The first self-consistent field calculations with multiple configurations have been presented by Hartree et al. in 1939 [24], where multiple electron configurations were used to describe the oxygen ion. First ideas have also been outlined in the 1950s by Slater [25], Löwdin [26], and McWeeny [27]. The name *multiconfiguration self-consistent-field* has been introduced by Gilbert in 1965 [28] and was

established soon after the publication. The first MCSCF methods have been presented by Das and Wahl [29–33] in 1966 and Hinze et al. [34–37] in 1967 in which the orbitals were optimized in a self-consistency procedure similar to the HF method. Few electron configurations were hand-picked manually, and the convergence of the early methods turned out to be very fragile [38, 39]. The numerical minimization of the MCSCF energy has been presented by Levy in 1969 [40] in order to improve the convergence. Since then, various approximations of the second-order derivatives have been proposed [38, 41–48], but a more robust convergence could be achieved by including the full orbital Hessian [49–51] in a Newton-Raphson (NR) optimization.

Another approach has been developed after formulating the generalized Brillouin theorem (GBT) by Levy and Berthier [52, 53] which states that the overlap of the optimized MCSCF wavefunction with the Hamiltonian and singly excited configurations vanishes. A consequence was the development of the GBT methods in which an update of the orbitals is determined from the coefficients of singly excited configurations. Today, these methods are better known as the Super-CI methods, and they have been pioneered by Grein and Chang in 1971 [54]. Further improvements have been made by co-workers of Grein and Chang [55–59] and by Ruedenberg and Cheung [60–62]. The early Super-CI methods featured a more robust convergence than the early self-consistent procedures, but they required third-order densities which made them less advantageous compared to the later developed second-order orbital optimization [50]. An improved Super-CI method has been introduced by Roos in 1980 [63–65] in which the computational complexity could be strongly reduced through approximations. This Super-CI method is still often used today, and a detailed review is presented in Chapter 7.

In the late 1970s, the CI optimization has been further developed, and the treatment of much larger configuration spaces was possible through direct methods in which only the product of the Hamiltonian matrix is required. A strong improvement has been made by the graphical unitary group approach (GUGA) [66–70] in which properties of the unitary group are used in the evaluation of the required coupling coefficients. The proper choice of the configurations has been a difficulty from the beginning, and the treatment of large CI expansions allows the inclusion of all possible configurations, i.e. full configuration interaction (full-CI) within a pre-selected set of active orbitals. This idea dates back to Ruedenberg et al. [60, 62], where the active orbitals are also called reaction orbitals. However, this approach was popularized by Roos under the name complete active space (CAS) [23, 51, 63, 64]. Today, it is by far the most common used MCSCF wavefunction, and a MCSCF with a CAS wavefunction is denoted as complete active space self-consistent field (CASSCF).

The 1980s were dominated by the development of second-order MCSCF methods [71–73] which consider the full second-order derivatives of the energy with respect to the CI coefficients and the orbitals [74]. Here, the energy shows a quadratic decay in the final iterations, which was first shown by Jørgensen et al. in 1979 [39, 75] by including the orbital-CI coupling in the NR optimization. Major developments in the second-order MCSCF have been driven by Lengsfeld and co-workers [76–78], by the trio of Jørgenson, Yeager and Olsen [79–85], and by Jensen and Ågren [86–89]. An alternative second-order MCSCF has been introduced by Werner et al. [90, 91], where the quadratic expansion of the energy includes higher-order terms such that the periodic behavior of the energy with respect to orbital rotations is reproduced. This increases the convergence radius of the quadratic approximation, and the convergence is therefore superior to the classic NR optimization. The method has been further improved by Werner and Knowles [21, 92, 93] to work with a large number of configurations. It is denoted in the following as the Werner-Meyer-Knowles (WMK) method, and a detailed review of the WMK method is presented in Chapter 5.

After the second-order MCSCF, the multireference developments have been more focused on post-MCSCF methods as for example multireference perturbation theory (MRPT) [94–103], multireference CI (MRCI) [104–113], and MRCC [17–19, 114–120]. Additionally, the calculation of properties and derivatives have been implemented for the MCSCF wavefunction [121–132]. Since then, several minor improvements have been published on the MCSCF theory [133–137], and most calculations have been performed with the programs developed in the 80s.

The factorial increase of the configurations in the CAS wavefunction limits the number of possible active orbitals, and the current maximum is reached by 22 electrons in 22 orbitals [138] exploiting massive parallelization. A possible solution is to restrict orbital occupations in the configuration generation [139–141], as for example done in the restricted active space (RAS) method [65, 142], or the generalized active space (GAS) methods [143, 144]. Another path is the development of approximated full-CI solvers, which have also been integrated into existing MCSCF programs. Examples are the full-CI quantum Monte Carlo (FCIQMC) method [145–147], the heat-bath CI [148–150], or the density matrix renormalization group (DMRG) methods [151–156]. However, approximations in the CI space remove the invariance of the CASSCF energy with respect to active-active orbital rotations. The inclusion of these rotations leads to difficult optimization problems [156], and a satisfying solution for this problem is still missing today. The approximated CI solvers allow calculations with massive active spaces, and examples with up to 44 electrons in 44 orbitals have been reported recently [150].

Also, approximated CI methods including the dynamical correlation are currently in development [157–161].

Until recently, the CASSCF starting orbitals are often hand-picked from a preceding HF or DFT calculation. A lot of experience and many trials are often necessary until a reasonable active space is found [162]. In the last five years, a variety of tools have been proposed for simplifying or even automatize the active space generation, driving the CASSCF method closer to a black-box application [163–170]. Most tools estimate the density for a large set of given orbitals. Afterwards, the relevant orbitals are picked with a selection criterion according to their occupation numbers [165–168, 170] or by orbital entanglement [171–173]. However, the orbital occupation can change during the MCSCF optimization [172], and a real black-box method can only be achieved if these changes are somehow included in the selection procedure [167–169].

The computational efficiency of the MCSCF method can be improved through an approximated evaluation of the required intermediates [174, 175] as for example with density fitting [176, 177]. Additionally, atomic orbital (AO) driven MCSCF codes have been presented [178, 179] that enable an efficient use of the computation power in graphics processing units (GPUs), and these methods have been majorly used for large scale nonadiabatic dynamic calculations [180, 181]. Another completely different recent development is the combination of MCSCF with a relativistic treatment [176, 182–185].

The MCSCF energy depends on both the orbitals and the CI coefficients, and the optimization can become extremely challenging due to a strong coupling between the orbitals and the CI coefficients. Often, the optimization of the orbitals and the CI coefficients is separated and performed in alternating steps. This is also known as a two-step optimization, and it yields a linear (first-order) convergence of the energy. However, the linear decay of the energy can become extremely slow if there is a strong orbital-CI coupling, and a large number of iterations is the consequence.

The primary goal in this thesis is the development of a robust MCSCF method which enables an optimization of large molecules with over hundred atoms. A second objective is the general improvement of the two-step optimization for strongly coupled systems. Our starting point is the WMK method in which the uncoupled optimization has been used to optimize the higher-order energy expansion. Here, a poor convergence has been observed for strongly coupled systems. In order to solve this problem, we developed a new optimization of the energy expansion in which explicit coupling terms are included [1]. The approach is presented in Chapter 5 and utilizes ideas of the coupled NR optimization. However, it allows more

control of the coupling level in order to reduce the number of CI evaluations. Here, we consider only the coupling with a reduced CI space obtained from the previous CI optimization. The intensity of the coupling can be increased by additional expansion vectors obtained from the coupled residual. This solves the slow convergence but requires numerous CI evaluations which can only be compensated for in extremely coupled cases. In order to solve this rather unfortunate result, we developed a convergence accelerator based on the quasi-Newton (QN) optimization [186] in which a correction to the orbital Hessian is constructed from the gradient and the step along the optimization [2]. The coupling is included, since the orbital gradient is evaluated after the CI optimization [65] which is discussed in more detail in Chapter 6. This QN-coupling solves the potentially slow convergence of the two-step optimization without introducing additional CI evaluations.

The second-order MCSCF requires the computation of the full orbital Hessian, and the construction of the required integrals limits the applications to small and medium sized molecules with less than hundred atoms. However, recent developments in local post-MCSCF methods [187–189] allow a calculation of the dynamical correlation for substantially larger systems. The first-order Super-CI method of Roos [64,65] solves this problem by approximating the Hessian such that only the computation of the Fock matrix is required. Since the Fock matrix is also needed in the orbital gradient, no large computational overhead is introduced. This permits an optimization of larger molecules than it is possible with the second-order optimization, but often shows a rather unsatisfying convergence with nearly a hundred iterations.

In order to improve the convergence of the first-order method, we developed a new approximated orbital optimization. Here, the active orbitals are still treated on a second-order level while the optimization of the other orbitals is approximated by the Super-CI treatment. The density fitting intermediates in the Super-CI method can be reused to evaluate the two-electron integrals required in the Hessian matrix. The second-order treatment of the active orbitals considerably accelerates convergence while introducing only a small additional computational overhead. The resulting method is denoted as SO-SCI [2] and it is presented in Chapter 7 together with a detailed review of the Super-CI method. Combined with the QN convergence acceleration, it shows a fast and reliable convergence even for difficult cases. This is demonstrated by various benchmark calculations in Chapter 8, where we discuss the excitation in aromatic systems, the strong coupling in an isomerization, and calculations with various transition metals with up to 231 atoms and 5154 basis functions.

This thesis summarizes results which have been published in

- [1]: D. A. Kreplin, P. J. Knowles, and H.-J. Werner: *Second-order MCSCF optimization revisited. I. Improved algorithms for fast and robust second-order CASSCF convergence*. The Journal of Chemical Physics **150** (19), 194106 (2019)
- [2]: D. A. Kreplin, P. J. Knowles, and H.-J. Werner: *MCSCF optimization revisited. II. Combined first- and second-order orbital optimization for large molecules*. The Journal of Chemical Physics **152** (7), 074102 (2020)

Reference [1] focuses on the second-order MCSCF, and it presents the derivation of the coupling in the WMK method and the first version of the QN-coupling. However, we found a more general way of the convergence acceleration after publishing [1]. This is discussed in Reference [2] together with the SO-SCI method. In this work, only the QN-coupling as presented in Reference [2] is discussed, since it is now employed in the first- and second-order program. Nearly the entire MCSCF program in Molpro [190] has been rewritten to make it more efficient, especially in parallel executions, and the efficiency is also discussed in Chapter 8. The first two chapters introduce the basic many-electron and MCSCF theory. Details about the numerical methods used throughout this thesis are presented in Chapter 4.

2 | Electronic structure theory

This chapter lays the theoretical foundation of the thesis. Starting point is the quantum molecular description of molecules. From here, we discuss the approximations made in electronic structure theory and how to build the many-electron wavefunction in order to solve the electronic Schrödinger equation. The notations and definitions used in subsequent chapters are also introduced here.

2.1 The Born-Oppenheimer approximation

The total Hamiltonian \hat{H}_{tot} of a molecular system reads [191]

$$\hat{H}_{tot} = - \sum_K^{N_{nuc}} \frac{\hbar^2}{2m_K} \nabla_K^2 - \sum_i^{N_{el}} \frac{\hbar^2}{2m_e} \nabla_i^2 - \sum_{K,i} \frac{q_e^2}{4\pi\epsilon_0} \frac{Z_K}{|\mathbf{r}_i - \mathbf{R}_K|} + \frac{q_e^2}{4\pi\epsilon_0} \sum_{K>L} \frac{Z_K Z_L}{|\mathbf{R}_K - \mathbf{R}_L|} + \frac{q_e^2}{4\pi\epsilon_0} \sum_{i>j} \frac{1}{|\mathbf{r}_i - \mathbf{r}_j|} \quad (2.1)$$

$$= \hat{T}_N + \hat{T}_e + \hat{V}_{eN} + \hat{V}_{NN} + \hat{V}_{ee}, \quad (2.2)$$

with the kinetic energy of the nuclei \hat{T}_N and electrons \hat{T}_e , the Coulomb repulsion between the nuclei \hat{V}_{NN} and electrons \hat{V}_{ee} , respectively, and the Coulomb attraction between the nuclei and the electrons \hat{V}_{eN} . In the following, the spatial coordinates of the nuclei are written as \mathbf{R} , and the positions of the electrons are denoted with \mathbf{r} . The solution of the time-independent Schrödinger equation

$$\hat{H}_{tot} |\Psi_k^{tot}(\mathbf{R}, \mathbf{x})\rangle = E_k^{tot} |\Psi_k^{tot}(\mathbf{R}, \mathbf{x})\rangle \quad (2.3)$$

is the total wavefunction $|\Psi_k^{tot}(\mathbf{R}, \mathbf{x})\rangle$ depending on all nuclear and electron coordinates, and the energy E_k^{tot} of state k . The electron coordinates \mathbf{x} refer collectively to the three dimensional spatial coordinates \mathbf{r} and the spin coordinates s of the electrons. The spins of the nuclei, relativistic contributions, as well as spin-orbit coupling are neglected in this work.

In the Born-Oppenheimer approximation [192], it is possible to separate the treatment of the electrons from that of the nuclei. The separation is justified by the argument that electrons

can adjust instantaneously to the nuclear behavior because their mass differs by a magnitude of 10^3 . The derivation of the Born-Oppenheimer approximation in this section follows Reference [193] and [191]. In a first step, we freeze the nuclear movement and solve only the electron problem with a fixed nuclear arrangement. At this level of description, the kinetic term of the nuclei \hat{T}_N vanishes (it will be dealt with later), and the remaining contributions are summarized in the electronic Hamiltonian:

$$\hat{H} = \hat{T}_e + \hat{V}_{eN} + \hat{V}_{ee} + \hat{V}_{NN} = \hat{H}_{tot} - \hat{T}_N. \quad (2.4)$$

In this case, the nuclear repulsion energy is constant, and we set $E_{nuc} = \hat{V}_{NN}$. The solution for the electrons moving within the fixed molecular structure is obtained from the electronic Schrödinger equation:

$$\hat{H}(\bar{\mathbf{R}}) |\Psi_n(\bar{\mathbf{R}}, \mathbf{x})\rangle = E_n(\bar{\mathbf{R}}) |\Psi_n(\bar{\mathbf{R}}, \mathbf{x})\rangle. \quad (2.5)$$

Here, the bar over \mathbf{R} denotes the solution for a fixed nuclear arrangement $\bar{\mathbf{R}}$. The index n labels the n -th electronic state, and $E_n(\bar{\mathbf{R}})$ is the energy of state n .

The total wavefunction can now be expanded in the basis of the electronic solutions:

$$|\Psi_k^{tot}(\mathbf{R}, \mathbf{x})\rangle = \sum_m \Phi_{km}(\mathbf{R}) |\Psi_m(\mathbf{R}, \mathbf{x})\rangle, \quad (2.6)$$

where the expansion coefficients $\Phi_{km}(\mathbf{R})$ describe the solution for moving nuclei. Inserting this expansion into the full Schrödinger equation, and projecting the result from the left with $\langle \Psi_n(\mathbf{R}, \mathbf{x}) |$ yields:

$$\sum_m \langle \Psi_n(\mathbf{R}, \mathbf{x}) | \hat{T}_N | \Phi_{km}(\mathbf{R}) \Psi_m(\mathbf{R}, \mathbf{x}) \rangle + E_n(\mathbf{R}) \Phi_{nk}(\mathbf{R}) = E_k^{tot} \Phi_{nk}(\mathbf{R}). \quad (2.7)$$

The term including \hat{T}_N can be simplified by using the product rule of differentiation:

$$\begin{aligned} \sum_m \left[\langle \Psi_n | \hat{T}_N | \Psi_m \rangle - \sum_K \frac{\hbar^2}{m_K} \langle \Psi_n | \nabla_K | \Psi_m \rangle \cdot \nabla_K \right] \Phi_{mk}(\mathbf{R}) \\ + [\hat{T}_N + E_n(\mathbf{R})] \Phi_{nk}(\mathbf{R}) = E_k^{tot} \Phi_{nk}(\mathbf{R}), \end{aligned} \quad (2.8)$$

where we used $\Psi = \Psi(\mathbf{R}, \mathbf{x})$ for notional convenience. The matrix elements $\langle \Psi_n | \nabla_K | \Psi_m \rangle$ and $\langle \Psi_n | \hat{T}_N | \Psi_m \rangle$ are also known as the first- and second-order non-adiabatic coupling elements.

More about the calculation of the first-order non-adiabatic coupling elements for the MCSCF wavefunction is presented in Section 3.5.

In the Born-Oppenheimer approximation, both non-adiabatic coupling elements are neglected, since the variation of the wavefunction with respect to the nuclear arrangement is assumed to be negligible. The result is the Schrödinger equation of nuclear motion:

$$[\hat{T}_N + E_n(\mathbf{R})] \Phi_{nk}(\mathbf{R}) = E_k^{tot} \Phi_{nk}(\mathbf{R}). \quad (2.9)$$

This equation can be used to calculate vibrational spectra for molecules [194]. An important result is that the energy $E_n(\mathbf{R})$ from the electronic Schrödinger equation acts as the potential for the nuclei motion.

However, in case of strong changes in the wavefunction, as for example near conical intersections or in molecular collisions, the Born-Oppenheimer approximation is not justified anymore, and the inclusion of the non-adiabatic coupling terms is required. Here, the off-diagonal terms of the second-order non-adiabatic coupling elements $\langle \Psi_n | \hat{T}_N | \Psi_m \rangle$ are often neglected in the treatment [193].

2.2 The many-electron wavefunction

Throughout this work, we consider the electronic Schrödinger equation with a fixed nuclear arrangement. In the following, all equations are considered in atomic units, where all spatial coordinates are considered in Bohr, and the energies are given in Hartree.¹ The electronic Hamiltonian in atomic units reads

$$\hat{H} = - \sum_i \frac{1}{2} \nabla_i^2 - \sum_{Ki} \frac{1}{|\mathbf{r}_i - \mathbf{R}_K|} + \sum_{i>j} \frac{1}{|\mathbf{r}_i - \mathbf{r}_j|} + E_{nuc} = \sum_i \hat{h}_i + \sum_{i>j} \frac{1}{|\mathbf{r}_i - \mathbf{r}_j|}, \quad (2.10)$$

and the constant nuclear repulsion energy E_{nuc} is neglected in the following, since it only acts as a shift of the electronic energy. The electronic Schrödinger equation is now written without explicitly stating a dependency on the nuclear arrangement:

$$\hat{H} |\Psi_n(\mathbf{x})\rangle = E_n |\Psi_n(\mathbf{x})\rangle. \quad (2.11)$$

¹Bohr radius: $a_0 = \frac{4\pi\epsilon_0\hbar^2}{m_e q_e^2} = 0.529 \cdot 10^{-10}$ m, one Hartree $E_0 = \frac{\hbar^2}{m_e a_0^2} = 2625.5$ kJ/mol.

The Hamilton operator (2.10) commutes with the spin operators

$$[\hat{S}^2, \hat{H}] = \hat{S}^2 \hat{H} - \hat{H} \hat{S}^2 = 0 \quad \text{and} \quad [\hat{S}_z, \hat{H}] = 0, \quad (2.12)$$

and the electronic wavefunction can be characterized by the spin quantum numbers S and M_S :

$$\hat{S}^2 |\Psi\rangle = S(S+1) |\Psi\rangle \quad \text{and} \quad \hat{S}_z |\Psi\rangle = M_S |\Psi\rangle. \quad (2.13)$$

Since, the Hamiltonian does not include a spin component, the energy is invariant to the quantum number M_S , and we can assume $M_S = S$ for simplification.

The wavefunction $|\Psi\rangle$ has to fulfill the Pauli principle in which the wavefunction of electrons has to be antisymmetric with respect to permutations of any pair of electrons, as for example

$$\Psi(\mathbf{x}_1, \mathbf{x}_2, \dots, \mathbf{x}_N) = -\Psi(\mathbf{x}_2, \mathbf{x}_1, \dots, \mathbf{x}_N). \quad (2.14)$$

The wavefunctions can be represented in an orthonormal basis of antisymmetric configuration functions (CFs) Φ_I :

$$\Psi_n(\mathbf{x}_1, \dots, \mathbf{x}_N) = \sum_I c_I^n \Phi_I(\mathbf{x}_1, \dots, \mathbf{x}_N) \quad (2.15)$$

enumerated by the index I . The coefficients c_I^n are known as the CI coefficients of state n .

One possibility of constructing the CF basis are configuration state functions (CSFs) in which the CFs are constructed by the antisymmetrized product of a spatial function $\varphi_I(\mathbf{r})$ and a spin-eigenfunction $\Theta_I^S(\mathbf{s})$:

$$\Phi_I(\mathbf{x}) = \hat{\mathcal{A}}[\varphi_I(\mathbf{r})\Theta_I^S(\mathbf{s})] = \frac{1}{\sqrt{N!}} \sum_P (-1)^{|P|} [\hat{P}\varphi_I(\mathbf{r})][\hat{P}\Theta_I^S(\mathbf{s})]. \quad (2.16)$$

The operator $\hat{\mathcal{A}}$ is the antisymmetrizer which sums over all possible permutations P of the electrons, and multiplies with factor of 1 or -1 if the number of permutations (indicated by $|P|$) is even or odd, respectively. Since the permutation operator permutes with the spin operators, the spin-eigenfunction is not destroyed by its application, and the total wavefunction fulfills equation (2.13). The spatial function $\varphi_I(\mathbf{r})$ is constructed from a product of orthonormal real functions $\phi_i(\mathbf{r})$ which are the molecular orbitals (MOs):

$$\Phi_I(\mathbf{x}_1, \mathbf{x}_2, \dots, \mathbf{x}_N) = \hat{\mathcal{A}}[\phi_1(\mathbf{r}_1)\phi_2(\mathbf{r}_2) \dots \phi_N(\mathbf{r}_N)\Theta_I^S(s_1, s_2, \dots, s_N)]. \quad (2.17)$$

The orbitals ϕ_i are chosen from a larger set of MOs, and therefore the index I specifies a set of

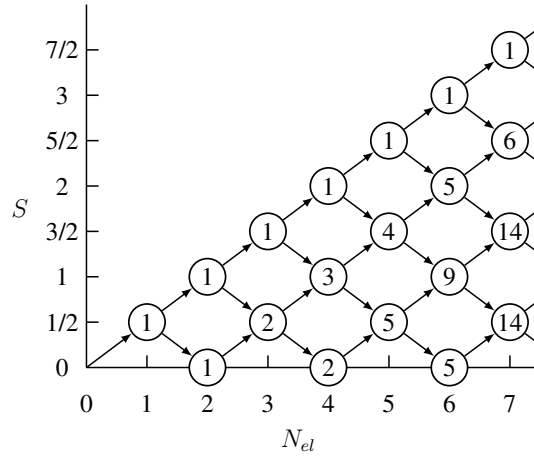


Figure 2.1: The branching diagram of the genealogical spin-eigenfunction generation (reproduced from Reference [195]).

the N molecular orbitals in the spatial function $\varphi_I(\mathbf{r})$ and the specific spin-eigenfunction Θ_I^S . If the same MO is occupied by more than two electrons, the CSF gets annihilated by the antisymmetrizer, since this violates the Pauli principle. Often, one is interested in a wavefunction in a specific spatial irreducible representation introduced by the symmetry of the molecular structure. In this case, the product of MO orbitals is restricted to be in the desired irreducible representation.

The spin-eigenfunctions can be constructed with the genealogical construction of spin-eigenfunctions [195] by successive angular momentum additions of the one-electron spin system. Each addition changes the spin quantum number S either by $+\frac{1}{2}$ or $-\frac{1}{2}$, since $\frac{1}{2}$ is the quantum number of the one-electron system.² For example, the two-electron triplet functions are obtained by an addition increasing $S = \frac{1}{2}$ by $+\frac{1}{2}$, while the singlet function is obtained by the $-\frac{1}{2}$ addition. The three-electron doublet eigenfunctions ($S = \frac{1}{2}$) are obtained either by the $+\frac{1}{2}$ addition to the two-electron singlet function ($S = 0$) or by the $-\frac{1}{2}$ addition to the two-electron triplet function ($S = 1$). Each spin state can be characterized by the history of $+\frac{1}{2}$ or $-\frac{1}{2}$ additions. This can be graphically visualized by the branching diagram which is shown in Figure 2.1. Each circle describes the spin states for N electrons and a spin quantum

²The angular momentum addition for the $M_S = S$ case can be written as [196]:

$$\Theta^{S+1/2}(s_1, \dots, s_N) = \Theta^S(s_1, \dots, s_{N-1})\alpha(s_N) \quad (2.18)$$

$$\Theta^{S-1/2}(s_1, \dots, s_N) = \frac{1}{(2S+1)} \left[(-\hat{S}^- \Theta^S(s_1, \dots, s_{N-1}))\alpha(s_N) + \sqrt{2S}\Theta^S(s_1, \dots, s_{N-1})\beta(s_N) \right], \quad (2.19)$$

with the one-electron functions $\Theta^{+1/2}(s_1) = \alpha(s_1)$ and $\Theta^{-1/2}(s_1) = \beta(s_1)$, and the ladder operator \hat{S}^- .

number S . The number of independent spin states is presented in circles, and it is equal to all spin-eigenfunctions with $M_S = S$. The number also represents all possible paths in the branching diagram leading to the circle.

In summary, each spin-eigenfunction can be uniquely written as a series of upward steps (denoted as \nearrow) and downwards steps (\searrow) in the branching diagram, which yields $|\nearrow\nearrow\searrow\rangle$ and $|\nearrow\searrow\nearrow\rangle$ for the two possible $\Theta^{S=\frac{1}{2}}(s_1, s_2, s_3)$ functions. Other spin-eigenfunction generation procedures can be found in the book on spin-eigenfunctions by Pauncz [195].

Furthermore, doubly occupied MOs can only contribute in a up and down sequence, since otherwise the CSF gets annihilated by the antisymmetrizer. This corresponds to a product with a two-electron singlet function which can be factored out of the spin-eigenfunction [195]. Therefore, we can consider the spin state generation only for electrons in singly occupied MOs. This enables another way of characterizing CSFs which is entirely focused on the MOs [67]. There are four possibilities how a MO ϕ_i can contribute in a CSF: non-occupied ($d_i = 0$), singly-occupied with an up-walk ($d_i = \nearrow$), singly-occupied with a down-walk ($d_i = \searrow$), and doubly occupied ($d_i = 2$). A CSF containing m orbitals can now be written as a step vector \mathbf{d} containing the different steps $|\Phi_I\rangle = |\mathbf{d}\rangle = |d_1 d_2 \dots d_m\rangle$. For example, all possible singlet CSFs with four electrons in three orbitals are given as (no spatial symmetry restrictions considered):

$$|\Phi_1\rangle = |220\rangle, \quad |\Phi_2\rangle = |202\rangle, \quad |\Phi_3\rangle = |022\rangle, \quad (2.20)$$

$$|\Phi_4\rangle = |2\nearrow\searrow\rangle, \quad |\Phi_5\rangle = |\nearrow 2\searrow\rangle, \quad |\Phi_6\rangle = |\nearrow\searrow 2\rangle. \quad (2.21)$$

Furthermore, it is possible to define an ordering of the CSFs, i.e. $|\Phi_I\rangle > |\Phi_J\rangle$ for $I > J$, which depends on the sequence in the step vector \mathbf{d} . This ordering is called lexical order [68].

By specifying the molecular orbitals, the number of electrons N , the spin quantum number S , and a spatial symmetry, it is possible to generate all possible CSFs within this set-up. This expansion is called the full configuration interaction (full-CI), and the number of all possible CSFs for a certain number of spatial orbitals m is given by Weyl's formula [197]:

$$n(N, S, m) = \frac{2S + 1}{m + 1} \binom{m + 1}{\frac{1}{2}N - S} \binom{m + 1}{\frac{1}{2}N + S + 1}, \quad (2.22)$$

where restrictions by spatial symmetry are neglected.

A second way of constructing CFs are Slater determinants. Here, we first construct spin-orbitals $\psi_i(\mathbf{x}_j)$ as a product of the spatial MO $\phi_i(\mathbf{r}_j)$ and the one-electron spin function $\sigma(s_j)$:

$$\psi_i(\mathbf{x}) = \phi_i(\mathbf{r})\sigma(s). \quad (2.23)$$

The spin function $\sigma(s)$ is one of the two possible spin-eigenfunctions $\alpha(s)$ or $\beta(s)$ of the one-electron spin operator. The determinant is built from the antisymmetrized product of the spin-orbitals, where index I specifies the set of spin-orbitals used in Φ_I :

$$\Phi_I = \hat{\mathcal{A}}[\psi_1(\mathbf{x}_1)\psi_2(\mathbf{x}_2)\dots\psi_N(\mathbf{x}_N)] = \frac{1}{\sqrt{N!}} \begin{vmatrix} \psi_1(\mathbf{x}_1) & \dots & \psi_N(\mathbf{x}_1) \\ \vdots & \ddots & \vdots \\ \psi_1(\mathbf{x}_N) & \dots & \psi_N(\mathbf{x}_N) \end{vmatrix}. \quad (2.24)$$

The antisymmetrized product can be written as a determinant of a matrix shown in the latter part of the equation. To achieve the correct spin quantum number M_S , the sum of the α - and β -spins (N_α and N_β) has to fulfill the relation $M_S = \frac{1}{2}(N_\alpha - N_\beta)$. Each spin-orbital can be occupied only once, since otherwise the configuration is annihilated by the antisymmetrizer. The spatial product can be restricted by the spatial symmetry similar to the CSF case. Furthermore, CSFs can also be expanded into combinations of determinants by expanding the spin-eigenfunction. The configuration space spanned by the determinants is therefore larger than the CSF space, since it includes other spin contributions as well. Per construction, a single determinant is an eigenfunction of the \hat{S}_z operator, but that is not necessarily true for the \hat{S}^2 operator. Therefore, the CI coefficients in the determinant basis cannot be freely chosen, since certain combinations of determinants are required to ensure that the total wavefunction is a spin-eigenfunction.

The larger number of determinants is usually compensated for by a faster computation time, since less complicated bookkeeping is required in the implementation. The use of determinants requires also some further technical details [198], as for example spin-projections if parts of the Hamiltonian are diagonalized exactly. The MCSCF program discussed in this thesis allows the usage of both CF types, and the CI part is based on code written by Knowles et al. [198, 199].

2.3 Second-quantization and the coupling coefficients

To simplify changes in the wavefunction we utilize the framework of second quantization [200]. In order to manipulate a spin-orbital configuration, we define the creation operator \hat{a}_r^\dagger and the annihilation operator \hat{a}_r . These operators act on determinants, but since CSFs can be represented in a determinant basis, the action is also well defined for CSFs. The creation operator \hat{a}_r^\dagger adds a spin-orbital ψ_r and an extra electron into the configuration, and antisymmetrizes the resulting function afterwards. If the spin-orbital is already part in the determinant the creation operator destroys the configuration yielding zero through the antisymmetrization. The application of the annihilation operator has the opposite effect: it returns zero if the spin orbital is not part of the configuration, otherwise the spin-orbital and the electron are removed. Every determinant can be described as a consecutive application of creation operators on the empty vacuum state. The operators fulfill the following anticommutation relation [200]

$$\hat{a}_r^\dagger \hat{a}_s^\dagger + \hat{a}_s^\dagger \hat{a}_r^\dagger = 0, \quad \hat{a}_r \hat{a}_s + \hat{a}_s \hat{a}_r = 0, \quad \text{and} \quad \hat{a}_r^\dagger \hat{a}_s + \hat{a}_s \hat{a}_r^\dagger = \delta_{rs} \quad (2.25)$$

which ensures the permutation relation in the Pauli principle. We further distinguish between α - and β -spins by labeling the creation and annihilation operator of the spin-orbitals with β -spins by an extra bar: \hat{a}_r and \hat{a}_r^\dagger . Next, we define the excitation operators

$$\hat{E}_{rs} = \hat{a}_r^\dagger \hat{a}_s + \hat{a}_r \hat{a}_s^\dagger \quad (2.26)$$

$$\hat{E}_{pq,rs} = \hat{a}_p^\dagger \hat{E}_{rs} \hat{a}_q + \hat{a}_p \hat{E}_{rs} \hat{a}_q^\dagger = \hat{E}_{pq} \hat{E}_{rs} - \delta_{qr} \hat{E}_{ps}. \quad (2.27)$$

The latter term can be derived from the anticommutator relations in equation (2.25). These operators do not modify the spin of the configuration, since only the MO in the spin-orbital is replaced or the configuration is destroyed otherwise.

In the framework of second quantization, a spin-independent one-electron operator can be represented with the excitation operator \hat{E}_{rs} [200]:

$$\hat{A} = \sum_{rs} A_{rs} \hat{E}_{rs} \quad \text{with} \quad A_{rs} = \int \phi_r^*(\mathbf{r}) \hat{A}(\mathbf{r}) \phi_s(\mathbf{r}) d\mathbf{r}. \quad (2.28)$$

An analogous result holds for two-electron electron operator:

$$\hat{B} = \sum_{pq,rs} B_{pq,rs} \hat{E}_{pq,rs} \quad \text{with} \quad B_{pq,rs} = \int \phi_p^*(\mathbf{r}_1) \phi_r^*(\mathbf{r}_2) \hat{B}(\mathbf{r}_1, \mathbf{r}_2) \phi_q(\mathbf{r}_1) \phi_s(\mathbf{r}_2) d\mathbf{r}_1 d\mathbf{r}_2. \quad (2.29)$$

Since we assume real orbitals, the complex conjugation is neglected in the following. The second quantization allows us to evaluate the one- and two-electron operators in the Hamiltonian (2.10) as matrices and tensors in the MO basis:

$$\hat{H} = \sum_{rs} h_{rs} \hat{E}_{rs} + \frac{1}{2} \sum_{pqrs} (pq|rs) \hat{E}_{pq,rs} \quad (2.30)$$

with

$$h_{rs} = \int \phi_r(\mathbf{r}) \hat{h}_1 \phi_s(\mathbf{r}) \mathbf{d}\mathbf{r} \quad (2.31)$$

$$(pq|rs) = \int \phi_p(\mathbf{r}_1) \phi_q(\mathbf{r}_1) \frac{1}{|\mathbf{r}_1 - \mathbf{r}_2|} \phi_r(\mathbf{r}_2) \phi_s(\mathbf{r}_2) \mathbf{d}\mathbf{r}_1 \mathbf{d}\mathbf{r}_2. \quad (2.32)$$

Throughout this thesis, the two-electron integral $(pq|rs)$ is used in the Mulliken notation as defined in (2.32), and the evaluation of these integrals is briefly reviewed in Section 2.4. Next, the second-quantized Hamiltonian is represented in the CF basis. Here, the overlap of the spin-free excitation-operators and the CFs yields the one- and two-electron coupling coefficients:

$$\gamma_{rs}^{IJ} = \langle \Phi_I | \hat{E}_{rs} | \Phi_J \rangle \quad \text{and} \quad \Gamma_{pq,rs}^{IJ} = \langle \Phi_I | \hat{E}_{pq,rs} | \Phi_J \rangle. \quad (2.33)$$

The two-electron coupling coefficient can be evaluated from the one-electron coupling coefficients by inserting the CF basis (Φ_K) as a resolution of identity:³

$$\Gamma_{pq,rs}^{IJ} = \langle \Phi_I | \hat{E}_{pq} \hat{E}_{rs} - \delta_{qr} \hat{E}_{ps} | \Phi_J \rangle = \sum_K \gamma_{pq}^{IK} \gamma_{rs}^{KJ} - \delta_{qr} \gamma_{ps}^{IJ}. \quad (2.34)$$

This trick can also be used to evaluate higher-order coupling coefficients if needed [21]. Determinants offer the advantage that the evaluation of the one-electron coupling coefficient is rather simple. It follows directly from the spin-orbital occupation and ordering, and the coupling coefficient γ_{ij}^{IJ} is either -1 , 0 or 1 . With a powerful addressing algorithm [199], the evaluation is fast and compensates for the larger number of CFs.

In case of the CSFs, the evaluation is less straightforward. Here, it is possible to use properties from the unitary group theory to evaluate the coupling coefficients, which has been pioneered by Paldus [66, 201, 202] and Shavitt [67, 68, 203, 204] for the CI problem. The connection to the unitary group $U(m)$ (m equals to the number of MOs) is based on the

³Resolution of identity: $1 = \sum_I |\Phi_I\rangle \langle \Phi_I|$

commutator relation of the single excitation operator:

$$[\hat{E}_{rs}, \hat{E}_{pq}] = \hat{E}_{rq}\delta_{ps} - \hat{E}_{ps}\delta_{rq}, \quad (2.35)$$

which is also the commutator relation of the generators of the $U(m)$ group [202]. An efficient evaluation of the coupling coefficients is possible with the graphical unitary group approach (GUGA) method [67, 68, 204]. The derivation is rather complicated, and we only briefly illustrate the main results presented in Reference [204]. First, we recall the definition of the CSFs using the step vector $\mathbf{d} = (d_1, d_2, \dots, d_m)$ and define a range between the index r and s in the excitation operator \hat{E}_{rs} :

$$(r, s) = \{\min(r, s), \dots, \max(r, s)\}. \quad (2.36)$$

It was found that the coupling coefficient vanishes if the definition of the CSFs $\Phi_I = |\mathbf{d}^I\rangle$ and $\Phi_J = |\mathbf{d}^J\rangle$ differs outside the range, in another words if $d_i^I \neq d_i^J$ for $i \notin (r, s)$. Otherwise, the coupling coefficient only depends on the definitions within the range (r, s) . If $r = s$, the evaluation of the coupling coefficient is trivial:

$$\langle \Phi_I | \hat{E}_{rr} | \Phi_J \rangle = \delta_{IJ} n(r) \quad (2.37)$$

with $n(r) = 0, 1, 1, 2$ for $d_r = 0, \nearrow, \searrow, 2$, respectively. Furthermore, we can use that

$$\langle \Phi_I | \hat{E}_{rs} | \Phi_J \rangle = \langle \Phi_J | \hat{E}_{sr} | \Phi_I \rangle, \quad (2.38)$$

which limits the necessary range to $r < s$. If the lexical order is assumed, it is possible to show that the coupling coefficients also vanishes for $r < s$ and $|\Phi_I\rangle \geq |\Phi_J\rangle$. The remaining non-zero coupling coefficients can be evaluated by a product of segment values W_k [68]

$$\langle \Phi_I | \hat{E}_{rs} | \Phi_J \rangle = \prod_{k \in (r, s)} W_k(\mathbf{d}_k^I, \mathbf{d}_k^J) \quad (2.39)$$

depending on the history of the previous k orbitals: $\mathbf{d}_k = (d_1, \dots, d_k)$. Here, the history \mathbf{d}_k is only needed for notational reasons, since we avoided the introduction of any group theoretical tableaux. In practice, the segment values W_k depend only on k and the evaluation can be efficiently done using the distinct row table introduced by Shavitt [67]. A summary of the possible values can be found in Reference [204]. A similar technique is also available for computing the two-electron coupling coefficients.

After evaluating the coupling coefficients, the final electronic Hamiltonian in the CF basis reads

$$H_{IJ} = \sum_{rs} h_{rs} \gamma_{rs}^{IJ} + \frac{1}{2} \sum_{pqrs} (pq|rs) \Gamma_{pq,rs}^{IJ}, \quad (2.40)$$

and it is a (real) symmetric matrix. The Schrödinger equation (2.11) is now an eigenvalue problem of the matrix H_{IJ} , and its solution yields the energy E_n and the CI coefficients c_I^n . The one- and two-electron integrals are symmetric with respect to the interchange of $p \leftrightarrow q$, $r \leftrightarrow s$, and $pq \leftrightarrow rs$. Without losing generality, it is possible to symmetrize the coupling coefficients in a similar way:

$$\bar{\gamma}_{rs}^{IJ} = \frac{1}{2} [\gamma_{rs}^{IJ} + \gamma_{sr}^{IJ}] \quad \text{and} \quad \bar{\Gamma}_{pq,rs}^{IJ} = \frac{1}{4} [\Gamma_{pq,rs}^{IJ} + \Gamma_{qp,rs}^{IJ} + \Gamma_{pq,sr}^{IJ} + \Gamma_{qp,sr}^{IJ}]. \quad (2.41)$$

Symmetrized coupling coefficients are assumed in the following unless otherwise noted, and the bar is omitted for simplicity.

2.4 Basis functions and integral evaluation

The MOs are constructed by a linear combination of a finite set of basis functions $\chi_\mu(\mathbf{r})$:

$$\phi_i(\mathbf{r}) = \sum_{\mu} \chi_{\mu}(\mathbf{r}) M_{\mu r}. \quad (2.42)$$

This is the linear combination of atomic orbitals (LCAO) approximation and $M_{\mu r}$ are the MO coefficients. Typically, the basis functions are approximations of a specific set of AOs from each atom in the molecule. The AO basis functions are non-orthogonal, and the overlap matrix $S_{\mu\nu} = \langle \mu | \nu \rangle$ has to be included if an overlap of two AO functions is needed. Nevertheless, the MO orbitals are considered to be orthonormal, i.e.

$$\langle \phi_r | \phi_s \rangle = [\mathbf{M}^T \mathbf{S} \mathbf{M}]_{rs} = \delta_{rs}. \quad (2.43)$$

The number of basis functions limits the number of possible MOs, and therefore restricts the number of possible configurations in the full-CI expansion. The finite basis introduces an error to the exact energy known as the basis incompleteness error.

The one- and two-electron integrals (2.32) are evaluated at the AO level, and the two-

electron integral in AO basis reads:

$$(\rho\sigma|\mu\nu) = \int \chi_\rho(\mathbf{r}_1)\chi_\sigma(\mathbf{r}_1) \frac{1}{|\mathbf{r}_1 - \mathbf{r}_2|} \chi_\mu(\mathbf{r}_2)\chi_\nu(\mathbf{r}_2) d\mathbf{r}_1 d\mathbf{r}_2. \quad (2.44)$$

The basis functions $\chi_\mu(\mathbf{r})$ are chosen to be as computationally advantageous as possible to reduce the numerical costs in the integral evaluation routines. Today, nearly all basis sets use contracted Gaussian type orbitals (GTOs) in which the radial part $R(r)$ of the atomic orbital is given by an approximation including Gaussian functions [200]:

$$\chi_{nlm\mathbf{R}}(\mathbf{r}) = R_{nl}(|\mathbf{r} - \mathbf{R}|)Y_{lm}(\theta, \varphi) \quad \text{with} \quad R_{nl}(r) = \sum_i d_{ni} N_{l\zeta_i} r^l \exp(-\zeta_i r^2). \quad (2.45)$$

Here, $Y_{lm}(\theta, \varphi)$ are the spherical harmonics and R_{nl} is the radial part expanded in a series of Gaussian functions with the contraction coefficient d_{ni} . \mathbf{R} is the nuclear coordinate from the associated atom, and $N_{l\zeta_i}$ is a normalization coefficient. The use of Gaussian functions allows an analytical evaluation of the integrals without any expensive grid based quadrature [205]. Furthermore, it is possible to derive efficient recursive evaluations of the integrals [206–209]. Today, various series of basis sets exist, and they are often labeled by a cardinal number $n = \text{D, T, Q, 5, 6}$ that is associated with the number of contracted exponential functions R_{nl} in each atomic valence orbital. With a growing cardinal number, more contracted Gaussians and also higher angular momentum functions are introduced to the basis set. The accuracy is gradually improved by an increasing n approximating the basis-set limit. Here, the energy converges polynomially such that an extrapolation of the energy is possible [210,211]. Popular basis-sets are the Dunning basis sets cc-pV n Z [15,211,212] or the Karlsruhe basis sets def2- n ZVP [213] both used in this thesis.

However, the approximation with Gaussian functions comes with the disadvantage that GTOs can hardly represent the wavefunction cusp at $r_{ij} = |\mathbf{r}_i - \mathbf{r}_j| = 0$. The reason for this cusp is the singularity of the Coulomb potential which results in a discontinuity in the first derivative of the wavefunction at $r_{ij} = 0$, and high-order angular momentum basis functions are required for an improved description of the cusp. This problem has been solved in the last 20 years by including correction terms depending explicitly on r_{ij} in the dynamical correlation treatment. This explicit correlation improves the accuracy considerably for smaller basis sets, and often a triple-zeta basis ($n=3$) is sufficient for accurate results [214]. Today, the explicit correlation is available for most of the electron-structure methods [215] including post-MCSCF methods [216–219].

2.4.1 Density fitting

The evaluation of the integrals and the transformation from the AO basis into the MO basis become more and more dominating with the growing system size. This can be accelerated by using density fitting (DF) in which products of functions $\chi_\mu(\mathbf{r})\chi_\nu(\mathbf{r})$ are fitted by an auxiliary basis set $\tilde{\chi}_A(\mathbf{r})$. Using this auxiliary basis (also called fitting basis), it is possible to approximate the two electron integral as [220, 221]:

$$(\rho\sigma|\mu\nu) \approx \sum_{AB} (\rho\sigma|A) J_{AB}^{-1} (B|\mu\nu), \quad (2.46)$$

where J_{AB} as defined as

$$J_{AB} = \int \tilde{\chi}_A(\mathbf{r}_1) \frac{1}{|\mathbf{r}_1 - \mathbf{r}_2|} \tilde{\chi}_B(\mathbf{r}_2) \mathbf{d}\mathbf{r}_1 \mathbf{d}\mathbf{r}_2. \quad (2.47)$$

The three index integrals read

$$(\mu\nu|A) = \int \chi_\mu(\mathbf{r}_1) \chi_\nu(\mathbf{r}_1) \frac{1}{|\mathbf{r}_1 - \mathbf{r}_2|} \tilde{\chi}_A(\mathbf{r}_2) \mathbf{d}\mathbf{r}_1 \mathbf{d}\mathbf{r}_2. \quad (2.48)$$

The evaluation of J_{AB}^{-1} is achieved with a Cholesky decomposition [222] or by solving a linear system of equations [221]. The Cholesky decomposition is only needed once, and it is calculated and stored in the beginning. The auxiliary basis is contracted with the Cholesky decomposition $\mathbf{J} = \mathbf{L}\mathbf{L}^\top$ after the integral evaluation:

$$(\rho\sigma|\bar{A}) = \sum_A (\rho\sigma|A) L_{A\bar{A}}^{-1} \quad \text{and} \quad (\rho\sigma|\mu\nu) = \sum_{\bar{A}} (\rho\sigma|\bar{A}) (\bar{A}|\mu\nu). \quad (2.49)$$

The bar denotes the auxiliary basis after the transformation with the Cholesky decomposition. The computation of the three-index integrals scales as $O(N_{ao}^2 N_{fit})$, and is therefore more efficient than the evaluation of the four-index integral. However, the assembly in equation (2.49) scales formally as $O(N_{ao}^4 N_{fit})$, but it can be efficiently computed with matrix multiplications leading to a significantly lower prefactor [220]. Furthermore, the assembly (2.49) with all AOs is not necessarily needed, since the transformation to the MO basis can be done beforehand. This is particularly interesting if only subsets of orbitals are required. Furthermore, steps of subsequent calculations with the integrals can also be computed before the assembling step, as for example the contraction with another matrix. Often, this further reduces the scaling of the assembly step, and for example the full density fitted calculation of the Fock matrix is achieved

in $O(N_{ao}^4)$ [221, 223].

If the auxiliary fitting basis is correctly chosen, the loss of accuracy through density fitting is negligible compared to other errors as for example the basis-set incompleteness error or the intrinsic error of the method [223–225]. Our MCSCF program is based on the well parallelized density fitting routines implemented by Werner et al. [222]. More details about the density fitting steps required for the MCSCF method can be found in the Supplementary Material of Reference [2].

3 | MCSCF theory

In case of the full-CI wavefunction, the energy does not explicitly depend on the shape of the orbitals, since all changes in the orbitals can be absorbed into the CI coefficients [226]. However, the number of possible CF increases factorially with the number of orbitals and electrons, as can be seen in the Weyl formula in equation (2.22). The application of the full-CI method is therefore limited to very few atoms.

In the MCSCF approach, only the strongly contributing CFs are included in the first-principles wavefunction. Since the full-CI structure is broken, the MCSCF wavefunction depends on both the MO and the CI coefficients. This chapter focuses on results which can be derived from the MCSCF wavefunction structure. Additionally, we discuss the access to excited states with state-averaging and the theory of analytical energy derivatives with the coupled-perturbed MCSCF (CP-MCSCF). Finally, the post-MCSCF calculation of the dynamic correlation with the MRPT is briefly outlined.

In the early MCSCF methods, single CFs have been carefully hand-picked to construct the MCSCF wavefunction, which often leads to convergence difficulties. Today, most MCSCF calculations are done with a complete active space (CAS) wavefunction, where a set of active orbitals is chosen a priori. The CF are generated by a full-CI expansion within the active orbitals for a given number of electrons [20, 23, 60, 62, 63, 227], and the remaining electrons doubly occupy the energetically lower orbitals. In the following, an active space with N_{el} electrons and N_{act} active orbitals is denoted as $CAS(N_{el}, N_{act})$. The MCSCF method with a CAS wavefunction is also known as the CASSCF method.

The CAS wavefunction suffers from the same exponential scaling as the full-CI expansion which limits the size of the active space. The number of generated CF can be reduced by introducing restrictions, as for example done in the commonly used restricted active space self-consistent field (RASSCF) method [65, 142]. Here, the active orbitals are divided into three subgroups RAS1, RAS2, and RAS3, and the CFs are constructed according to the following rules: (i) only configurations with a maximum of a certain number of holes in the RAS1 orbitals are allowed, (ii) no occupation restrictions are considered for the RAS2 orbitals (similar to CAS), and (iii) only configurations with a certain number of electrons in the RAS3

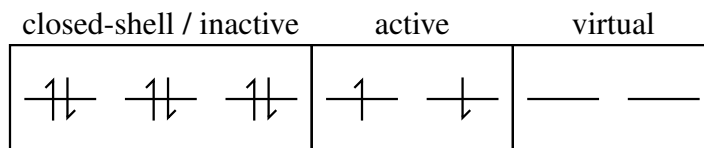


Figure 3.1: Occupation scheme of a single MCSCF determinant. MOs are symbolized by horizontal lines, the occupation with an α - or β -spin is denoted by the upwards or downwards pointing arrow, respectively.

orbitals are included. This approach has been further generalized by introducing additional subspaces and restrictions [143, 144]. Nevertheless, all further discussions are independent on the exact MCSCF wavefunction structure, and the presented methods are applicable to all possible MCSCF wavefunctions.

3.1 MCSCF energy and density

In the following, we categorize the orbitals with respect to their occupations in the CF basis. Orbitals which are doubly occupied in all CFs are called inactive or closed-shell orbitals. MOs with varying occupations are referred to as active orbitals, and non-occupied orbitals are denoted as virtual orbitals. A graphical representation of a single determinant following this structure is displayed in Figure 3.1. From now on, we employ the following index notation to label these orbitals in equations: The indices r, s, p, q are used when referring to all orbitals. The inactive orbitals are denoted by i, j and the active orbitals by t, u, v, w . The labels k, l represent the occupied orbitals, hence the inactive and active orbitals together. The virtual orbitals are distinguished by a, b .

This structure of the CFs allows a direct evaluation of some of the one-electron coupling coefficients:

$$\gamma_{ij}^{IJ} = 2\delta_{IJ}\delta_{ij}, \quad \gamma_{ar}^{IJ} = \gamma_{ra}^{IJ} = 0, \quad \text{and} \quad \gamma_{iu}^{IJ} = \gamma_{ui}^{IJ} = 0. \quad (3.1)$$

The remaining non-trivial one-electron coupling coefficient is γ_{tu}^{IJ} of the two active orbitals t and u . Because of the trivial treatment of the closed-shell orbitals, they can be removed from the CFs without loss of generality. This can be also seen in the Hamiltonian, if the evaluated coupling coefficients are inserted:

$$H_{IJ} = \delta_{IJ}E_c + \sum_{tu}^{\text{act}} F_{tu}^c \gamma_{tu}^{IJ} + \frac{1}{2} \sum_{tuvw}^{\text{act}} (tu|vw) \Gamma_{tu,vw}^{IJ}. \quad (3.2)$$

The contribution of the closed-shell orbitals can be separated into the closed-shell energy E_c and the closed-shell Fock matrix F_{rs}^c :

$$E_c = \sum_i^{\text{cs}} [h_{ii} + F_{ii}^c] \quad \text{and} \quad F_{rs}^c = h_{rs} + \sum_i^{\text{cs}} [2J_{rs}^{ii} - K_{rs}^{ii}], \quad (3.3)$$

and only the coupling coefficients involving purely active orbitals remain. In the last equation, the two-electron integrals in MO basis are represented in matrix form with $J_{rs}^{kl} = (kl|rs)$ for the Coulomb integral and $K_{rs}^{kl} = (rk|ls)$ for the exchange integral.

The evaluated coupling coefficients allow us to rewrite the energy $E = \mathbf{c}^\top \mathbf{H} \mathbf{c}$ for a given set of CI coefficients \mathbf{c} :

$$E = E_c + \sum_{tu}^{\text{act}} F_{tu}^c D_{tu} + \frac{1}{2} \sum_{tuvw}^{\text{act}} (tu|vw) D_{tu,vw}. \quad (3.4)$$

The coupling coefficients are contracted with the given CI vector, and the result are the active one- and two-particle reduced density matrices (RDMs):

$$D_{tu} = \sum_{IJ} c_I \gamma_{tu}^{IJ} c_J \quad \text{and} \quad D_{tu,vw} = \sum_{IJ} c_I \Gamma_{tu,vw}^{IJ} c_J. \quad (3.5)$$

The remaining non-vanishing density matrices read:

$$D_{ij} = 2\delta_{ij}, \quad D_{ij,kl} = 4\delta_{ij}\delta_{kl} - \delta_{ik}\delta_{jl} - \delta_{jk}\delta_{il}, \quad (3.6)$$

$$D_{tu,ij} = D_{ij,tu} = 2\delta_{ij}D_{tu}, \quad \text{and} \quad D_{it,uj} = -\frac{1}{2}\delta_{ij}D_{tu}. \quad (3.7)$$

Since we already consider the coupling coefficients to be symmetrized, the RDMs show the same symmetry as the the integral F_{tu}^c and $(tu|vw)$.

3.2 Variational conditions and the Brillouin theorem

Changes in the molecular orbitals can be represented by a unitary transformation \mathbf{U} . Since we only deal with real orbitals, \mathbf{U} is an orthogonal transformation, i.e. $\mathbf{U}^{-1} = \mathbf{U}^\top$. This maintains the orthogonality of the orbitals without losing any generality:

$$\tilde{\phi}_k = \sum_r \phi_r U_{rk} = \sum_{\mu r} \chi_\mu M_{\mu r} U_{rk} = \sum_\mu \chi_\mu \tilde{M}_{\mu k} \quad \text{and} \quad \tilde{\mathbf{M}} = \mathbf{M} \mathbf{U}. \quad (3.8)$$

$$\mathbf{R} = \begin{array}{|c|c|c|} \hline R_{ij} = 0 & -R_{it} & -R_{ia} \\ \hline R_{ti} & \begin{array}{c} -R_{ut} \\ \hline R_{tu} \end{array} & -R_{ua} \\ \hline R_{ai} & R_{au} & R_{ab} = 0 \\ \hline \end{array}$$

Figure 3.2: Elements in the rotational matrix \mathbf{R} . The rotation $R_{tu} = -R_{ut}$ are fully redundant for a CASSCF wavefunction.

The unitary transformation can be constructed from a set of rotational parameters R_{rk} which describe the rotation between the orbitals r and k ($r > k$). The rotation parameters are arranged in an antisymmetric matrix $\mathbf{R}^T = -\mathbf{R}$, and the unitary transformation is obtained by the matrix exponential of the matrix \mathbf{R} :

$$\mathbf{U} = \exp(\mathbf{R}) = 1 + \mathbf{R} + \frac{1}{2!}\mathbf{R}^2 + \frac{1}{3!}\mathbf{R}^3 + \dots \quad (3.9)$$

The rotations R_{ij} between inactive orbitals and R_{ab} between virtual orbitals are fully redundant and removed, since the energy is independent to these rotations.¹ In case of a CAS wavefunction, the rotational parameters R_{tu} are redundant as well, since changes in the active orbitals can be fully described by the CI expansion [226]. In this case, the energy is independent of the explicit form of the orbitals, and only the optimization of the three orbital subspaces is relevant. In case of restrictions in the CF generation, some active-active rotations are needed while others are redundant. The determination of the redundant and non-redundant rotations is described for example in Reference [85] or [124]. An overview of the different rotational parameters is displayed in Figure 3.2.

The change of the wavefunction by the orbital transformation can also be described by a transformation operator [22]:

$$|\tilde{\Psi}\rangle = \exp(\hat{R}) |\Psi\rangle \quad (3.10)$$

¹In case of closed-shell orbitals, this is due to the invariance of the trace with respect to unitary transformations.

in which the operator $\hat{R}^\dagger = -\hat{R}$ is defined as:

$$\hat{R} = \sum_{r>k} R_{rk} (\hat{E}_{rk} - \hat{E}_{kr}). \quad (3.11)$$

The rotation parameters R_{rk} are equivalent to the lower left of the antisymmetric matrix \mathbf{R} . Expanding the expectation value of the transformed wavefunction with help of the Baker-Campbell-Hausdorff (BCH) formula yields a series of commutators:

$$\begin{aligned} E(\mathbf{R}) &= \langle \Psi | \exp(-\hat{R}) \hat{H} \exp(\hat{R}) | \Psi \rangle \\ &= \langle \Psi | \hat{H} | \Psi \rangle + \langle \Psi | [\hat{H}, \hat{R}] | \Psi \rangle + \frac{1}{2!} \langle \Psi | [[\hat{H}, \hat{R}], \hat{R}] | \Psi \rangle + \dots \\ &= E_0 + \sum_{r>k} g_{rk} R_{rk} + \frac{1}{2} \sum_{\substack{r>k \\ s>l}} R_{rk} h_{rk,sl} R_{sl} + \dots \end{aligned} \quad (3.12)$$

Sorting the elements with respect to the power of \mathbf{R} yields a Taylor expansion of the energy including the orbital gradient g_{rk} and Hessian $h_{rk,sl}$. The gradient can be obtained by evaluating the first commutator relation:

$$g_{rk} = 2 \langle \Psi | [\hat{H}, \hat{E}_{rk}] | \Psi \rangle. \quad (3.13)$$

Another derivation of the quadratic expansion is achieved by inserting the transformation with the exponential expansion of $\mathbf{U}(\mathbf{R})$ into the MCSCF energy expression (3.4) and sorting for the linear and quadratic terms of \mathbf{R} . The second-order expansion in the orbital rotation generators R_{rk} can be written as [21]:

$$E^{(2)}(\mathbf{R}) = E_0 + 2 \sum_{rk} A_{rk} (R_{rk} + \frac{1}{2} [\mathbf{R}^2]_{rk}) + \sum_{rk,sl} R_{rk} G_{rs}^{kl} R_{sl} \quad (3.14)$$

in which the matrix A_{rk} is defined as

$$A_{ri} = 2F_{ri}, \quad A_{rt} = \sum_u^{\text{act}} F_{ru}^c D_{ut} + \sum_{uvw}^{\text{act}} J_{ru}^{vw} D_{tu,vw}, \quad \text{and} \quad A_{ra} = 0. \quad (3.15)$$

F_{rs} is known as the general Fock matrix, and it is built from the closed-shell Fock matrix F_{rs}^c

and the contribution of the active orbitals through the active density D_{tu} :

$$F_{rs} = F_{rs}^c + \sum_{tu}^{\text{act}} D_{tu} \left[J_{rs}^{tu} - \frac{1}{2} K_{rs}^{tu} \right]. \quad (3.16)$$

The intermediate \mathbf{G}^{kl} is required for the orbital Hessian and reads

$$G_{rs}^{ij} = 2[F_{rs}\delta_{ij} + L_{rs}^{ij}], \quad (3.17)$$

$$G_{rs}^{tj} = \sum_v^{\text{act}} D_{tv} L_{rs}^{vj} = G_{sr}^{jt}, \quad (3.18)$$

$$G_{rs}^{tu} = F_{rs}^c D_{tu} + \sum_{vw}^{\text{act}} \left[J_{rs}^{vw} D_{tu,vw} + 2K_{rs}^{vw} D_{tu,uw} \right], \quad (3.19)$$

with

$$L_{rs}^{kl} = 4K_{rs}^{kl} - K_{rs}^{lk} - J_{rs}^{kl}. \quad (3.20)$$

The gradient g_{rk} and the Hessian $h_{rk,sl}$ are obtained by differentiating the energy $E^{(2)}(\mathbf{R})$ with respect to \mathbf{R} and evaluating the terms for $\mathbf{R} = 0$ afterwards. Here, the antisymmetry of the \mathbf{R} matrix has to be respected in the differentiation which introduces the permutation operator $\hat{\tau}_{rk}$ interchanging the indices $r \leftrightarrow k$.² The orbital gradient reads

$$g_{rk} = \left. \frac{\partial E^{(2)}(\mathbf{R})}{\partial R_{rk}} \right|_{\mathbf{R}=0} = 2(1 - \hat{\tau}_{rk})A_{rk} = 2(A_{rk} - A_{kr}), \quad (3.21)$$

and the orbital Hessian matrix $h_{rk,sl}$ can be obtained as [21]

$$h_{rk,sl} = \left. \frac{\partial^2 E^{(2)}(\mathbf{R})}{\partial R_{rk} \partial R_{sl}} \right|_{\mathbf{R}=0} = (1 - \hat{\tau}_{rk})(1 - \hat{\tau}_{sl}) \left[2G_{rs}^{kl} - \delta_{kl}(A_{rs} + A_{sr}) \right]. \quad (3.22)$$

If the energy is optimal, the gradient vanishes:

$$A_{kl} - A_{lk} = 0 \quad \text{and} \quad A_{ak} = 0 \quad (3.23)$$

which constitutes the variational condition for the orbitals. It is a necessary condition for an optimized MCSCF wavefunction. In combination with equation (3.13), we can see that the vanishing gradient also reproduces the generalized Brillouin theorem discovered by Levy and Berthier [52, 53] in which the overlap of the commutator including the Hamiltonian and a

²Permutation operator: $\tau_{rk}A_{rk} = A_{kr}$

single excitation vanishes for the optimal MCSCF wavefunction $|\Psi\rangle$:

$$\langle\Psi|[\hat{H}, \hat{E}_{rk}]|\Psi\rangle = \langle\Psi|\hat{H}(\hat{E}_{rk} - \hat{E}_{kr})|\Psi\rangle = 0. \quad (3.24)$$

The variational condition of the CI coefficients can be obtained by minimizing the expectation value with the constraint that the CI vector stays normalized:

$$L(\mathbf{c}, \lambda) = \mathbf{c}^T \mathbf{H} \mathbf{c} - \lambda(\mathbf{c}^T \mathbf{c} - 1). \quad (3.25)$$

Differentiating with respect to c_I and projecting by \mathbf{c}^T yields the Lagrangian multiplier $\lambda = E(\mathbf{c})$, and the final variational condition of the CI problem reads

$$\sum_J H_{IJ} c_J - E c_I = 0. \quad (3.26)$$

The Hamiltonian matrix and the energy are given in equation (3.2) and (3.4), respectively, and the Schrödinger equation of the CI expansion is reproduced. Both variational conditions have to be satisfied simultaneously, which can become rather challenging for a numerical optimization as discussed in more detail in Chapter 4.

3.3 Restricted open-shell Hartree-Fock

The restricted open-shell Hartree-Fock (ROHF) method [228] is a special case of the MCSCF method, where the wavefunction consist only of a single determinant in which all active orbitals are singly occupied with the same one-electron spin function. This is also known as the high-spin case, and the number of electrons and active orbitals are equal to $2S$, as for example two electrons in two active orbitals and a triplet wavefunction. In case of a singlet, there are no active orbitals and the method is better known as the conventional HF method. In this single determinant case, the one- and two-electron RDMs can be evaluated analytically:

$$D_{tu} = \delta_{tu} \quad \text{and} \quad D_{tu,vw} = \delta_{tu} \delta_{vw} - \delta_{uv} \delta_{tw}. \quad (3.27)$$

Inserting the evaluated densities into the MCSCF energy (3.4) yields the ROHF energy:

$$E_{ROHF} = E_c + \sum_t^{\text{act}} F_{tt} - \frac{1}{2} \sum_{tu}^{\text{act}} J_{uu}^{tt} = \sum_i^{\text{cs}} [h_{ii} + f_{ii}^c] + \frac{1}{2} \sum_t^{\text{act}} [h_{tt} + f_{tt}^c + f_{tt}^o]. \quad (3.28)$$

The latter equation is based on the matrices f^c and f^o , which are more suitable for the ROHF method:

$$f_{rs}^c = F_{rs} \quad \text{and} \quad f_{rs}^o = -\frac{1}{2} \sum_t^{\text{act}} K_{rs}^{tt}. \quad (3.29)$$

The variational conditions (3.23) can be expressed with the matrices f^c and f^o as well:

$$A_{ai} = 2f_{ai}^c = 0, \quad A_{ti} - A_{it} = f_{ti}^c - f_{ti}^o = 0 \quad \text{and} \quad A_{at} = f_{at}^c + f_{at}^o = 0, \quad (3.30)$$

resulting in the ROHF Brillouin conditions. If the energy E_{ROHF} is minimized with the constraint that the orbitals stay orthonormal, one obtains after some rearrangements the following matrix equation [229]:

$$f_{rs} = \begin{pmatrix} f_{ij}^c & f_{iu}^c - f_{iu}^o & f_{ib}^c \\ f_{tj}^c - f_{tj}^o & f_{tu}^c + f_{tu}^o & f_{tb}^c + f_{tb}^o \\ f_{aj}^c & f_{au}^c + f_{au}^o & f_{ab}^c + f_{ab}^o \end{pmatrix} = \begin{pmatrix} \epsilon_i \delta_{ij} & 0 & 0 \\ 0 & \epsilon_t \delta_{tu} & 0 \\ 0 & 0 & \epsilon_a \delta_{ab} \end{pmatrix}. \quad (3.31)$$

Note that the Brillouin elements are located at the off-diagonal entries in the ROHF Fock matrix f_{rs} . If there are no active orbitals, f^o and all entries with active indices vanish, and the equation reduces to the Hartree-Fock-Roothaan equation [200].

The diagonalization of the ROHF Fock matrix f_{rs} yields a unitary transformation \mathbf{U} which is used to transform the orbitals. Afterwards, a new (not necessarily diagonal) ROHF Fock matrix is computed from the transformed orbitals. This defines a self-consistency cycle, which is repeated until convergence is reached and the Brillouin elements vanish. However, convergence acceleration with the direct inversion of the iterative subspace (DIIS) method [230,231] is vital to achieve a robust convergence.

In principle, it is possible to derive a similar set of equations for the general MCSCF case, as already indicated in equation (3.30). In the early days of MCSCF development, similar concepts have been tried for the MCSCF problem [28–32, 232–234] resulting in an often unsatisfactory convergence [38,39]. Therefore, other MCSCF optimization techniques have been developed soon, as for example the numerical optimization of the energy.

3.4 Excited states

The MCSCF theory can also be used to access electronically excited states. Today, the most common approach is state-averaging where all states share the same set of orbitals [35,48,61,91,235]. Here, the weighted energy average of the N_{av} states is minimized:

$$E = \sum_n^{N_{av}} W_n E_n \quad \text{and} \quad \sum_n W_n = 1, \quad (3.32)$$

with the weights W_n of the different states. Often, all weights are equal, but other choices, or even dynamically adjusted weighting [236], are possible as well. Each state n is described by the CI coefficients \mathbf{c}^n , which are determined by the CI eigenvalue problem:

$$\mathbf{H}\mathbf{c}^n = E_n \mathbf{c}^n. \quad (3.33)$$

This is possible, since the Hamiltonian is the same for all states. The state-specific energy E_n can be calculated with the state-specific RDMs:

$$D_{tu}^n = \sum_{IJ} c_I^n \gamma_{tu}^{IJ} c_J^n \quad \text{and} \quad D_{tu,vw}^n = \sum_{IJ} c_I^n \Gamma_{tu,vw}^{IJ} c_J^n \quad (3.34)$$

and the MCSCF energy equation (3.4). Furthermore, it is possible to move the weighted summation to the state-specific RDMs, and the averaged energy can be calculated from the state-averaged RDMs:

$$D_{tu}^{av} = \sum_n W_n D_{tu}^n \quad \text{and} \quad D_{tu,vw}^{av} = \sum_n W_n D_{tu,vw}^n. \quad (3.35)$$

However, a definition of a state-averaged wavefunction is not possible, and the averaged energy (3.32) cannot be expressed as an expectation value. Instead, the total energy is the weighted sum of the expectation values of the different states. Minimizing this energy functional for fixed CI coefficients yields the same gradient and Hessian expressions as in the single-state case with the RDMs being replaced by the state-averaged ones (3.35). The state-averaged optimization has the great advantage that it is not prone to root-flipping [61,91], since the optimization does not depend on the ordering of the states. All of the discussed MCSCF methods in this thesis use the state-averaged approach to calculate excited states.

Another possibility is the state-specific optimization using the NR method. This can be

achieved by a saddle-point optimization with the full Hessian including the CI coefficients and the orbitals. The level-shifting in the Hessian can be adjusted such that convergence to specific states is possible [71, 87–89, 136]. However, it is difficult to ensure the convergence into the correct state because of root-flipping problems. Here, the ordering of the states can change during the optimization, since the targeted state can become lower in energy because of a more accurate representation of the wavefunction [91].

3.5 Coupled-perturbed MCSCF

The CP-MCSCF is required to calculate state-specific first-order derivatives or non-adiabatic coupling elements in a state-averaged calculation. Here, an additional linear equation similar to the coupled NR equation has to be solved. This is necessary, since the state-averaged wavefunction is not variationally optimized for specific states. We begin this section with a more general derivation of the first-order derivatives with respect to a small perturbation q . In case of analytic energy gradients, the perturbation is an infinitesimal displacement of a nuclear coordinate, for example $q = \Delta x$. We are interested in the calculation of the first-order derivative of a functional $f(q, \mathbf{c}(q))$ depending on the perturbation q and the wavefunction solution \mathbf{c} at $q = 0$. In the following discussion, all independent parameters of the wavefunction are summarized in the variable \mathbf{c} . In case of the MCSCF wavefunction, \mathbf{c} includes all CI coefficients and (non-redundant) orbital rotation parameters. If nuclear gradients are computed, the functional is simply the energy, but this formalism can be also used to compute energy-difference gradients or the non-adiabatic coupling elements $\langle \Psi_m | \nabla_K | \Psi_n \rangle$. The first derivative of f with respect to the perturbation q can be formally written as

$$\left. \frac{df}{dq} \right|_{q=0} = \left. \frac{\partial f}{\partial q} \right|_{q=0} + \sum_j \left. \frac{\partial f}{\partial c_j} \frac{dc_j}{dq} \right|_{q=0}. \quad (3.36)$$

In the following, the notation of the $q = 0$ evaluation is omitted, since the derivatives are always evaluated at $q = 0$ in this discussion. However, this approach is not very promising, since the derivatives dc_j/dq are not easy to access, and the dependency of the CI and MO coefficients on the perturbation has to be considered explicitly.

Fortunately, the evaluation of these derivatives can be completely avoided [237] by introducing a Lagrangian functional L including the functional f and the variational conditions of

the wavefunction $\mathbf{g}(q, \mathbf{c}(q)) = 0$ [238]:

$$L(q, \mathbf{c}(q), \mathbf{z}(q)) = f(q, \mathbf{c}(q)) + \mathbf{z}(q)^\top \mathbf{g}(q, \mathbf{c}(q)). \quad (3.37)$$

In case of the MCSCF wavefunction, the function \mathbf{g} captures the variational conditions introduced in Section 3.2. The parameters $\mathbf{z}(q)$ are the Lagrangian multipliers, which have to be determined to make the Lagrangian stationary with respect to the coefficients c_j :

$$\frac{\partial L}{\partial c_j} = \frac{\partial f}{\partial c_j} + \sum_i z_i \frac{\partial g_i}{\partial c_j} = 0. \quad (3.38)$$

This linear system of equation is also known as the Z-vector equation, and the solutions are the Lagrangian multipliers z_i . Per construction, the Lagrangian reproduces the functional f at $(q, \mathbf{c}(q))$ because of the vanishing stationary conditions $\mathbf{g}(q, \mathbf{c}(q))$, and therefore, the derivative of f can be obtained from the total differential of the Lagrangian function:

$$\frac{df}{dq} = \frac{dL}{dq} = \frac{\partial L}{\partial q} + \sum_j \frac{\partial L}{\partial c_j} \frac{dc_j}{dq} + \sum_i \frac{\partial L}{\partial z_i} \frac{dz_i}{dq}. \quad (3.39)$$

If the Z-vector equation is solved, the derivatives $\partial L/\partial c_j$ are zero. Also, the derivatives of the Lagrangian multipliers $\partial L/\partial z_i$ are zero by construction, and the final derivative can be obtained from

$$\frac{df}{dq} = \frac{\partial L}{\partial q} = \frac{\partial f}{\partial q} + \sum_i z_i \frac{\partial g_i}{\partial q}. \quad (3.40)$$

The partial derivatives $\partial f/\partial q$ and $\partial g_i/\partial q$ can be evaluated with integral derivatives, for instance $\partial h_{\mu\nu}/\partial q$ and $\partial(\rho\sigma|\mu\nu)/\partial q$. These derivatives have to be computed separately, and in Molpro this is done for the MCSCF case with the Cambridge analytic derivation package (CADPAC) [239] or Alaska [240].

Next, we derive the explicit form of the Z-vector equation of the MCSCF problem. The explicit form of the Lagrangian reads [241]:

$$L(q, \mathbf{c}^n, \mathbf{U}(\mathbf{R}), \mathbf{z}^n, \mathbf{Z}, x_n) = f(q, \mathbf{c}^n, \mathbf{U}(\mathbf{R})) + \sum_{r>k} Z_{rk}(A_{rk} - A_{kr}) \\ + \sum_n W_n \left[(\mathbf{z}^n)^\top (\mathbf{H} - E_n) \mathbf{c}^n - \frac{1}{2} x_n ((\mathbf{c}^n)^\top \mathbf{c}^n - 1) \right]. \quad (3.41)$$

The stationary condition $\mathbf{g}(q, \mathbf{c}(q))$ is given by the MCSCF variational conditions (3.23) and

(3.26), and the associated Lagrangian multipliers are Z_{rk} and z_I^n , respectively. Here, we use the MO parameterization with the orbital rotation parameters R_{rk} . Additionally, the normalization of the CI coefficients has to be added separately (parameter x_n), since this is not captured in the CI variational condition. Differentiating the Lagrangian L with respect to the orbital rotation parameters R_{rk} yields the first Z-vector equation:

$$\frac{\partial L}{\partial R_{rk}} = \underbrace{\frac{\partial f}{\partial R_{rk}}}_{=b_{rk}} + \sum_{s>l} h_{rk,sl} Z_{sl} + \sum_{In} h_{rk,In} z_{In} = 0. \quad (3.42)$$

The first terms is the orbital right-hand side (RHS) b_{rk} . The differentiation of the orbital variational condition reproduces the orbital Hessian matrix $h_{ri,sj}$ given in equation (3.22), and $h_{rk,In}$ results from differentiating the CI variational condition with respect to the orbital rotation parameters:

$$h_{In,rk} = h_{rk,In} = 2W_n \left[A_{rk}^{In} - A_{kr}^{In} - c_I^n (A_{rk}^n - A_{kr}^n) \right]. \quad (3.43)$$

This mixed derivative block in the Hessian captures the coupling between the CI coefficients and the orbitals, and the matrices A_{rk}^{In} and A_{rk}^n are defined as

$$A_{rk}^{In} = \sum_l^{\text{occ}} h_{rl} D_{lk}^{In} + \sum_{ijl}^{\text{occ}} J_{rl}^{ij} D_{kl,ij}^{In} \quad \text{and} \quad A_{rk}^n = \sum_l^{\text{occ}} h_{rl} D_{lk}^n + \sum_{ijl}^{\text{occ}} J_{rl}^{ij} D_{kl,ij}^n. \quad (3.44)$$

For simplicity, the matrices are shown here with the full density matrix, and the indices i, j, k, l represent the occupied orbitals. The matrices A_{rk}^{In} and A_{rk}^n are constructed from the transition densities matrices

$$D_{kl}^{In} = \sum_J \gamma_{kl}^{IJ} c_J^n \quad \text{and} \quad D_{kl,ij}^n = \sum_{IJ} \Gamma_{kl,ij}^{IJ} c_J^n \quad (3.45)$$

and the state-specific RDMs D_{kl}^n and $D_{kl,ij}^n$ defined in equation (3.34), respectively. If the transition density matrices are evaluated for the closed-shell orbitals, the definition of A_{rk}^{In} and A_{rk}^n is equivalent to equation (3.15) where the RDMs are replaced by the transition density matrices of the active orbitals. More details about an efficient construction of the different A matrices are presented in Section 5.2.

The second Z-vector equation is obtained by the differentiation of the Lagrangian L with

respect to the CI coefficients c_I^n of state n :

$$\frac{\partial L}{\partial c_I^n} = \underbrace{\frac{\partial f}{\partial c_I^n}}_{=b_I^n} + \sum_{Jn} h_{In,Jn} z_J^n + 2W_n \sum_{r>k} (A_{rk}^{In} - A_{kr}^{In}) Z_{rk} - W_n x_n c_I^n = 0, \quad (3.46)$$

which results in the RHS b_I^n and the CI Hessian:

$$h_{In,Jm} = \delta_{nm} W_n [H_{IJ} - \delta_{IJ} E_n]. \quad (3.47)$$

Projecting equation (3.46) by $(c^n)^\top$ from the left-hand side yields an explicit formula for the Lagrangian multiplier

$$x_n = 2 \sum_{r>k} [A_{rk}^n - A_{kr}^n] Z_{rk} + \frac{(c^n)^\top \mathbf{b}^n}{W_n}, \quad (3.48)$$

and therefore the final Z-vector equation of the CI RHS is:

$$\sum_{Jn} h_{In,Jn} z_J^n + \sum_{i>r} h_{In,ri} Z_{ri} = -b^n - ((c^n)^\top \mathbf{b}^n) c_I^n. \quad (3.49)$$

In case of single-state MCSCF, the right-hand sides b_I^n and b_{rk} vanish for the energy gradient, since the MCSCF energy is already optimized variationally. In this case, the solution of the Z-vector equation is zero, and the first-order derivatives can be directly obtained from $\partial f / \partial q$. However, this is not true for the state-averaged optimization, since the MOs are optimized for the state-averaged energy and not for specific states. If state-specific gradients ($f = E_n$) or state difference gradients ($f = E_m - E_n$) are computed, the Z-vector equation has to be solved with the following RHS:

$$\text{State-specific gradients:} \quad b_{rk} = [A_{rk}^n - A_{kr}^n] \quad \text{and} \quad b_I^n = 0, \quad (3.50)$$

$$\text{State-difference gradients:} \quad b_{rk} = [A_{rk}^m - A_{kr}^m] - [A_{rk}^n - A_{kr}^n] \quad \text{and} \quad b_I^n = 0. \quad (3.51)$$

Following the work of Lengsfeld et al. [123, 125, 130], the first-order non-adiabatic coupling term can be rewritten as

$$\frac{\partial f}{\partial q} = \left\langle \Psi^m \left| \frac{\partial}{\partial q} \right| \Psi^n \right\rangle = D_{rs}^{mn} \left\langle \phi_r \left| \frac{\partial}{\partial q} \right| \phi_s \right\rangle - (E^m - E^n)^{-1} (\mathbf{c}^m)^\top \frac{\partial \mathbf{H}}{\partial q} \mathbf{c}^n \quad (3.52)$$

with a non-symmetrized transition density $D_{rs}^{mn} = \sum_I c_I^m D_{rs}^{In}$. From here, one obtains the

following RHS:

$$b_{rk} = (D_{rk}^{mn} - D_{kr}^{mn}) - (E^m - E^n)^{-1} [A_{rk}^{mn} - A_{kr}^{mn}] \quad \text{and} \quad b_I^n = 0. \quad (3.53)$$

The matrix A_{rk}^{mn} is constructed as shown in equation (3.44) from the one- and two-electron transition density matrices D_{ij}^{mn} and $D_{kl,ij}^{mn}$. The term $(\mathbf{c}^n)^\top \mathbf{b}^n$ in equation (3.49) is zero for all shown properties, and is therefore neglected in the following.

The Z-vector equation can be summarized into a single linear equation:

$$\begin{pmatrix} \mathbf{h}_{cc} & \mathbf{h}_{co} \\ \mathbf{h}_{co} & \mathbf{h}_{oo} \end{pmatrix} \begin{pmatrix} \mathbf{z}_c \\ \mathbf{z}_o \end{pmatrix} = - \begin{pmatrix} \mathbf{b}_c \\ \mathbf{b}_o \end{pmatrix}. \quad (3.54)$$

The size of the Hessian matrix can become massive, and this system of linear equations has to be solved iteratively. This is typically done with a preconditioned conjugate gradient method [132,242,243]. In order to improve the convergence of the linear equation solver, we developed an iterative subspace method including an a priori chosen primary space, which is presented in more detail in Chapter 4.

3.6 Multi-reference perturbation theory

The MCSCF description misses the contributions of the dynamic correlation, i.e. the missing configurations with respect to full-CI. This limits the accuracy of the MCSCF method, and the method is primarily used to obtain a first-principles approximation of the wavefunction. Missing parts of the dynamical correlation are added in subsequent post-MCSCF methods by excitations of electrons into non-occupied orbitals. An important and commonly used post-MCSCF method is the multireference perturbation theory (MRPT) [94–102, 244]. It is derived from Rayleigh-Schrödinger perturbation theory [200], where the Hamilton operator is partitioned into a zeroth-order term $H^{(0)}$ and the first-order perturbation $\lambda H^{(1)}$:

$$\hat{H}(\lambda) = \hat{H}^{(0)} + \lambda \hat{H}^{(1)}. \quad (3.55)$$

The general Rayleigh-Schrödinger perturbation theory can be analogously derived by including higher-order terms in the Hamiltonian expansion. The parameter λ can have a physical meaning, but here it is used to simplify the derivation, and it will be later set to $\lambda = 1$. The

wavefunction and the energy are expanded in a power series in the perturbation parameter λ :

$$|\Psi(\lambda)\rangle = \sum_n \lambda^n |\Psi^{(n)}\rangle \quad \text{and} \quad E(\lambda) = \sum_n \lambda^n E^{(n)}. \quad (3.56)$$

In the next step, the equations (3.55) and (3.56) are inserted into the Schrödinger equation, and the result is sorted with respect to the power of λ :

$$\lambda^0 \rightarrow [\hat{H}^{(0)} - E^{(0)}] |\Psi^{(0)}\rangle = 0, \quad (3.57)$$

$$\lambda^1 \rightarrow [\hat{H}^{(0)} - E^{(0)}] |\Psi^{(1)}\rangle + [\hat{H}^{(1)} - E^{(1)}] |\Psi^{(0)}\rangle = 0, \quad (3.58)$$

$$\lambda^2 \rightarrow [\hat{H}^{(0)} - E^{(0)}] |\Psi^{(2)}\rangle + [\hat{H}^{(1)} - E^{(1)}] |\Psi^{(1)}\rangle - E^{(2)} |\Psi^{(0)}\rangle = 0. \quad (3.59)$$

This yields a hierarchy of equations which can be solved successively. We further assume the intermediate normalization $\langle \Psi^{(0)} | \Psi^{(0)} \rangle = 1$ and $\langle \Psi^{(n)} | \Psi^{(0)} \rangle = 0$, and the perturbation energies $E^{(n)}$ are obtained by projecting equations (3.57) and (3.58) from the left by $\langle \Psi^{(0)} |$:

$$E^{(0)} + E^{(1)} = \langle \Psi^{(0)} | \hat{H}^{(0)} | \Psi^{(0)} \rangle + \langle \Psi^{(0)} | \hat{H}^{(1)} | \Psi^{(0)} \rangle, \quad (3.60)$$

$$E^{(2)} = \langle \Psi^{(0)} | \hat{H}^{(1)} | \Psi^{(1)} \rangle. \quad (3.61)$$

The equation for energy $E^{(2)}$ can be rearranged, and by adding equation (3.58) one obtains the Hylleraas functional:

$$E^{(2)} = \langle \Psi^{(1)} | \hat{H}^{(0)} - E^{(0)} | \Psi^{(1)} \rangle + 2 \langle \Psi^{(1)} | \hat{H}^{(1)} | \Psi^{(0)} \rangle. \quad (3.62)$$

In the next step, we set $H^{(1)} = H - H^{(0)}$ and $\lambda = 1$. Therefore, the first-order Hamiltonian $H^{(1)}$ describes the correction from the zeroth-order Hamiltonian. The energies $E^{(0)} + E^{(1)}$ reproduce the eigenvalue of the zeroth-order wavefunction as can be seen in equation (3.60). The approach is usually used to add dynamical correlation to the system by calculating the contribution from the Hylleraas functional (3.62). In the single-reference case, this is known as the Møller-Plesset (MP) perturbation theory [10], where $\hat{H}^{(0)}$ is the Fock operator

$$\hat{F} = \sum_{rs} F_{rs} \hat{E}_{rs}, \quad (3.63)$$

and $|\Psi^{(0)}\rangle$ is given by the HF determinant. The first-order wavefunction is built from all possible double excitations from the HF determinant.³ The higher-order energies $E^{(n)}$ yield

³Single excitations do not contribute because of the Brillouin theorem. Triple excitations vanish because of the Slater-Condon rules.

energy corrections to the Hartree-Fock energy adding some parts of the missing dynamical correlation. The associated post-HF methods are known as MP_n . Today, only the MP2 method is regularly used, since cheaper and more accurate post-HF methods are available for $n > 2$ [200].

In the multireference case, the choice of the zeroth-order Hamiltonian is not unique and several options exist [95–97, 100, 101, 245–247]. A commonly used Hamiltonian [101, 103, 245] is

$$\hat{H}^{(0)} = \hat{P}\hat{F}\hat{P} + \hat{Q}\hat{F}\hat{Q} \quad \text{with} \quad \hat{P} = |\Psi\rangle\langle\Psi| \quad \text{and} \quad \hat{Q} = \hat{1} - |\Psi\rangle\langle\Psi|. \quad (3.64)$$

Here, \hat{F} is the Fock operator (3.63) built from the general Fock matrix (3.16). The zeroth-order wavefunction is the MCSCF wavefunction $|\Psi^{(0)}\rangle = |\Psi\rangle$, and the projection operators \hat{P} and \hat{Q} ensure that the MCSCF wavefunction is an eigenfunction of operator $\hat{H}^{(0)}$:

$$\hat{H}^{(0)}|\Psi\rangle = |\Psi\rangle\langle\Psi|\hat{F}|\Psi\rangle\langle\Psi|\Psi\rangle = E^{(0)}|\Psi\rangle. \quad (3.65)$$

This is necessary to fulfill equation (3.57) of the perturbation theory, and the zeroth-order energy $E^{(0)}$ is given by

$$E^{(0)} = \langle\Psi|\hat{F}|\Psi\rangle = 2 \sum_i^{\text{cs}} F_{ii} + \sum_{tu}^{\text{act}} D_{tu} F_{tu}. \quad (3.66)$$

A similar Hamiltonian has been proposed by Wolinski and Pulay [94, 95] but with additional projection operators into the first-order wavefunction contributions. This Hamiltonian has later been used by Andersson and Roos [96] in their CAS perturbation theory (CASPT2) method. Another choice for the zeroth-order Hamiltonian is the Dyll Hamiltonian [247]:

$$\hat{H}^{(0)} = \hat{H}_D = \sum_{ij}^{\text{cs}} F_{ij}^c \hat{E}_{ij} + \sum_{ab}^{\text{vrt}} F_{ab} \hat{E}_{ab} + \sum_{tu}^{\text{act}} F_{tu}^c \hat{E}_{tu} + \frac{1}{2} \sum_{tuvw}^{\text{act}} (tu|vw) \hat{E}_{tu,vw} \quad (3.67)$$

in which no additional projections are required to feature the MCSCF wavefunction as an eigenfunction. The Dyll Hamiltonian has been used by Angeli et al. to derive the n-electron valence state perturbation theory (NEVPT2) method [100, 244, 248].

The first-order wavefunction includes single and double excitations from the occupied space into empty active or virtual orbitals. In case of a non-CASSCF, the missing configurations from the equivalent CAS wavefunction are added as well [101]. Often, the excitations

are classified into three different types [96]: (i) internal excitations where only excitation into active orbitals are considered (e.g. $\hat{E}_{ti}\hat{E}_{uj}$), (ii) semiinternal excitations with mixed excitations into active and virtual space (e.g. $\hat{E}_{ti}\hat{E}_{aj}$), and (iii) external excitations with excitations only into the virtual orbitals (e.g. $\hat{E}_{ai}\hat{E}_{bj}$). For simplicity, the first-order wavefunction is written as

$$|\Psi^{(1)}\rangle = \sum_I T_I |\tilde{\Phi}_I\rangle, \quad (3.68)$$

where $|\tilde{\Phi}_I\rangle$ represent the excited configurations also known as the first-order interaction space. In case of an internal contraction, which means that $|\tilde{\Phi}_I\rangle$ is constructed by applying the excitation to the whole MCSCF wavefunction, the first-order interaction space is not orthonormal. This is solved by an additional orthonormalization in the beginning, where nearly redundant contributions are removed as well [97]. The coefficients T_I are obtained by minimizing the Hylleraas functional (3.62) yielding the following linear equation:

$$\sum_J \langle \tilde{\Phi}_I | \hat{H}^{(0)} - E^{(0)} | \tilde{\Phi}_J \rangle T_J = - \langle \tilde{\Phi}_I | \hat{H} | \Psi \rangle. \quad (3.69)$$

How this equation is solved depends on the choice of the zeroth-order Hamiltonian. A block-diagonal structure can be achieved in the Dyll Hamiltonian [100] or by additional projection operators [96, 200], and the coupling between the single and double excitations is zero. Another possibility is to use contravariant configurations replacing $\langle \tilde{\Phi}_I |$ in the linear equation to simplify the equations [188]. The final MRPT energy correction is obtained from the Hylleraas functional after solving equation (3.69).

Calculation with MRPT can suffer from the intruder states problem. This is typically observed in excited-states calculations, but also ground-state calculations can be affected [249]. A famous example is the dissociation of chromium dimer investigated by Andersson et al. [250–252], where jumps on the potential energy surface occur. The reason for these problems can be found in the matrix $\langle \tilde{\Phi}_I | \hat{H}^{(0)} - E^{(0)} | \tilde{\Phi}_J \rangle$ which can become singular or even negative definite, since possible solutions of first-order wave-function may yield a slightly lower energy than the zeroth-order energy $E^{(0)}$. These states are the intruder states, and the singular matrix can strongly affect the final MRPT energy. A solution was found by Roos and Andersson [251] by introducing a level-shift into the zeroth-order Hamiltonian, which is equivalent to level-shifting the matrix in equation (3.69):

$$\sum_J \langle \tilde{\Phi}_I | \hat{H}^{(0)} - E^{(0)} + \epsilon | \tilde{\Phi}_J \rangle T_J = - \langle \tilde{\Phi}_I | \hat{H} | \Psi \rangle \quad \text{with } \epsilon > 0. \quad (3.70)$$

Negative or zero eigenvalues are removed by the shift ϵ , and typical values of the level-shift are $\epsilon = 0.1 - 0.3$ Hartree. The effect of the level-shift on the second-order energy is removed afterwards:

$$E^{(2)} = E^{(2)}(\epsilon) - \langle \Psi^{(1)} | \Psi^{(1)} \rangle \epsilon, \quad (3.71)$$

and the difference in the final energy is negligible in comparison with the intrinsic error of MRPT [251]. Nevertheless, the level-shift correction can fix convergence problems and smooth the energy in potential energy surfaces as shown in Reference [251] for the chromium dimer.

The simultaneous optimization of multiple states is possible with the multi-state CASPT2 method [253] which includes the coupling between different states and allows a more accurate treatment of avoided crossings. Furthermore, the accuracy of the MRPT can be improved by a third-order MRPT [102, 244] or by the integration of explicit correlation [216, 219, 254, 255]. Recent developments are the local MRPT methods in which a linear scaling can be achieved through local approximations, which allows an application to much larger molecules. Examples for the local methods are the pair natural orbitals (PNO)-NEVPT2 of Guo et al. [187] and the PNO-CASPT2 method of Menezes, Katz and Werner [188, 189, 256]. The MRPT can be also used to derive the Super-CI method of Roos et al [64, 65], which is discussed in detail in Chapter 7.

4 | The numerical optimization of the MCSCF energy

The numerical optimization of the CI coefficients and the orbital rotation parameters \mathbf{R} is based on the variational principle [257]:

$$E_{exact} \leq \frac{\langle \Psi(c, R) | \hat{H} | \Psi(c, R) \rangle}{\langle \Psi(c, R) | \Psi(c, R) \rangle} = E(\mathbf{c}, \mathbf{R}). \quad (4.1)$$

The numeric minimization of $E(\mathbf{c}, \mathbf{R})$ yields the best possible approximation of the exact energy with respect to the restrictions of the MCSCF wavefunction. The variational conditions correspond to the gradient of the energy, and therefore they are fulfilled at a minimum. However, the numerical optimization cannot guarantee to find the optimal solution, since only local information can be taken into account. Convergence to a local minimum is not uncommon, and a good starting guess close to the optimal solution is necessary. On the other hand, the global minimum is in some cases not the most desired solution. Often, it is more important to find a solution with a specific set of active orbitals that is used in a subsequent calculation of the dynamic correlation.

The variety of MCSCF methods divides into two categories: first-order and second-order methods. The difference between these two categories is best shown in a semi-logarithmic graph of the energy convergence in Figure 4.1. Second-order methods show a quadratic decay of the energy and the gradient near the final solution, which is achieved by determining the minimum of a quadratic expansion at the current position. That is usually accomplished with a NR optimization [258,259], where the update \mathbf{x} is calculated from the current Hessian \mathbf{h} and the gradient \mathbf{g} :

$$\mathbf{h}\mathbf{x} = -\mathbf{g}. \quad (4.2)$$

The NR optimization includes the orbital-CI coupling in the mixed derivatives in the Hessian, and in the following, this optimization is also called coupled optimization.

As soon as the quadratic model is approximated in some way, only a linear decay of the energy can be achieved in the semi-logarithmic graph. This defines the group of the first-order

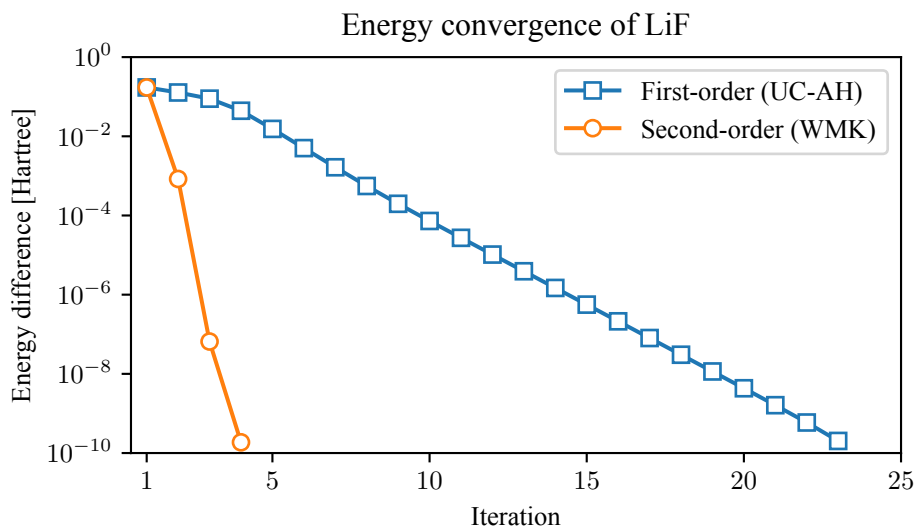


Figure 4.1: First- and second-order energy convergence for stretched LiF illustrated by the energy difference to the converged solution. The calculation is the ground-state optimization of LiF ($r_{\text{Li-F}} = 3\text{\AA}$), with a full valance active space, the cc-pVTZ basis [15], and the atomic density starting guess.

methods. Typically, the optimization of the CI coefficients and the orbitals is separated in first-order methods and performed in alternating steps. The updated RDMs and orbitals are used in the next step, respectively. This is also called the two-step method or the uncoupled optimization. An advantage of the uncoupled optimization is that the CI problem can be solved as an eigenvalue problem to which robust methods exist. On the other hand, the linear decay in the uncoupled optimization can become extremely flat for strongly coupled problems resulting in a large number of iterations. The optimization level of the orbitals is not to be confused with the optimization of the MCSCF energy, as unfortunately sometimes done in the literature. For example, a second-order NR optimization of the orbitals used in the two-step method will yield a first-order convergence of the MCSCF energy. Furthermore, if the orbital Hessian is approximated, a coupled optimization does not make sense, since only a first-order convergence is achieved anyway.

This chapter introduces the numerical framework that is utilized in all presented MCSCF methods. A stable NR optimization can be achieved with the augmented Hessian (AH) method presented in Section 4.1. Large eigenvalue problems, as they may occur in the CI problem, are best solved with the P-space Davidson method presented afterwards. In Section 4.3, the AH method and the CI optimization are combined in a simple first-order MCSCF method. Finally,

another application of the P-space method is presented for the coupled-perturbed MCSCF (CP-MCSCF) which is required to compute state-specific first-order derivatives in state-averaged calculations.

4.1 The augmented Hessian method

The NR optimization guarantees a second-order convergence, but only for convex functions where the Hessian is positive definite. However, the MCSCF energy is by no means a convex function, and often the starting guess is far from the convex region around a minimum. This can cause severe convergence problems, as for example the convergence to maxima or saddle points. A solution for this problem is to level-shift the Hessian matrix, such that \mathbf{h} becomes positive definite:

$$(\mathbf{h} - \mathbf{1}\epsilon)\mathbf{x} = -\mathbf{g} \quad \text{with} \quad \epsilon < 0. \quad (4.3)$$

This equation can be derived by restricting the optimization within a trust radius, and it can be shown that the quadratic approximation $E^{(2)}$ of the energy E is lowered, if the Hessian is shifted to be positive definite [258]. The trust radius describes the area where the quadratic approximation $E^{(2)}$ is an adequate description of the energy such that a decay of the real energy can be expected. It is possible to guarantee the convergence by rejecting steps and adjusting the trust radius if the updated energy increases [258].

The level-shift can be automatically computed with the AH method [260] in which the level-shift is set to the first-order update:

$$\epsilon = \mathbf{g}^T \mathbf{x}. \quad (4.4)$$

This allows to transform the shifted NR equation (4.3) into an eigenvalue problem of the AH matrix:

$$\begin{pmatrix} 0 & \mathbf{g}^T \\ \mathbf{g} & \mathbf{h} \end{pmatrix} \begin{pmatrix} 1 \\ \mathbf{x} \end{pmatrix} = \epsilon \begin{pmatrix} 1 \\ \mathbf{x} \end{pmatrix}, \quad (4.5)$$

where the eigenvalue ϵ is the level-shift of the Hessian. An additional control of the step-length is needed though, since the step \mathbf{x} might be too large to be within the trust radius. This can be achieved by introducing a damping factor λ and setting the level-shift to $\epsilon = \lambda^2 \mathbf{g}^T \mathbf{x}$ [21]:

$$\begin{pmatrix} 0 & \mathbf{g}^T \\ \mathbf{g} & \mathbf{h}/\lambda \end{pmatrix} \begin{pmatrix} 1/\lambda \\ \mathbf{x} \end{pmatrix} = \epsilon \begin{pmatrix} 1/\lambda \\ \mathbf{x} \end{pmatrix}. \quad (4.6)$$

The damping factor λ is determined such that the step-length $|\mathbf{x}|$ is within the trust radius. However, the step-length can be very sensitive to changes of the damping factor, and a severe over-damping can occur. In order to avoid this, we used a bisection method to determine the damping parameter λ , which is only switched on when the step-length exceeds the trust-radius. The bisection methods then tries to find a step-length which is lower but still close enough to the trust-radius. If the energy increases after the update, the trust-radius is halved.

Furthermore, we found that the AH method can become numerically chaotic, if the lowest eigenvalues of the AH matrix are degenerate [1]. The problem is that the update vector \mathbf{x} is not uniquely defined for degenerate eigenvalues, since it can be arbitrarily rotated within the degenerate subspace. A solution to this problem is to rotate the degenerate vectors with two by two rotations such that the first entry of one eigenvector is maximized. The rotation angle γ of the two vectors is given by

$$\tan(\gamma_1) = \frac{v_1}{v_2} \quad \text{and} \quad \tan(\gamma_2) = \frac{v_2}{v_1}, \quad (4.7)$$

where v_1 and v_2 are the first entries of the two degenerate vectors. A rotation with either γ_1 or γ_2 maximizes the first entry. The solution with the larger first entry is kept and rotated with the next degenerate vector. This is repeated until no more rotations are observed and a unique solution is defined. Throughout this work, the AH method is used for all optimizations even if the Hessian matrix is approximated. Also, it is not necessary to solve the eigenvalue equation exactly. In a first-order MCSCF optimization it is accurate enough to let the solver improve the error of the solution until it is lower than the current gradient multiplied by 0.1.

4.2 The P-space Davidson method

The large eigenvalue problems in the MCSCF optimization are best solved with a direct method in which only the action of the matrix on a vector is required. In our MCSCF implementation, all eigenvalue problems are numerically solved with the Davidson method [261, 262] in which the problem is projected into a subspace which is then iteratively enlarged by the preconditioned residual. The Davidson method is explained here first for the CI optimization. A strong improvement in the CI optimization has been achieved by the introduction of an a priori chosen primary space (P-space) [92]. Here, dominant CI configurations are pre-selected, and the Hamiltonian is explicitly constructed within the P-space. This accelerates convergence considerably and solves root-flipping problems, since a good starting guess is

obtained from the diagonalization of the P-space matrix.

The P-space contains a set of indices $\{I\}$ chosen a priori by some criteria. In the following, we consider a mapping $I(P)$ which maps the P-space index P to the configuration I in the full space. Hence, the P-space is spanned by the unit vectors of the configurations $I(P)$.¹ The complementary space is approximated by a secondary Q-space which is spanned by the dense expansion vectors $B_{Q\alpha}$. The Q-space is iteratively constructed along the iterations. In the CI case, the diagonal dominance of the Hamiltonian is used to select the P-space CFs with the diagonal criterion: $H_{II} - H_{\min} \leq \epsilon_p$. Here, H_{\min} is the lowest entry in the diagonal, and ϵ_p is the P-space threshold (usually $\epsilon_p = 0.5$). If a large number of states are included in the optimization, a larger P-space threshold can be necessary to capture at least as many P-space CFs as states, i.e. $N_P \geq N_{av}$. If a guess of the CI vector is available from a previous calculation, the CFs with the largest entries, which are not already captured by the diagonal criterion, are also added into the P-space. Furthermore, existing CI vectors are orthogonalized to the P-space and afterwards added into the Q-space. Otherwise, the Q-space is empty in the beginning, i.e. $N_Q = 0$.

The reduced matrix $\bar{\mathbf{H}}$ is built in the $N_c = N_P + N_Q$ dimensional reduced space:

$$\bar{\mathbf{H}} = \begin{pmatrix} \bar{H}_{PP'} & \bar{H}_{P\alpha'} \\ \bar{H}_{\alpha P'} & \bar{H}_{\alpha\alpha'} \end{pmatrix} \quad \text{with} \quad \begin{aligned} \bar{H}_{PP'} &= H_{I(P)I(P')}, & \bar{H}_{P\alpha} &= \bar{H}_{\alpha P} = [\mathbf{HB}]_{I(P)\alpha}, \\ \text{and } \bar{H}_{\alpha\alpha'} &= [\mathbf{B}^T \mathbf{HB}]_{\alpha\alpha'}. \end{aligned} \quad (4.8)$$

Here, α labels the N_Q Q-space vectors, and $I(P)$ is the P-space index mapping. The P-space block $\bar{H}_{PP'}$ is a sub-block of the exact Hamiltonian matrix. It is important that its computation is very efficient, since otherwise, the improved convergence may not compensate the extra computation time. In case of determinants, all CFs with the same spatial orbital occupation have to be added into the P-space, and an additional projection into the spin-adapted space is necessary [93] to avoid spin contamination. The Q-space part is calculated from the Hamiltonian action on the Q-space vectors $[\mathbf{HB}]_{Q\alpha}$, which is calculated only once per Q-space vector and is stored afterwards. Typically, this Hamiltonian action is the dominating step in the CI optimization.

The reduced problem is solved by diagonalizing $\bar{\mathbf{H}}$:

$$[\bar{\mathbf{C}}^T \bar{\mathbf{H}} \bar{\mathbf{C}}]_{nm} = [\mathbf{C}^T \mathbf{H} \mathbf{C}]_{nm} = E_n \delta_{nm}. \quad (4.9)$$

¹In general, it is also possible to consider sparse vectors instead of unit vectors. But this is not explicitly used in this work.

Here, $c_I^n = C_{I_n}$ are the N_c approximated eigenvectors which are back transformed from the reduced solution \bar{C} into the full space:

$$c_{I(P)}^n = \bar{C}_{Pn} \quad \text{and} \quad c_Q^n = B_{Q\alpha} \bar{C}_{\alpha n}. \quad (4.10)$$

The current residual $\mathbf{r}^n = \mathbf{H}\mathbf{c} - E_n \mathbf{c}$ of the eigenvector c_I^n is calculated by

$$r_{I(P)}^n = 0 \quad \text{and} \quad r_Q^n = \sum_{\alpha=1}^{N_Q} [\mathbf{H}\mathbf{B}]_{Q\alpha} \bar{C}_{\alpha n} + \sum_P^{N_P} H_{QP} c_P^n - E_n c_Q^n, \quad (4.11)$$

and no additional Hamiltonian action $\mathbf{H}\mathbf{c}$ with the full vector is required. The P-space residual is zero by construction, but the Hamiltonian action on the P-space solution vector c_P^n has to be computed separately. However, c_P^n is very sparse with values only at the P-space configurations such that this Hamiltonian action is negligible.

A new Q-space vector is obtained for each state from the preconditioned residual and Gram-Schmidt orthonormalization on the excising Q-space.

$$\Delta c_Q^n = -\frac{r_Q^n}{H_{QQ} - E_n} \quad \text{and} \quad B_{Q\alpha} = \text{ortho}_{\mathbf{B}}(\Delta c^n) \quad \text{with} \quad \alpha = N_Q + 1. \quad (4.12)$$

In case of determinants, the denominator has to be averaged for the configurations with the same orbital occupation, since otherwise spin contamination occurs [198].

We utilize the P-space not only in the CI optimization but also in the diagonalization of the AH matrix [1]. The derivation for the AH matrix is exactly the same, but the structure is kept by projecting the gradient \mathbf{g} and the Hessian \mathbf{h} separately into the P- and Q-space:

$$\begin{pmatrix} 0 & \bar{g}_{P'}^T & \bar{g}_{\alpha}^T \\ \bar{g}_P & \bar{h}_{PP'} & \bar{h}_{P\alpha'} \\ \bar{g}_{\alpha} & \bar{h}_{\alpha P'} & \bar{h}_{\alpha\alpha'} \end{pmatrix} \quad \text{with} \quad \begin{aligned} \bar{g}_P &= g_{I(P)}, & \bar{g}_{\alpha} &= [\mathbf{B}^T \mathbf{g}]_{\alpha}, & \bar{h}_{PP'} &= h_{I(P)I(P')}, \\ \bar{h}_{P\alpha} &= \bar{h}_{\alpha P} & &= [\mathbf{h}\mathbf{B}]_{I(P)\alpha}, & \bar{h}_{\alpha\alpha'} &= [\mathbf{B}^T \mathbf{h}\mathbf{B}]_{\alpha\alpha'}. \end{aligned} \quad (4.13)$$

The creation of the orbital rotation P-space is also different to the CI case. Here, we first estimate the update by calculating the quotient $|g_{ri}/h_{ri,ri}|$ of the orbital gradient and Hessian diagonal. Defining a selection threshold is not as straightforward as in the CI case, since the estimated step will decrease with the advancing optimization. Instead, we simply add the $N_P = 200$ rotations with the largest quotient, which is in our experience enough for a reliable convergence.

In principle, other types of preconditioning are possible as well. Here, better approxima-

tions than the diagonal can further improve the convergence. A route to follow is the Jacobi-Davidson method [263] in which the preconditioning is obtained by solving the following system of linear equations approximately:

$$(\mathbf{1} - \mathbf{c}^n \mathbf{c}^{n\top}) [\tilde{\mathbf{H}} - E_n \mathbf{1}] (\mathbf{1} - \mathbf{c}^n \mathbf{c}^{n\top}) \Delta \mathbf{c} = -\mathbf{r}^n. \quad (4.14)$$

This can be done for example with a LU decomposition with a sparse approximation $\tilde{\mathbf{H}}$, which has been implemented by Lipparini et al. [185] for the orbital optimization. Nevertheless, in our experience, the convergence with the diagonal preconditioning and the P-space is already satisfying enough. It is also possible to modify the P-space approach for linear equations, which is discussed in more detail in Section 4.4 for the CP-MCSCF.

4.3 The uncoupled optimization (UC-AH)

A simple MCSCF optimization is achieved by combining the P-space Davidson optimization of the CI coefficients with the second-order orbital optimization using the AH method into a two-step method. The orbital gradient and Hessian are already derived in Section 3.2 in equation (3.21) and (3.22), respectively. The rotation parameters are optimized using the AH method, and the orbitals are transformed by the unitary transformation $\mathbf{U}(\mathbf{R})$ generated from the rotational parameters (3.9). This yields a robust second-order convergence of the pure orbital problem, and we never encountered a failing convergence of the second-order orbital optimization. The explicit orbital-CI coupling is neglected, and thus a first-order MCSCF convergence is achieved. This method is denoted in the following as "UC-AH" which is an abbreviation of uncoupled AH. Each iteration of the UC-AH method is started with a computation of the two-electron integrals J_{rs}^{kl} and K_{rs}^{kl} which are required in the orbital Hessian. Afterwards, the CI coefficients are optimized until the total CI residual is reduced by the factor of 0.1 or if a maximum of ten Davidson iterations is reached. The last step is the optimization of the orbitals with the AH method in which the orbital gradient and Hessian are constructed from the updated densities.

The computation of the two-electron integrals easily dominates each iteration, and therefore the number of two-electron integral computations should be reduced to a minimum. This can be accomplished by including the orbital-CI coupling to reach the second-order MCSCF convergence [39], which solves the potentially slow first-order convergence but requires still many integral evaluations. A better solution has been developed by Werner et al. [21, 90–93], and it is discussed in detail in Chapter 5. Here, a model energy based on the exact same

two-electron integrals is introduced, and the optimization is shifted to the model energy. This drastically reduces the number of two-electron integral evaluations and easily outperforms the UC-AH method, as can be seen in Chapter 8. Another possibility is to avoid the evaluation of these integrals by introducing approximations into the orbital Hessian, which is presented in Chapter 7. Although faster and more robust methods are available, the UC-AH method is still commonly used today [146, 176, 264], since it provides a reasonable robust convergence for simple systems with a less complicated implementation.

4.4 Z-vector equation solver for CP-MCSCF

Because of our good experience with the P-space in the eigenvalue problem, we also developed a P-space method for solving the Z-vector equation in the CP-MCSCF discussed in Section 3.5. The linear equation solver is very similar to the P-space Davidson method described in Section 4.2, and the linear equation is projected into a similar iteratively enlarged reduced space. Here, the P- and Q-space capture both the CI coefficients and the orbital rotation parameters. The linear equation is then solved in the reduced space $\bar{\mathbf{h}}\bar{\mathbf{z}} = \bar{\mathbf{b}}$, and the Q-space vectors are obtained from the preconditioned residual as shown in equation (4.12). The construction of the P-space is exactly the same as described in Section 4.2.

However, the coupled-perturbed Hessian shows eigenvalues which are zero and they are associated with the CI vectors of the N_{av} states. This requires some additional considerations when the linear equation system is solved. Without a P-space, this problem can be simply avoided by projecting each new expansion vector onto the orthogonal complement of the CI vectors [132]. However, this changes with the introduction of the P-space, since the P-space unit vectors are not orthogonal to the CI vectors. Removing the CI vector contributions by an extra projection destroys the sparse structure of the P-space vectors and therefore ruins the efficient evaluation.

Instead, the orthogonal projection with the CI vectors is done within the reduced space. Here, the reduced space is now separated into the subspace spanned by the reduced CI vectors $\bar{\mathbf{C}}$

$$\bar{C}_{\alpha n} = B_{\alpha Q}^T c_Q^n \quad \text{and} \quad \bar{C}_{Pn} = c_{I(P)}^n, \quad (4.15)$$

and the $N_P+N_Q-N_{av}$ dimensional orthogonal complement. The basis vectors of the orthogonal complement are constructed with a Gram-Schmidt orthogonalization including $\bar{\mathbf{C}}$ and $N_P+N_Q-N_{av}$ unit vectors. This requires one additional Cholesky decomposition in the N_P+N_Q dimensional space. Afterwards, the reduced problem $\bar{\mathbf{h}}\bar{\mathbf{z}} = \bar{\mathbf{b}}$ is projected into this N_P+

Table 4.1: Iterations needed for solving the CP-MCSCF equations for the state-specific gradients of $[\text{Fe}(\text{NO})(\text{CO})_3]^-$ with an active space of CAS(10,8) [164].

State	Energy [Hartree]	Pople	With P-space		Without P-space	
			united	separated	united	separated
$1^1A'$	-1730.073403	78	27	33	52	63
$1^3A'$	-1730.005203	92	27	33	52	73
$2^3A'$	-1729.992157	199	27	38	52	79
$1^3A''$	-1729.992157	183	27	38	52	79
$2^3A''$	-1729.992021	92	27	33	52	73

$N_Q - N_{av}$ dimensional subspace, and the zero eigenvalues from the CI states are removed. Additionally, convergence can be improved if the CI vectors are added as Q-space vectors in the beginning, which guarantees that $\bar{\mathbf{h}}\bar{\mathbf{C}} = \mathbf{0}$. The reason for this rather complicated procedure is that one has to distinguish between small eigenvalues of the coupled Hessian and the zero eigenvalues associated with the CI states. Therefore, the removal of small eigenvalue contributions, for example with a singular value decomposition, cannot distinguish between the important contributions of some small eigenvalues and the negligible contributions of the CI states.

An example is shown in Table 4.1 where the convergence is compared with the old CP-MCSCF implementation in Molpro. In the old program, the Z-vector equation is solved with the Pople linear equation solver [242] which is a special form of a preconditioned conjugate gradient method [243]. In the new CP-MCSCF program, the Z-vector equation can be solved with all RHS vectors united or for each RHS separately, and the results are shown with and without a P-space. All methods are iterated until the residual is lower than 10^{-7} . The example is the calculation of the five state-specific gradients of $[\text{Fe}(\text{NO})(\text{CO})_3]^-$ with an active space of CAS(10,8) [164] and the def2-tzvp basis [213]. The difficulty in this calculation is the near degeneracy of the two triplet states in the A' and A'' symmetry. Therefore, the coupled-perturbed Hessian shows small eigenvalues which have to be included in the equation solver. This causes severe convergence problems in the old linear equation solver, and several restarts after getting stuck have been reported by the program. No such problems occur in the new program in which a smooth convergence is obtained in all calculations. Here, it is advantageous to solve the Z-vector equation for all RHS together, since expansion vectors of each RHS can contribute to other solutions as well. This yields a 30 percent reduction of iterations without any additional costs. The P-space halves the number of iterations for both the united and the separated

RHS treatment. However, the reduced coupled-perturbed Hessian is relatively large, since it includes the P-space Hessian of the orbitals and the five states. In this particular example, solving the reduced system requires a significant amount of time, such that no improvement in the computation time could be achieved using the P-space. This might change for larger active spaces where the action of the coupled-perturbed Hessian becomes more dominant.

5 | Second-order MCSCF

The development of second-order algorithms [1, 21, 39, 70, 74, 76–93, 156, 179, 185, 265–268] has been mainly driven in the 1980s to improve convergence of the MCSCF method. A second-order convergence as shown in Figure 4.1 can be achieved by a NR optimization including both a parameterization of the CI problem (\mathbf{x}_c) and the non-redundant orbital rotation parameters (\mathbf{x}_o):

$$\begin{pmatrix} \mathbf{h}_{cc} & \mathbf{h}_{co} \\ \mathbf{h}_{oc} & \mathbf{h}_{oo} \end{pmatrix} \begin{pmatrix} \mathbf{x}_c \\ \mathbf{x}_o \end{pmatrix} = - \begin{pmatrix} \mathbf{g}_c \\ \mathbf{g}_o \end{pmatrix} \quad (5.1)$$

The Hessian includes a CI block \mathbf{h}_{cc} , the orbital block \mathbf{h}_{oo} , and the block $\mathbf{h}_{co} = \mathbf{h}_{oc}^\top$ which accounts for the coupling between the CI coefficients and the orbitals. The Hessian can be similar to the CP-MCSCF Hessian discussed in Section 4.4.

The parameterization of the CI problem differs in various second-order MCSCF methods. The reason for different CI parameterizations is the redundancy in the CI problem due to the normalization and orthogonality of the CI states. One possibility of removing this redundancy is to describe changes in the CI vectors with another unitary transformation as done in the orbital problem [39, 70, 74, 76, 78, 79, 83, 265, 266]. Here, the parameters \mathbf{x}_c in the NR equation (5.1) describe the CI rotation parameters of the unitary transformation. As an alternative, it is also possible to work directly in the CF basis by determining the update of the CI coefficients in the space orthogonal to the current CI vector. This can be achieved by projecting the Hessian onto the orthogonal subspace, which was first proposed by Lengsfeld [77] and extended by Jensen et al. [86–89] later. All optimization methods based on a coupled NR approach show a second-order convergence when starting close enough to the solution. However, the starting guesses of a MCSCF optimization can be far away from this second-order region and many NR steps are required in the beginning until the second-order convergence becomes visible. Also, the coupled Hessian matrix often exhibits negative eigenvalues in the beginning of the optimization. This has to be considered when the update step is computed, and the negative eigenvalues produced convergence problems in the beginning of the second-order method development [268]. The convergence can even be guaranteed [82] with an appropriate level-shifting algorithm, although it might become very slow in the beginning. A level-shift can be

also determined with the AH method for the coupled problem.

The reason for this slow convergence in the beginning is due to the fact that the second-order expansion $E^{(2)}(\mathbf{R})$ of the energy cannot describe the periodicity of the unitary transformation $\mathbf{U}(\mathbf{R})$, and therefore the convergence radius of the second-order orbital optimization can be relatively small. A solution for this problem has been presented by Werner and Meyer [90,91] where the energy is expanded up to second-order in the orbital changes $\mathbf{T} = \mathbf{U} - \mathbf{1}$ instead of the rotation parameters \mathbf{R} . This increases the convergence radius for the occupied-virtual rotations drastically and results in a strong reduction of MCSCF iterations while still showing a second-order convergence. Furthermore, the expansion in \mathbf{T} requires the exact same integrals \mathbf{J}^{kl} and \mathbf{K}^{kl} as the orbital Hessian and therefore does not introduce a large computational overhead. However, the optimization with the Werner-Meyer expansion requires additional sub-iterations in order to determine the minimum of the expansion. The method has been further improved and extended to large CASSCF cases by Werner and Knowles [21,92,93] yielding the Werner-Meyer-Knowles (WMK) method. In most cases, the WMK method is superior to the coupled NR optimization, since the number of iterations, and therefore, the number of integral evaluations, is significantly reduced [21,92,93]. Often, the WMK method reaches convergence in just four iterations.

This entire chapter focuses on the second-order method by Werner and Knowles, and a detailed review of the WMK method is presented in the first sections. The second part of this chapter presents new improvements of the WMK method based on ideas and concepts of the coupled NR optimization [1]. Furthermore, we did an entire reimplemention of the WMK method in Molpro [190], not only to improve the convergence of the program, but also to increase computational efficiency and introduce parallelization.

5.1 The WMK method

The foundation of the WMK method is the second-order expansion of the energy in the orbital change $\mathbf{T} = \mathbf{U} - \mathbf{1}$ [90,91]:

$$E^{(2)}(\mathbf{T}) = E_0 + 2 \sum_{rk} T_{rk} A_{rk} + \sum_{rk,sl} T_{rk} G_{rs}^{kl} T_{sl}. \quad (5.2)$$

The intermediates A_{rk} and G_{rs}^{kl} are exactly the same as in the second-order expansion $E^{(2)}(\mathbf{R})$ in equation (3.14). A comparison of both energy expansion $E^{(2)}(\mathbf{R})$ and $E^{(2)}(\mathbf{T})$ with the exact energy is presented in Figure 5.1 for a single orbital rotation R_{rk} . The figure of the

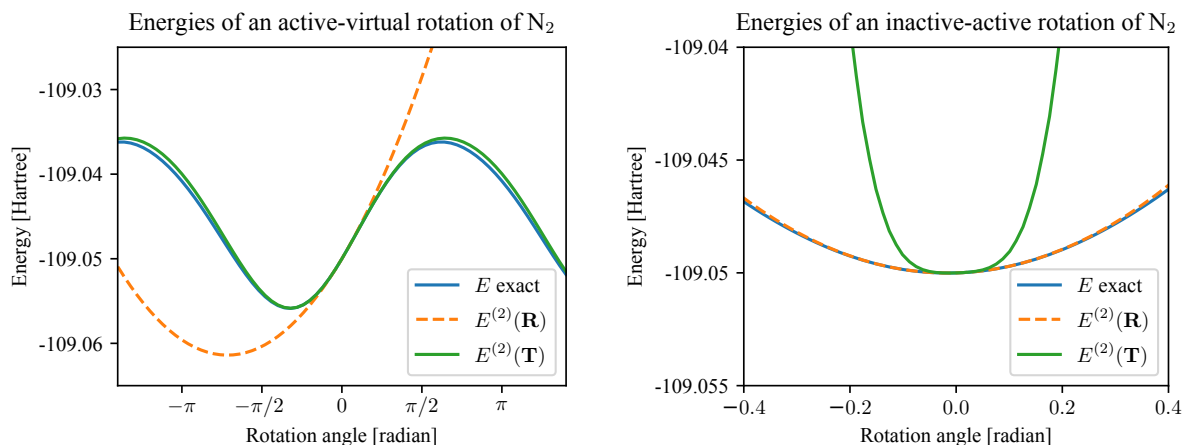


Figure 5.1: Energy plots of the exact energy, the $E^{(2)}(\mathbf{R})$ expansion, and the WMK expansion $E^{(2)}(\mathbf{T})$ for a single active-virtual rotation (left) and for an inactive-active rotation (right). The system is a N_2 molecule with $r_{\text{N-N}} = 1.09 \text{ \AA}$, cc-pVTZ basis [15], full valence active space, and starting from Hartree-Fock orbitals. The left figure shows the rotation between orbital $3b_{1u}$ and $5b_{1u}$, the plot on the right hand side shows the rotation between orbital $1a_g$ and $2a_g$ in D_{2h} symmetry.

active-virtual rotation on the left hand side shows clearly the good approximation of the WMK energy $E^{(2)}(\mathbf{T})$ for occupied-virtual rotations. A similarly good representation can be observed for other occupied-virtual rotations, although the shape of the energy can vary strongly. The convergence radius of $E^{(2)}(\mathbf{T})$ is therefore substantially larger compared to the second-order energy $E^{(2)}(\mathbf{R})$ which shows up as the parabola in Figure 5.1. However, the energy $E^{(2)}(\mathbf{T})$ exhibits a systematically wrong behavior for the inactive-active rotations, and an underestimation of the orbital update is the consequence. This problem requires a separate treatment [21,92] called the internal optimization, which is discussed in more detail in Section 5.1.1. In contrast to the $E^{(2)}(\mathbf{R})$ expansion, it is not possible to determine the minimum of the $E^{(2)}(\mathbf{T})$ energy from a linear equation, since higher-order terms are included in the WMK expansion. Instead, an additional optimization of the $E^{(2)}(\mathbf{T})$ energy is required, which is substantially faster compared to the exact energy minimization.

It is very helpful to regard the $E^{(2)}(\mathbf{T})$ expansion as a surrogate of the exact energy, and the optimization of the energy is shifted to the surrogate model. The WMK energy is optimized up to a certain degree, which constitutes a single iteration in the MCSCF optimization. In context of the WMK method, these iterations are also called macro-iterations. Each macro-iteration requires a computation of the \mathbf{J}^{kl} and \mathbf{K}^{kl} integrals, just as it is necessary in the UC-AH

method. The additional steps in the optimization of the WMK energy are hereinafter referred to as micro-iterations.

The variational conditions of the WMK energy can be obtained by minimizing $E^{(2)}(\mathbf{T})$ with the constraint that \mathbf{U} stays unitary:

$$L(\mathbf{T}, \kappa) = E^{(2)}(\mathbf{T}) - \sum_{rs} ([\mathbf{U}^\top \mathbf{U}]_{rs} - \delta_{rs}) \kappa_{rs}. \quad (5.3)$$

By solving the constrained minimization one obtains the Lagrangian multiplier $\kappa_{rs} = [\mathbf{U}^\top \mathbf{B}]_{rs}$ where the intermediate B_{rk} is defined as:

$$B_{rk} = A_{rk} + \sum_{sl} G_{rs}^{kl} T_{sl}. \quad (5.4)$$

Using the symmetry of the Lagrangian multiplier $\kappa_{rs} = \kappa_{sr}$ one obtains the orbital variational condition:

$$\mathbf{U}^\top \mathbf{B} - \mathbf{B}^\top \mathbf{U} = 0. \quad (5.5)$$

If $\mathbf{U} = \mathbf{1}$, the orbital variational condition of the exact energy in equation (3.23) is reproduced. The numerical minimization of the energy $E^{(2)}(\mathbf{T})$ is described in more detail in Section 5.1.1.

An analogue second-order expansion in \mathbf{T} can be also derived for the Hamilton operator. This is achieved by replacing the RDMs in A_{kl} and G_{rs}^{kl} by the coupling coefficients γ_{tu}^{IJ} and $\Gamma_{tu,vw}^{IJ}$. Reordering the terms with respect to the coupling coefficients yields:

$$H_{IJ}^{(2)}(\mathbf{T}) = \delta_{IJ} E_c^{(2)} + \sum_{tu}^{\text{act}} F_{tu}^c{}^{(2)} \gamma_{tu}^{IJ} + \frac{1}{2} \sum_{tuvw}^{\text{act}} (tu|vw)^{(2)} \Gamma_{tu,vw}^{IJ}. \quad (5.6)$$

The closed-shell energy $E_c^{(2)}$ and the second-order transformed close-shell Fock matrix $F_{tu}^c{}^{(2)}$ read:

$$E_c^{(2)} = \sum_i^{\text{cs}} [h_{ii} - F_{ii}^c + 2(\mathbf{U}^\top \mathbf{F}^c \mathbf{U})_{ii}] + 2 \sum_{ij}^{\text{cs}} (\mathbf{T}^\top \mathbf{L}^{ij} \mathbf{T})_{ij}, \quad (5.7)$$

$$F_{tu}^c{}^{(2)} = (\mathbf{U}^\top \mathbf{F}^c \mathbf{U})_{tu} + \sum_i^{\text{cs}} \left[2(\mathbf{U}^\top \mathbf{J}^{tu} \mathbf{U} - \mathbf{J}^{tu})_{ii} - (\mathbf{U}^\top \mathbf{K}^{tu} \mathbf{U} - \mathbf{K}^{tu})_{ii} + (\mathbf{T}^\top \mathbf{L}^{ui} \mathbf{T})_{ti} + (\mathbf{T}^\top \mathbf{L}^{ti} \mathbf{T})_{ui} \right]. \quad (5.8)$$

The second-order transformed integral $(tu|vw)^{(2)}$ can be alternatively derived by inserting the

unitary transformation (3.8) into the two-electron integral, building the expansion, and keeping only terms up to quadratic order:

$$(tu|vw)^{(2)} = - (tu|vw) + (\mathbf{U}^\top \mathbf{J}^{vw} \mathbf{U})_{tu} + (\mathbf{U}^\top \mathbf{J}^{tu} \mathbf{U})_{vw} + (1 + \tau_{tu})(1 + \tau_{vw})(\mathbf{T}^\top \mathbf{K}^{tv} \mathbf{T})_{uw}. \quad (5.9)$$

Both expansions are equivalent and the state-averaged energy $E^{(2)}(\mathbf{T})$ is obtained from the second-order transformed Hamiltonian $H_{IJ}^{(2)}(\mathbf{T})$ by:

$$E^{(2)}(\mathbf{c}, \mathbf{T}) = \sum_n W_n \sum_{IJ} c_I^n H_{IJ}^{(2)}(\mathbf{T}) c_J^n. \quad (5.10)$$

Therefore, the variational condition of the CI coefficients within the \mathbf{T} model is:

$$\left[\mathbf{H}^{(2)}(\mathbf{T}) - \mathbf{1} E_n^{(2)}(\mathbf{T}) \right] \mathbf{c}^n = 0. \quad (5.11)$$

In each macro-iteration, the orbital and CI variational condition are solved up to a certain degree of accuracy, which is equivalent to an optimization of the model energy $E^{(2)}(\mathbf{c}, \mathbf{T})$. In the original WMK method [21, 92, 93], this optimization is done with a first-order two-step optimization similar to the UC-AH method described in Section 4.3. The minimization of the model energy $E^{(2)}(\mathbf{c}, \mathbf{T})$ is computationally less expensive, since all intermediates can be stored in memory and no recomputation of the integrals \mathbf{J}^{kl} and \mathbf{K}^{kl} is required. An overview of all steps in a single macro-iterations is presented in Figure 5.2.

5.1.1 Micro-iterations

The micro-iterations are the optimization steps of the energy $E^{(2)}(\mathbf{c}, \mathbf{T})$ in each macro-iteration. In the beginning of the WMK development, the optimization of the orbital rotation generators has been achieved by a preconditioned descending gradient optimization [90]. However, a second-order orbital optimization is required for robust convergence [21, 92, 93] because of the close relationship with the exact energy. In order to derive the gradient and the Hessian of $E^{(2)}(\mathbf{T})$, an update for a given $\mathbf{T}(\mathbf{R})$ is defined [92, 93]:

$$\mathbf{T}(\mathbf{R} + \Delta\mathbf{R}) = \mathbf{T}(\mathbf{R}) + \mathbf{U}(\mathbf{R})(\Delta\mathbf{R} + \frac{1}{2!}\Delta\mathbf{R}^2 + \dots). \quad (5.12)$$

This is obtained from the iterative update of the unitary transformation $\mathbf{U}(\mathbf{R} + \Delta\mathbf{R}) \approx \mathbf{U}(\mathbf{R})\mathbf{U}(\Delta\mathbf{R})$. Inserting the update formula into equation (5.2), differentiating with respect

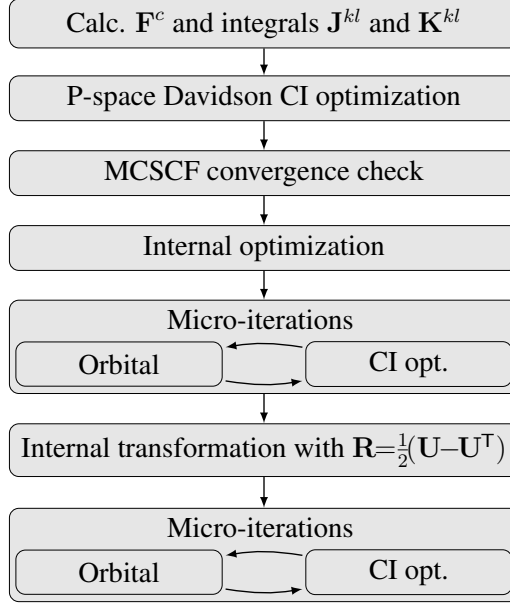


Figure 5.2: Flowchart of a single macro-iteration. The micro-iterations and the internal optimization are discussed in Section 5.1.1 and 5.1.2.

to ΔR_{kl} , and evaluating at $\Delta \mathbf{R} = 0$ yields the gradient \tilde{g}_{rk} and the Hessian $\tilde{h}_{rk,sl}$ for a given \mathbf{T} matrix:

$$\tilde{g}_{rk} = 2(\tilde{A}_{rk} - \tilde{A}_{kr}) \quad (5.13)$$

$$\tilde{h}_{rk,sl} = (1 - \tau_{rk})(1 - \tau_{sl}) \left[2\tilde{G}_{rs}^{kl} - \delta_{kl}(\tilde{A}_{rs} + \tilde{A}_{sr}) \right], \quad (5.14)$$

where

$$\tilde{A}_{rk} = [\mathbf{U}^T \mathbf{B}]_{rk}, \quad \tilde{A}_{ra} = 0 \quad \text{and} \quad \tilde{G}_{rs}^{kl} = [\mathbf{U}^T \mathbf{G}^{kl} \mathbf{U}]_{rs}. \quad (5.15)$$

With the update-equation (5.12), the gradient reproduces the variational conditions of the energy $E^{(2)}(\mathbf{T})$ in equation (5.5). Furthermore, the orbital gradient (3.21) and Hessian (3.22) of the exact energy are reproduced at the starting point $\mathbf{U} = \mathbf{1}$.

It is important to point out that the computation of \tilde{G}_{rs}^{kl} is not needed if the update step $\Delta \mathbf{R}$ is computed with a direct method:

$$\sum_{sl} \tilde{G}_{rs}^{kl} \Delta R_{sl} = \sum_{\bar{r}} U_{r\bar{r}}^T \left[\sum_{sl} G_{\bar{r}s}^{kl} (\mathbf{U} \Delta \mathbf{R})_{sl} \right]. \quad (5.16)$$

This reduces the scaling from $O(N_{\text{occ}}^2 N_{\text{orb}}^3)$ for the \tilde{G}_{rs}^{kl} computation to $O(N_{\text{occ}}^2 N_{\text{orb}}^2)$ for each direct step. In our new implementation, the orbital step $\Delta \mathbf{R}$ is obtained from the P-space AH

method as described in Chapter 4. This allows a more accurate computation of the orbital update compared to the old implementation in which only few iterations of a simple Davidson procedure are used. After calculating $\Delta\mathbf{R}$, the matrices \mathbf{U} and \mathbf{T} are updated with equation (5.12) where the fast evaluation of the energy $E^{(2)}(\mathbf{T})$ allows us to verify the energy decay for the updated \mathbf{T} . If the step is too large and the energy increases, the trust-radius of the AH method is adjusted and a new step $\Delta\mathbf{R}$ is computed. This procedure guarantees the minimization of the model energy in every step.

After the update of \mathbf{U} and \mathbf{T} , the second-order transformed integrals (5.7) - (5.9) are computed and the CI coefficients are optimized with the P-space Davidson method and the transformed Hamiltonian $H_{IJ}^{(2)}(\mathbf{T})$. Finally, the one- and two-particle RDMs are recalculated, and the orbital optimization is restarted. This uncoupled optimization is repeated until the current orbital gradient \mathbf{g} and CI residual \mathbf{r} are lower than the squared norm of the initial gradient $|\mathbf{g}_0|$ which is obtained after the internal optimization: $\sqrt{|\mathbf{g}|^2 + |\mathbf{r}|^2} \leq |\mathbf{g}_0|^2 = \epsilon$. This is necessary to ensure the second-order convergence of the macro-iterations. Because of the good approximation of the WMK energy, it is also reasonable to converge the micro-iterations in the first macro-iterations with a tighter threshold, and the final convergence criterion of the micro-iterations is $\epsilon = \min(|\mathbf{g}_0|^2, 0.01|\mathbf{g}_0|)$. Furthermore, the micro-iterations are terminated for tiny energy changes or after reaching 20 updates of the \mathbf{U} matrix to avoid an overdoing of the model optimization.

The separated optimization of the orbital and the CI problem allows various options for fine-tuning the micro-iterations by changing the number of orbital updates and Davidson iterations in each micro-iteration. In the original implementation, the orbital problem is nearly fully converged before the Davidson optimization is started. This procedure is designed to reduce the number of CI updates in the micro-iterations and is denoted "Uncoupled (CI)". However, we found that this optimization strategy often leads to a slow convergence of the micro-iterations [1]. It can be improved if more Davidson steps are done in the CI update and, secondly, if the frequency between the orbital and CI updates is increased. We therefore implemented a second micro-iteration strategy that is very similar to the previously described UC-AH method. Here, the CI optimization is started after each update of the \mathbf{U} matrix, and the CI residual is lowered by 0.1 in each CI optimization. The increased number of CI optimization steps is partially compensated for by a faster convergence of the micro-iterations. Often, the number of macro-iterations are reduced as well, which is demonstrated in the benchmark chapter. Since this strategy focuses on minimizing the orbital optimization steps, it is denoted as "Uncoupled (Orb)".

The efficiency of both strategies strongly depends on the problem. For example, an enormous active space justifies the use of the Uncoupled (CI) method, since less Davidson iterations are preferable to potentially more macro-iterations. It is possible to choose the optimization strategy automatically by comparing the approximated computational cost of a single Hamiltonian with the most dominant step in the orbital optimization, the generation of the G^{kl} matrices:

$$q = \frac{O_{CI}}{O_{orb}} = \frac{n_{CF}N_{av}n_{act}^4}{[n_{act}^4 + n_{act}^2n_{cs} + n_{cs}^2/2]n_{orb}^2} \approx \frac{n_{CF}N_{av}}{n_{orb}^2}. \quad (5.17)$$

In the last step, the contributions of n_{cs} are neglected if $n_{cs} \ll n_{act}^2$, which is usually the case in a second-order optimization. We found $q = 10$ to be a reasonable threshold for switching from the Uncoupled (Orb) strategy ($q \leq 10$) to the Uncoupled (CI) method ($q > 10$). The choice may not be optimal near the switching point, but typically, the computation times of both strategies are similar at $q = 10$.

Nevertheless, both optimization strategies yield a first-order convergence of the micro-iterations, since no explicit coupling terms are considered. This can cause severe convergence problems if there is a strong coupling between the CI coefficients and the orbitals. In order to fix this problem, we developed a new micro-iteration solver featuring an explicit orbital-CI coupling. This coupled optimization is described in more detail in Section 5.2.

5.1.2 Internal optimization

As shown in Figure 5.1, the inactive-active rotations feature a systematically wrong x^4 behavior [21,92]. This inactive-active rotations are also called internal rotations, since only occupied orbitals are involved. The wrong asymptotic behavior reduces the convergence radius of these internal rotations and results in an underestimation of the internal update. The problem can be solved by starting each macro-iteration with an additional optimization restricted to the internal rotations [21, 92]. Fortunately, this internal optimization is very efficient, since all required internal integrals involve only occupied orbitals and can be held in memory for the entire optimization. Also, transformations of the internal integrals is very efficient, since only transformation among occupied orbitals occur. The internal optimization is equivalent to an UC-AH optimization of the inactive-active rotations. Since the number of internal rotations is small, the full Hessian and can be directly calculated from the internal integrals, and the AH matrix can be diagonalized without a direct method. A CI optimization is also done after each orbital update to include the first-order orbital-CI coupling. Typically, only 3 iterations are required to converge the internal optimization. After finishing the internal optimization, a

final transformation of the full integrals with the internal update U_{kl} is required:

$$J_{\tilde{r}\tilde{s}}^{kl} = \sum_r U_{r\tilde{r}} \sum_s U_{s\tilde{s}} \sum_k U_{k\tilde{k}} \sum_l U_{\tilde{l}l} J_{rs}^{kl}, \quad (5.18)$$

and the same transformation is also performed for the K_{rs}^{kl} integral. Here, \mathbf{U} only differs from the identity in the occupied-occupied block. The transformation scales as $O(N_{\text{orb}}N_{\text{occ}}^4)$ and can still be done in memory. We also implemented a parallelized version in which the loops over l and k are done in parallel. This transformation avoids the expensive recomputation of the integrals J_{rs}^{kl} and K_{rs}^{kl} if only internal rotations are involved. The number of macro-iterations are considerably reduced with the additional internal optimization, as shown in Reference [21].

Additionally, the number of macro-iterations can be further reduced by an additional internal transformation (5.18) after converging the micro-iterations [21, 92]. Here, the internal rotations R_{kl} are approximated by the antisymmetric part of the total transformation \mathbf{U} obtained from the micro-iterations:

$$R_{kl} \approx \frac{1}{2} [\mathbf{U} - \mathbf{U}^T]_{kl}. \quad (5.19)$$

If the internal step is larger than a certain threshold, the additional internal transformation is performed with the unitary matrix obtained from the rotations R_{kl} . Afterwards, the micro-iterations are repeated with the transformed integrals starting with the previously obtained \mathbf{U} matrix. All these extra steps efficiently correct the wrong asymptotic behavior in the WMK energy, and the additional computational effort is easily compensated for by the faster convergence of the macro-iteration.

5.2 Coupled optimization of the micro-iterations

The optimization in the micro-iteration does not include any explicit coupling between the CI coefficients and the orbitals. It therefore shows only a first-order convergence which can potentially become very slow. A consequence is either an extremely large number of CI optimization steps or a large number of macro-iterations if the micro-iterations are terminated prematurely by reaching the given maximum iteration number. This problem can be solved by including the explicit coupling between the CI coefficients c_I^n and the orbital rotation parameters R_{rk} in a shared Hessian matrix (5.1) as done in many other second-order MCSCF methods. A prototype of such a coupled optimization was already developed in my master

thesis [269] which is based on the coupled optimization of Jensen et al. [86–89]. The coupled optimization of the energy $E^{(2)}(\mathbf{c}, \mathbf{T})$ solves the problem of the slow convergence but, unfortunately, required a massive number of Hamiltonian actions and RDM evaluations. The reason behind is that each block in the coupled Hessian (5.1) requires either a Hamiltonian action (\mathbf{Hc}) or RDM evaluation for each action of the Hessian. This can also be seen in the equations of the CP-MCSCF in Section 4.4 which are very similar to the coupled optimization of the WMK energy.

In order to reduce the number of Hamiltonian actions and RDM evaluations, we modified the approach of coupling the CI coefficients and the orbitals [1]. We keep the basic structure of the Uncoupled (Orb) method and start with the pure CI optimization first. In the subsequent orbital optimization, the reduced CI space from the Davidson method is kept and coupled with the orbital rotation parameters in an united Hessian matrix. A second update of the CI vector is then obtained from the coupled AH problem. This way, only the coupling with the reduced space is included and the number of CI evaluations is reduced. The level of coupling can be increased by adding additional CI expansion vectors derived from the coupled residual. The advantage of this method is that we can optimize the CI problem first where only a single Hamiltonian action is required for each Q-space vector and state. Afterwards, we reuse the reduced space from the Davidson method for the coupling in the orbital optimization.

We recall the definitions of the reduced space in the Davidson method introduced in Section 4.2. The reduced space is spanned by the N_c solution vectors \mathbf{C} which are constructed from the P- and Q-space vectors. The second optimization of the CI problem is done with a unitary transformation $\mathbf{V}(\mathbf{S})$ parameterized by the rotation parameters S_{pq} as done in many other second-order MCSCF methods [39, 70, 74, 76, 78, 79, 83, 265, 266]:

$$\mathbf{V} = \exp(\mathbf{S}) \quad \text{with} \quad \mathbf{S} = -\mathbf{S}^T. \quad (5.20)$$

We assume that the vectors in \mathbf{C} are sorted according to their energy such that the current solution of the CI vectors are $c_I^n = C_{In}$. The updated CI solution \tilde{c} then reads:

$$\tilde{c}_I^n = [\mathbf{C} \exp(\mathbf{S})]_{In}. \quad (5.21)$$

Only rotations with the N_{av} states are required, since all other rotations are redundant and removed, i.e. S_{pq} for $q < N_{av}$ are redundant. As shown below, rotations between states with equal weights W_n are redundant as well and also excluded.

The WMK energy depending on the CI rotations \mathbf{S} and the orbital changes \mathbf{T} can be ob-

tained from equation (5.10) where the updated CI vectors \tilde{c}_I^n are inserted:

$$E^{(2)}(\mathbf{S}, \mathbf{T}) = \sum_n W_n \sum_{IJ} \tilde{c}_I^n H_{IJ}^{(2)}(\mathbf{T}) \tilde{c}_J^n = \sum_n W_n [\exp(\mathbf{S}) \bar{\mathbf{H}}^{(2)}(\mathbf{T}) \exp(\mathbf{S})]_{nn}. \quad (5.22)$$

Here, $\bar{\mathbf{H}}^{(2)}(\mathbf{T})$ is the transformed Hamiltonian $H_{IJ}^{(2)}(\mathbf{T})$ in equation (5.6) projected into the reduced space \mathbf{C} :

$$\bar{\mathbf{H}}^{(2)}(\mathbf{T}) = \mathbf{C}^\top \mathbf{H}^{(2)}(\mathbf{T}) \mathbf{C}. \quad (5.23)$$

If \mathbf{C} includes all CFs, the energy $E^{(2)}(\mathbf{S}, \mathbf{T})$ is an equivalent parameterization of $E^{(2)}(\mathbf{c}, \mathbf{T})$. The update formula (5.12) is inserted into the energy $E^{(2)}(\mathbf{S}, \mathbf{T})$ to express the dependency on $\Delta \mathbf{R}$ for a given \mathbf{T} which is indicated in the following by the subscript \mathbf{T} . A second-order expansion of the resulting energy $E_{\mathbf{T}}^{(2)}(\mathbf{S}, \Delta \mathbf{R})$ in \mathbf{S} and $\Delta \mathbf{R}$ reads:

$$E_{\mathbf{T}}^{(2)}(\mathbf{S}, \Delta \mathbf{R}) = E^{(2)}(\mathbf{T}) + \tilde{\mathbf{g}}_c^\top \mathbf{x}_c + \tilde{\mathbf{g}}_o^\top \mathbf{x}_o + \frac{1}{2} \mathbf{x}_c^\top \tilde{\mathbf{h}}_{cc} \mathbf{x}_c + \frac{1}{2} \mathbf{x}_o^\top \tilde{\mathbf{h}}_{oo} \mathbf{x}_o + \mathbf{x}_o^\top \tilde{\mathbf{h}}_{oc} \mathbf{x}_c, \quad (5.24)$$

where \mathbf{x}_o and \mathbf{x}_c contain the non-redundant parameters of $\Delta \mathbf{R}$ and \mathbf{S} , respectively. $\tilde{\mathbf{g}}$ and $\tilde{\mathbf{h}}$ are the gradient and the Hessian where the subscript o and c indicate the orbital and the CI sub-blocks as done in equation (5.1).

The orbital gradient and Hessian in equation (5.13) and (5.14) are reproduced, since the energy $E^{(2)}(\mathbf{S}, \mathbf{T})$ is equal to $E^{(2)}(\mathbf{T})$ for $\mathbf{S} = \mathbf{0}$. The CI gradient and Hessian reads:

$$[\tilde{\mathbf{g}}_c]_{pm} = 2[W_m - W_p] \bar{H}_{pm}^{(2)}(\mathbf{T}) \quad (5.25)$$

$$[\tilde{\mathbf{h}}_{cc}]_{pm,qn} = (1 - \tau_{pm})(1 - \tau_{qn}) \left[\delta_{mn} \bar{H}_{pq}^{(2)}(\mathbf{T}) (2W_m - W_p - W_q) \right], \quad (5.26)$$

where we assume $p > m$, $q > n$, and $W_p = 0$ for $p > N_{av}$. Both derivatives become zero for rotations between states with equal weights which shows that these rotations are redundant. Furthermore, the CI Hessian is block diagonal, since it vanishes for different states where $m \neq n$. The coupling block $\tilde{\mathbf{h}}_{oc}$ is given by:

$$[\tilde{\mathbf{h}}_{oc}]_{rk,pm} = 4(W_m - W_p) \left[\tilde{A}_{rk}^{pm} - \tilde{A}_{kr}^{pm} \right]. \quad (5.27)$$

Here, the \tilde{A}_{rk}^{pm} is defined analogously to \tilde{A}_{rk} , but the density is replaced by the transition density matrices D_{tu}^{pm} and $D_{tu,vw}^{pm}$ between the N_{av} states (m) and the other vectors in \mathbf{C} (p):

$$D_{tu}^{pm} = \sum_{IJ} C_{Ip} \gamma_{tu}^{IJ} c_J^m = \sum_I C_{Ip} D_{tu}^{Im} \quad \text{and} \quad D_{tu,vw}^{pm} = \sum_{IJ} C_{Ip} \Gamma_{tu,vw}^{IJ} c_J^m. \quad (5.28)$$

The expensive computation of the \mathbf{A} and \mathbf{G}^{kl} matrix for every transition density \mathbf{D}^{pm} is not required at all. Instead, the \tilde{A}^{pm} matrix can be constructed from additional intermediates P_{rk} and Q_{rk}^{vw} :

$$\tilde{A}_{ri}^{pm} = 2\delta_{pm}P_{ri} + \sum_{tu}^{\text{act}} D_{tu}^{pm} Q_{ri}^{tu} \quad \text{and} \quad \tilde{A}_{ru}^{pm} = \sum_u^{\text{act}} P_{ru} D_{ut}^{pm} + \sum_{uvw}^{\text{act}} D_{tu,vw}^{pm} Q_{ru}^{vw}. \quad (5.29)$$

The intermediates \mathbf{P} and \mathbf{Q}^{vw} are defined as

$$P_{rk} = (\mathbf{U}^T \mathbf{F}^c \mathbf{U})_{rk} + \sum_j^{\text{cs}} (\mathbf{U}^T \mathbf{L}^{kj} \mathbf{T})_{rj} \quad (5.30)$$

and

$$Q_{ri}^{vw} = 2(\mathbf{U}^T \mathbf{J}^{vw} \mathbf{U})_{ri} - (\mathbf{U}^T \mathbf{K}^{vw} \mathbf{U})_{ri} + (\mathbf{U}^T \mathbf{L}^{iw} \mathbf{T})_{rv} \quad (5.31)$$

$$Q_{ru}^{vw} = (\mathbf{U}^T \mathbf{J}^{vw} \mathbf{U})_{ru} + 2(\mathbf{U}^T \mathbf{K}^{uw} \mathbf{T})_{rv}. \quad (5.32)$$

These intermediates are calculated alongside with the \mathbf{A} and \mathbf{G} matrices, and their computation is negligible compared to the \mathbf{G} matrix construction.

The optimization step of the energy $E^{(2)}(\mathbf{S}, \mathbf{T})$ is calculated with the AH method:

$$\begin{pmatrix} -\epsilon & \tilde{\mathbf{g}}_c^T & \tilde{\mathbf{g}}_o^T \\ \tilde{\mathbf{g}}_c & \tilde{\mathbf{h}}_{cc} - \epsilon & \tilde{\mathbf{h}}_{co} \\ \tilde{\mathbf{g}}_o & \tilde{\mathbf{h}}_{oc} & \tilde{\mathbf{h}}_{oo} - \epsilon \end{pmatrix} \begin{pmatrix} 1 \\ \mathbf{x}_c \\ \mathbf{x}_o \end{pmatrix} = \mathbf{0}. \quad (5.33)$$

The diagonalization of the AH matrix is again done with the P-space Davidson variant where all CI rotation parameters are added to the P-space. Since we consider only rotations within the reduced CI space, the number of CI rotations is typically relatively small. The rotational P-space is determined as described in Section 4.2. The solution of the AH equation yields the orbital and CI rotations ΔR_{rk} and S_{pm} , and the orbitals are transformed exactly as in the Uncoupled optimization. However, they are different compared to the pure orbital optimization because of the CI part in the Hessian. The CI rotations are also used for a second update of the CI vectors as shown in equation (5.21). The transformation of the CI vectors can have the side effect that the off-diagonal elements of the N_{av} states in the Hamiltonian are not necessarily zero after the update. This is due to the fact that only the subspace spanned by the CI vectors is optimized by the CI rotations for equal weights, since all rotations S_{mn} between

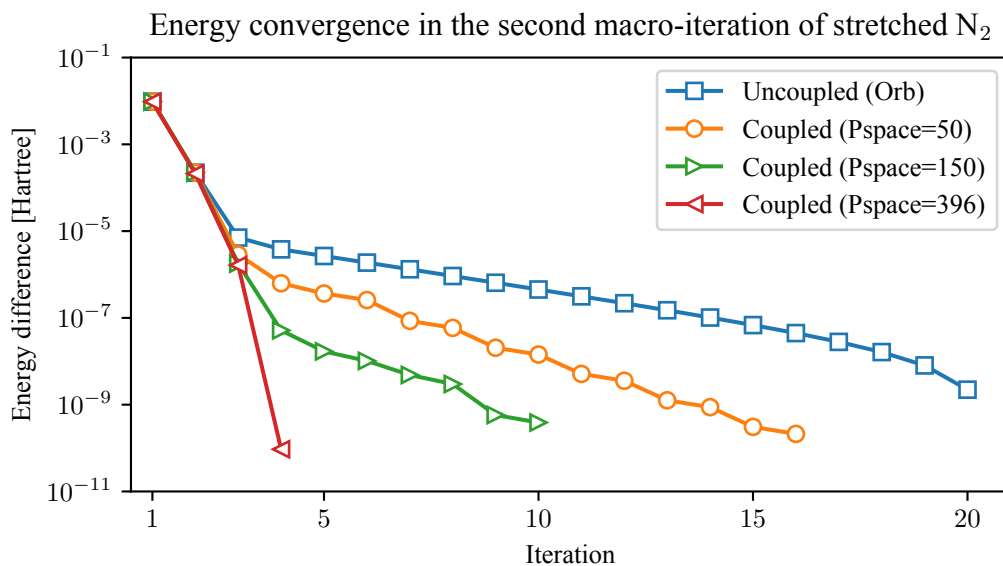


Figure 5.3: Micro-iteration convergence of the Uncoupled (orb) method and the coupled optimization with different sizes of the reduced space. The example shows the micro-iterations in the second macro-iteration of the ground state optimization of a stretched N_2 molecule ($r_{N-N} = 3 \text{ \AA}$) with a full valence active space and the cc-pVTZ basis [15].

the states are redundant. This can easily be fixed by a cheap extra diagonalization of the transformed Hamiltonian in the basis of the N_{av} transformed states. This is the last step in a single micro-iteration, and the subsequent micro-iteration is started again with CI optimization of the transformed Hamiltonian $H_{IJ}^{(2)}(\mathbf{T})$.

The additional computational costs from the coupling are essentially the evaluation of the one- and two-particle transition density matrices \mathbf{D}^{pm} . Here, one should definitely reuse the P- and Q-space structure from the Davidson method to compute only the transition densities $\mathbf{D}^{n\alpha}$ between the N_{av} states and the Q-space vectors $B_{Q\alpha}$. The evaluation of the P-space transition densities $D_{tu}^{I(P)n}$ and $D_{tu,vw}^{I(P)n}$ is rather cheap. The final transition-densities \mathbf{D}^{pm} can be assembled from the solution $\tilde{\mathbf{C}}$ of the reduced Hamiltonian and the P- and Q-space transition density matrices.

If the reduced space \mathbf{C} covers all CFs, the coupling is fully described and a second-order convergence of the micro-iterations can be observed. In practice, this is only possible for a tiny active space with several hundreds of CFs. The level of coupling depends on the size of the reduced space spanned by \mathbf{C} and increasing the size of \mathbf{C} reduces the number of iterations. This is demonstrated for the stretched N_2 molecule in Figure 5.3, where the uncoupled micro-

iterations in the second macro-iteration show a rather slow convergence. The convergence is improved with an increasing size of the reduced space, which is achieved by adding more P-space configurations. A second-order convergence is obtained if all 396 determinants are added. The full P-space is also used in the uncoupled optimization with Uncoupled (Orb). A more efficient way of increasing the coupling is presented in the next section, where specially constructed expansion vectors are added into the reduced space. These vectors are derived from the solution of the coupled AH problem (5.33).

5.2.1 Additional expansion vectors

New expansion vectors can be added to the reduced space in order to increase the coupling. They are derived from the residual of the coupled AH method in the full CF basis. The equation of the coupled Hessian in the full CFs basis is exactly the same as the coupled Hessian discussed in the CP-MCSCF method in Section 4.4, but with all intermediates replaced by their tilde version. The CI part of the residual \mathbf{r}^n of the current update $\Delta\mathbf{c}$ and $\Delta\mathbf{R}$ reads:

$$r_I^n = \left[[\mathbf{H}^{(2)}(\mathbf{T}) - \mathbf{1}E_n^{(2)}(\mathbf{T})](\mathbf{c}^n + \Delta\mathbf{c}^n) \right]_I - \epsilon\Delta c_I^n + 2 \sum_{r>k} \left[(\tilde{A}_{rk}^{In} - \tilde{A}_{kr}^{In})\Delta R_{rk} - c_I^n(\tilde{A}_{rk}^n - \tilde{A}_{kr}^n)\Delta R_{rk} \right], \quad (5.34)$$

where ϵ is the level-shift from the AH method. The summation over the orbital transformation generators $\Delta\mathbf{R}$ can be rewritten into a one-index transformation of the integrals (5.7) - (5.9). This can be efficiently computed by using the intermediates P_{rk} and Q_{rk}^{vw} from the $\tilde{\mathbf{A}}$ construction:

$$\tilde{F}_{tu}^{c(2)} = \frac{1}{2}(1 + \tau_{tu}) \left[\sum_i^{\text{cs}} (\Delta\mathbf{R}^\top \mathbf{Q}^{tu})_{ii} + (\Delta\mathbf{R}^\top \mathbf{P})_{tu} \right] \quad (5.35)$$

$$(\widetilde{tu|vw})^{(2)} = \frac{1}{8}(1 + \tau_{tu})(1 + \tau_{vw}) [(\Delta\mathbf{R}^\top \mathbf{Q}^{vw})_{tu} + (\Delta\mathbf{R}^\top \mathbf{Q}^{tu})_{vw}]. \quad (5.36)$$

Thus, it is possible to replace the coupling part in the residual by the Hamiltonian $\tilde{H}_{IJ}^{(2)}(\mathbf{T})$ and the energy $\tilde{E}_n^{(2)}(\mathbf{T})$ where both are constructed from the transformed integrals:

$$r_I^n = \left[[\mathbf{H}^{(2)}(\mathbf{T}) - \mathbf{1}E_n^{(2)}(\mathbf{T})](\mathbf{c}^n + \Delta\mathbf{c}^n) \right]_I - \epsilon\Delta c_I^n + 2 \left[[\tilde{\mathbf{H}}^{(2)}(\mathbf{T})\mathbf{c}^n]_I - \tilde{E}_n^{(2)}(\mathbf{T})c_I^n \right]. \quad (5.37)$$

In a last step, the update $\mathbf{c}^n + \Delta\mathbf{c}^n$ is replaced by the first-order update of the transformation $\mathbf{V}(\mathbf{S})$ in equation (5.21):

$$\mathbf{c}_I^n + \Delta\mathbf{c}_I^n = [\mathbf{C}(\mathbf{1} + \mathbf{S})]_{In}, \quad (5.38)$$

and the final residual reads:

$$\begin{aligned} r_I^n = & [\mathbf{H}^{(2)}(\mathbf{T})\mathbf{C}(\mathbf{1} + \mathbf{S})]_{In} - E_n^{(2)}(\mathbf{T})[\mathbf{C}(\mathbf{1} + \mathbf{S})]_{In} - \epsilon[\mathbf{CS}]_{In} + \\ & + 2 \left[[\tilde{\mathbf{H}}^{(2)}(\mathbf{T})\mathbf{c}^n]_I - \tilde{E}_n^{(2)}(\mathbf{T})\mathbf{c}_I^n \right]. \end{aligned} \quad (5.39)$$

N_{av} new expansion vectors are obtained by preconditioning the residual as it is done in the Davidson method (4.12) followed by an orthonormalization to the existing reduced space. Afterwards, the transition density matrices and the Hamiltonian action of the N_{av} CI vectors are computed and stored for each new expansion vector. They are used to calculate the additional rows and columns of $\tilde{\mathbf{h}}_{cc}$ and $\tilde{\mathbf{h}}_{oc}$. The first set of expansion vectors is determined when the Davidson-procedure of the AH matrix is converged. Afterwards, the updated AH problem is solved again where the Q-space can be reused. In case of multiple states, the number of transition density matrix evaluations can be reduced by excluding the rotation S_{np} if matrix element $\tilde{\mathbf{H}}_{np}^{(2)}(\mathbf{T})$ is close to zero. This is justified by the vanishing gradient \tilde{g}_{np} , indicating that this rotation is not important, and the exclusion of rotation S_{np} avoids the evaluation of \mathbf{D}^{np} .

One can either add a fixed number of m expansion vectors per state, which is denoted in the following as "Coupled (m)", or define an automatic criterion. In the automatic criterion the expansion vectors are added until the relative change of energy $E_{\mathbf{T}}^{(2)}(\mathbf{S}, \Delta\mathbf{R})$ is lower than ten percent. Typically, that is achieved after three update vectors, and the WMK method using the automatic criterion is named "Coupled (auto)". The calculation of the residual requires one Hamiltonian action, and each new expansion vector requires one action of the Hamiltonian and one transition density matrix evaluation with each of N_{av} states. Therefore, the number of expansion vectors should be as low as possible, and a maximum of five vectors is added in our program even though the automatic criterion is not fulfilled.

Figure 5.4 shows the convergence of the micro-iterations for the ${}^1\text{A}_2$ state optimization of the CrO_3 molecule [270] for a different number of additional expansion vectors. In the third macro-iteration, the convergence of the micro-iterations slows down considerably as can be seen in the blue curve of the Uncoupled (Orb) method. The calculation is done with the def2-TZVP basis set [213] and a CAS(10,10) active space, including the bonding and anti-bonding 3d orbitals of Chromium with the surrounding Oxygen atoms. The convergence successively improves the more expansion vectors are added. Strong improvements are obtained through

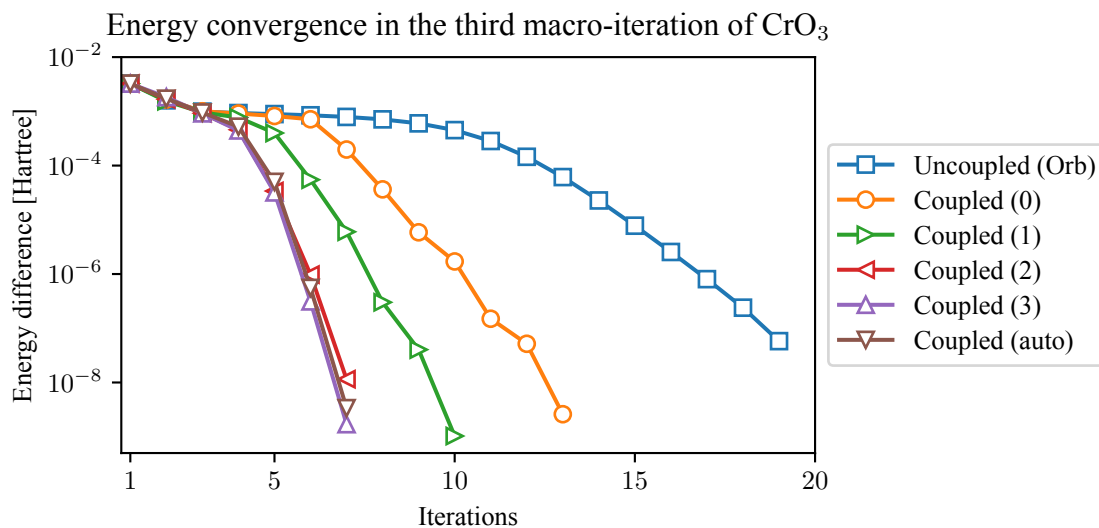


Figure 5.4: Micro-iteration convergence in the third macro-iteration of CrO_3 [270]. The number of additional expansion vectors is shown in parenthesis.

the coupling with the reduced space (Coupled (0)) and if one additional expansion vector is added (Coupled (1)). With the automatic criterion (Coupled (auto)), mostly three additional expansion vectors are added yielding nearly a second-order convergence.

5.2.2 Disadvantages of the explicit coupling

The explicit coupling solves the problem of the slow first-order convergence in the micro-iterations. However, this comes to the price of calculating numerous additional transition density matrices and Hamiltonian action vectors. Unfortunately, the additional cost in the CI optimization cannot always be compensated for by the faster convergence of the micro-iterations. This becomes especially critical for a larger number of CFs where the CI part becomes more and more dominant. An improvement compared to the uncoupled optimization can only be observed in few cases as shown in benchmark calculations in Chapter 8. This restricts the application of the explicitly coupled WMK method to very small active spaces or hardly converging cases. In the next section, we found another approach for including the orbital-CI coupling into the MCSCF method without performing any additional CI evaluations. In this method, the uncoupled optimization is combined with a limited-memory BFGS (L-BFGS) convergence acceleration which treats the coupling on a quasi-Newton level.

6 | Quasi-Newton coupling

In this section we present a more approximated way of including the orbital-CI coupling without introducing any further CI evaluations. This is possible through the development of quasi-Newton (QN) methods in which an approximated Hessian is iteratively constructed from the gradients and steps along the optimization. To illustrate how this works in a two-step environment, we recall the coupled NR equation (5.1) rearrange it to:

$$(\mathbf{h}_{oo} - \mathbf{h}_{oc}\mathbf{h}_{cc}^{-1}\mathbf{h}_{co})\mathbf{x}_o = -(\mathbf{g}_o - \mathbf{h}_{oc}\mathbf{h}_{cc}^{-1}\mathbf{g}_c) = \bar{\mathbf{g}}_o. \quad (6.1)$$

It is also possible to derive a second-order MCSCF based on equation (6.1) [70, 83, 85]. However, the Hessian blocks \mathbf{h}_{cc}^{-1} , \mathbf{h}_{co} , and \mathbf{h}_{oc} require also additional CI evaluations, and therefore these methods do not feature any strong advantage compared to the coupled NR method.

The gradient $\bar{\mathbf{g}}_o$ includes the orbital gradient \mathbf{g}_o and a second-order update introduced through the coupling block \mathbf{h}_{oc} and the uncoupled CI step $\Delta\mathbf{c} = -\mathbf{h}_{cc}^{-1}\mathbf{g}_c$. In the two-step optimization, the orbital gradient $\bar{\mathbf{g}}_o$ is computed from the updated densities, and therefore already includes the CI update on a higher-order level as in the shown $\bar{\mathbf{g}}_o$. This is the reason for the first-order convergence of the two-step method, since this already introduces a weak form of coupling. The Hessian on the right hand side can be seen as an effective Hessian which includes the orbital Hessian \mathbf{h}_{oo} and a correction term $-\mathbf{h}_{oc}\mathbf{h}_{cc}^{-1}\mathbf{h}_{co}$ accounting for the coupling. The idea behind the QN coupling is to approximate this correction term with a QN Hessian. This is possible since the QN Hessian is constructed from the orbital gradient which includes the coupling through the updated densities.

This idea has already been briefly described in 1990 by Malmqvist et al. [65], but details are not given. Nevertheless, it is successfully used to accelerate the Super-CI convergence in the Molcas program [271]. We first developed a QN coupling for the micro-iteration optimization of WMK method [1]. In this approach, the orbital Hessian is replaced by a QN Hessian when close to the convergence. The QN method utilized for the updates is the Broyden-Fletcher-Goldfarb-Shanno (BFGS) method, which is also briefly discussed in the next section. However, after publishing this approach, we found a general way to build a convergence accelerator based on the BFGS method [2], which is also derived in Section 6.2. In this work,

we therefore only present the QN coupling with the L-BFGS acceleration.

6.1 The L-BFGS optimization

In general, a QN method is based on a NR optimization with an approximated Hessian matrix \mathbf{h}^{QN} . There is a large variety of different QN methods, in this work, however, we mainly focus on the BFGS optimization, since it can be also employed as a convergence accelerator. The method is named after its discoverers Broyden [272], Fletcher [273] Goldfarb [274], and Shanno [275], and it is the most used QN method today. The BFGS method is described in various numerical optimization textbooks. Here, we follow the introduction given by Nocedal and Wright [259].

The general idea is to construct a model Hessian from the gradients and steps in an iterative minimization of an objective function $f(\mathbf{s})$. The optimization step \mathbf{x}_n at iteration n is calculated from the NR equation of the current model Hessian \mathbf{h}_n^{QN} :

$$\mathbf{h}_n^{QN} \mathbf{x}_n = -\mathbf{g}_n. \quad (6.2)$$

This step is used to update the current location $\mathbf{s}_{n+1} = \mathbf{s}_n + \alpha \mathbf{x}_n$, where α controls the length of the taken step. The parameter α is typically determined with a line-search algorithm. The Hessian is updated in each iteration such that a quadratic model f_{n+1} reproduces the gradient at \mathbf{s}_{n+1} and \mathbf{s}_n :

$$f_{n+1}(\mathbf{s}_{n+1} + \mathbf{x}) = f(\mathbf{s}_{n+1}) + \mathbf{g}_{n+1}^T \mathbf{x} + \mathbf{x}^T \mathbf{h}_{n+1}^{QN} \mathbf{x}. \quad (6.3)$$

By construction, this expansion reproduces the gradient \mathbf{g}_{n+1} for $\mathbf{x} = 0$. The second requirement that the gradient \mathbf{g}_n is reproduced at \mathbf{s}_n ($\mathbf{x} = \mathbf{s}_n - \mathbf{s}_{n+1}$) yields the following equation:

$$\mathbf{g}_{n+1} - \mathbf{h}_{n+1}^{QN} (\mathbf{s}_{n+1} - \mathbf{s}_n) = \mathbf{g}_n. \quad (6.4)$$

After rearranging, one obtains the secant equation which is the first condition for the Hessian update:

$$\mathbf{h}_{n+1}^{QN} \mathbf{z}_n = \mathbf{y}_n. \quad (6.5)$$

The displacements \mathbf{z}_n and the change in the gradient \mathbf{y}_n are the foundation of the BFGS method, and they are called BFGS vectors in the following:

$$\mathbf{y}_n = \mathbf{g}_{n+1} - \mathbf{g}_n \quad \text{and} \quad \mathbf{z}_n = \mathbf{s}_{n+1} - \mathbf{s}_n. \quad (6.6)$$

Furthermore, the QN Hessian should stay positive definite to avoid convergence problems. This is achieved by a second condition known as the curvature condition:

$$\rho_n = \mathbf{y}_n^\top \mathbf{z}_n > 0. \quad (6.7)$$

The curvature condition is not necessarily fulfilled for non-convex functions, and additional restrictions in the line-search procedures are necessary. This can be achieved, for example, with a line-search based on the Wolfe conditions [259]. In the one-dimensional case, the secant equation returns the finite difference approximation, and the QN method reproduces the secant method. In the multi-dimensional case, however, the secant equation and the curvature condition are both not enough to uniquely define an update of the QN Hessian, and indeed, there is a whole class of QN methods with different update equations [85, 259].

The lengthy derivation of the BFGS update formula is omitted here and can be found for example in Reference [259]:

$$\mathbf{h}_{n+1}^{QN} = \mathbf{h}_n^{QN} + \frac{\mathbf{y}_n \mathbf{y}_n^\top}{\rho_n} - \frac{(\mathbf{h}_n^{QN} \mathbf{z}_n)(\mathbf{h}_n^{QN} \mathbf{z}_n)^\top}{\mathbf{z}_n^\top \mathbf{h}_n^{QN} \mathbf{z}_n}. \quad (6.8)$$

The initial Hessian \mathbf{h}_0^{QN} is often chosen to be the identity matrix, but also other starting guesses are possible, as for example the diagonal of the Hessian [276]. It is not mandatory to store the full Hessian, since the Hessian consists of cheap rank one updates.¹ It is also possible to derive an update scheme for the inverse Hessian:

$$\left[\mathbf{h}_{n+1}^{QN}\right]^{-1} = \left(\mathbf{1} - \frac{\mathbf{z}_n \mathbf{y}_n^\top}{\rho_n}\right) \left[\mathbf{h}_n^{QN}\right]^{-1} \left(\mathbf{1} - \frac{\mathbf{y}_n \mathbf{z}_n^\top}{\rho_n}\right) + \frac{\mathbf{z}_n \mathbf{z}_n^\top}{\rho_n}, \quad (6.9)$$

which can efficiently be computed using the algorithm shown in Figure 6.1. Furthermore, it is not necessary to keep all BFGS vectors along the optimization, since the very old updates may not be relevant anymore. Instead, the BFGS Hessian can be built from the m recent BFGS vector pairs $\{\mathbf{y}_i, \mathbf{z}_i\}$. This is particularly important for high dimensional optimization problems in which the storing and the scalar products with the BFGS vectors may become critical. The method is known as the L-BFGS method and has been introduced by Nocedal [186].

In quantum chemistry, the major application of QN methods is the geometry optimization [276], since it provides fast convergence without the computation of the extremely ex-

¹A rank one update has the following structure: $\beta \mathbf{v} \mathbf{v}^\top$.

pensive molecular Hessian [277, 278]. Nevertheless, it has also been used for the MCSCF optimization as well. Already in 1975, a MCSCF optimization based on a QN updated Hessian has been presented [44]. Since then, the MCSCF orbital optimization with the BFGS method appears occasionally [85, 135, 136, 184, 279, 280] in order to avoid the computation of the orbital Hessian. Often, the approach of Fischer and Almlöf [276] is used, where the initial Hessian \mathbf{h}_0^{QN} is given by an approximated diagonal of the orbital Hessian calculated from the starting guess [135, 184, 279]. However, it has also been reported in a subsequent publication [176] that a NR optimization is “significantly more stable”.

We have also developed a BFGS orbital optimization [1] in order to improve the potentially slow two-step convergence of the micro-iterations in the WMK method. When the step-length becomes small, the orbital Hessian is replaced by the QN Hessian. Here, the initial Hessian in the BFGS method is given by the exact full orbital Hessian [136], which is then iteratively updated as shown in equation (6.8). In this process, it is only necessary to compute and store the rank one update vectors of the BFGS Hessian. The orbital update is calculated from the BFGS Hessian with the AH method. This already solves most of the convergence problems, and examples are given in Reference [1].

6.2 L-BFGS convergence acceleration

The iterative construction of the inverse L-BFGS Hessian can be completely avoided, if only the action on a vector is required. As shown by Nocedal [186, 259] and in Figure 6.1, it is possible to unroll the recursive construction of the inverse L-BFGS Hessian (6.9) which is called the two-loop recursion. It provides an efficient implementation of the L-BFGS method, and furthermore, it separates the action of the initial Hessian. The algorithm can be divided into three steps: the first loop (lines 2-6) can be seen as a preconditioning of the gradient ($\mathbf{g}_{n+1} \rightarrow \bar{\mathbf{g}}_1$). Afterwards, a step is calculated (line 7) from the preconditioned gradient by the action of the inverse initial Hessian ($\bar{\mathbf{g}}_1 \rightarrow \bar{\mathbf{x}}_1$). At the end, the second-loop (lines 8-12) is a post-processing of the calculated step ($\bar{\mathbf{x}}_1 \rightarrow x_{n+1}$). In a classical L-BFGS implementation, the initial Hessian \mathbf{h}_0 is either kept fix (e.g. the identity matrix) or changes during the iterations (e.g. a scaled identity matrix). However, as pointed out by Nocedal [259], the choice of the initial Hessian allows some flexibility as long as it stays positive definite. This can also be seen when the BFGS update (6.8) is inserted into the secant equation (6.5). The secant equation is fulfilled without imposing any restrictions on the previous Hessian \mathbf{h}_n^{QN} or the initial Hessian \mathbf{h}_0^{QN} . However, the initial Hessian has to be positive definite, since this cannot be fixed by the

Input: Gradient \mathbf{g}_{n+1} and the last m $\{\mathbf{y}_i\}$, $\{\mathbf{z}_i\}$, and $\{\rho_i\}$

Output: Step $\mathbf{x}_{n+1} = -[\mathbf{h}_{n+1}^{QN}]^{-1}\mathbf{g}_{n+1}$

```

1:  $\bar{\mathbf{g}}_{m+1} = \mathbf{g}_{n+1}$ 
2: for  $i = m, m-1, \dots, 1$  do
3:    $j = i + n - m$ 
4:    $\alpha_i = \rho_j \mathbf{z}_j^\top \bar{\mathbf{g}}_{i+1}$  (store  $\alpha_i$ )
5:    $\bar{\mathbf{g}}_i = \bar{\mathbf{g}}_{i+1} - \alpha_i \mathbf{y}_j$ 
6: end for
7:  $\bar{\mathbf{x}}_1 = -[\mathbf{h}_0^{QN}]^{-1} \bar{\mathbf{g}}_1$ 
8: for  $i = 1, \dots, m$  do
9:    $j = i + n - m$ 
10:   $\beta_i = \rho_j \mathbf{y}_j^\top \bar{\mathbf{x}}_i$ 
11:   $\bar{\mathbf{x}}_{i+1} = \bar{\mathbf{x}}_i + \mathbf{z}_j(-\alpha_i - \beta_i)$  (read  $\alpha_i$ )
12: end for
13:  $\mathbf{x}_{n+1} = \bar{\mathbf{x}}_{m+1}$ 

```

Figure 6.1: The L-BFGS two-loop recursion algorithm for calculating the action of the inverse L-BFGS Hessian [186].

BFGS updates. This flexibility allows us to replace the initial Hessian in each iteration by an approximation of the current Hessian.

We utilize the L-BFGS as a convergence acceleration of the MCSCF method. Here, the step calculation in line 7 is replaced by the AH method, which also ensures the non-negative eigenvalues through the level-shift. The Hessian in the AH can either be the true orbital Hessian or an approximated version of the orbital Hessian introduced in the next chapter. The coupling part in equation (6.1) is approximated by the L-BFGS method. This is more robust than replacing the complete orbital optimization with the L-BFGS method, since the current orbital Hessian is fully included. Furthermore, it is also possible to include the CI gradients and vectors into the L-BFGS procedure, since both are available after the Davidson optimization in the two-step method. Before going into detail how this is exactly done in the MCSCF two-step optimization, we first discuss a simplified example which is the optimization of the CI eigenvalue, where the L-BFGS is used to accelerate the direct-CI optimization. The convergence is compared to the P-space Davidson method.

Before the Davidson method was developed, the direct-CI optimization had been used for solving of the full-CI problem iteratively [281]. In the direct-CI method, an update of the CI coefficients is determined from the preconditioned residual, as it is done in the Davidson

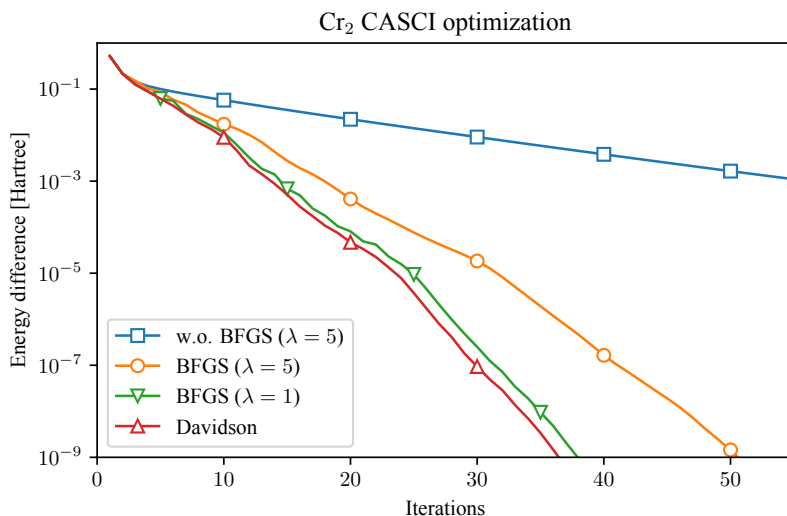


Figure 6.2: CAS-CI optimization of the chromium dimer ($r_{\text{Cr-Cr}} = 1.69 \text{ \AA}$), aug-cc-pVQZ basis [282], and a full valence active space. The orbitals are obtained from a previous CASSCF optimization. The difference to the final energy is shown for the non-accelerated direct-CI method (blue), the L-BFGS accelerated direct-CI (orange and green), and the conventional P-space Davidson method (red).

method to calculate a new expansion vector:

$$\Delta c_I = -\frac{g_I}{H_{II} - E - \lambda} \quad \text{with} \quad \mathbf{g} = \mathbf{H}\mathbf{c} - E\mathbf{c} \quad \text{and} \quad \mathbf{c}^\top \mathbf{c} = 1. \quad (6.10)$$

The parameter $\lambda > 0$ is a damping parameter and $E = \mathbf{c}^\top \mathbf{H}\mathbf{c}$ is the current energy. The CI vector is normalized after each update. The direct-CI method can be improved by introducing a P-space similar to the P-space Davidson method. The gradient is calculated by diagonalizing the reduced Hamiltonian built from the P-space configurations and the current CI solution. This is not significantly more expensive than the gradient calculation in equation (6.10), but yields the optimal coefficients for the P-space configurations. Therefore, the CI gradient calculation is equivalent to the Davidson method without any Q-space vectors. The P-space improves the direct-CI optimization considerably and makes the comparison with the P-space Davidson method fair.

To obtain the L-BFGS accelerated direct-CI method, the update step with the initial Hessian (Figure 6.1, line 7) is replaced by direct-CI update (6.10). Figure 6.2 shows the energy convergence of the direct-CI method with and without the L-BFGS acceleration. The convergence of the conventional P-space Davidson method is also shown. The example is a CAS-CI

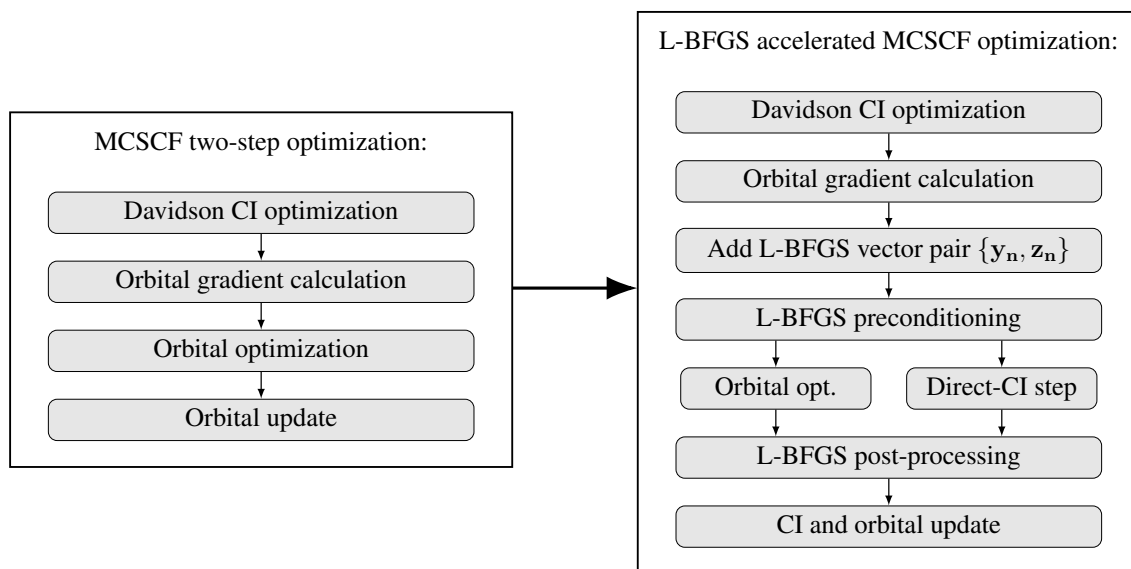


Figure 6.3: Flowchart of a single iteration in the MCSCF two-step optimization and the L-BFGS accelerated MCSCF optimization.

ground state optimization of the chromium dimer molecule with a full-valence CAS(12,12) active space (107216 Slater determinants, and D_{2h} symmetry used). This is a particularly difficult case, since multiple configurations are strongly contributing to the wavefunction, and the P-space Davidson method shows a rather slow convergence. The direct-CI optimization without the L-BFGS acceleration requires a large damping parameter $\lambda = 5$, since otherwise, the energy starts oscillating heavily. The result is a very slow linear convergence. When the L-BFGS acceleration is added the convergence significantly improves. Furthermore, the L-BFGS acceleration enables a lower damping parameter $\lambda = 1$, which improves the convergence considerably without introducing oscillations, and in the end, the convergence is very similar to the Davidson method. We found this result quite astonishing, since the Davidson method yields the optimal results within subspace spanned by the expansion vectors. In this particular example, the number of BFGS vectors and Davidson expansion vectors are equal.

Now we shift focus back on the MCSCF problem. An overview of the L-BFGS acceleration of the two-step optimization is shown in Figure 6.3. In order to improve the coupling, both the orbital rotation parameters and the CI coefficients are included in the acceleration. The CI part is very similar to the previously discussed example, and the CI residual is obtained from the Davidson solver. The displacement vector of the orbitals is given by the rotation update \mathbf{R} which has been used in the last orbital transformation with $\mathbf{U} = \exp(\mathbf{R})$. In summary, the

BFGS vectors of iteration $n+1$ in the MCSCF optimization read

$$\mathbf{y}_n = \begin{pmatrix} [\mathbf{g}_c]_{n+1} - [\mathbf{g}_c]_n \\ [\mathbf{g}_o]_{n+1} - [\mathbf{g}_o]_n \end{pmatrix} \quad \text{and} \quad \mathbf{z}_n = \begin{pmatrix} \mathbf{c}_{n+1} - \mathbf{c}_n \\ \mathbf{R}_n \end{pmatrix}. \quad (6.11)$$

The BFGS vectors are computed and stored after the CI optimization, and the orbital gradient is calculated with the updated density. At this point, we have a consistent set of the CI vector, the CI residual, the orbital gradient, and the orbital update to form a new BFGS vector pair $\{\mathbf{y}_i, \mathbf{z}_i\}$. The orbital optimization is done with the AH method, where the gradient is replaced by the preconditioned version. Afterwards, the orbitals are transformed with the exponential of the post-processed rotation parameters. In case of state-averaged calculations, only the orbital parameters are included in the BFGS vectors, since otherwise root-flipping problems can occur for nearly degenerate states. Fortunately, the L-BFGS acceleration performs also very well, if only the orbital rotation parameters are included. Nevertheless, the inclusion of the CI parameters in single-state calculations does not hurt, since no additional expensive computations are necessary, and it helps especially in case of a slowly converging CI.

However, there are some tricks necessary, to take the full advantage of the L-BFGS acceleration in the two-step procedure. Most of the tricks are required, because we cannot include any sophisticated step-length control without additional expensive energy evaluations. The final energy is only available after the next CI optimization, and therefore it is not possible to build a model function from the last energies and gradients as it is typically done in line-search procedures [259]. Instead, we use a very simple approach in which we rescale the orbital update \mathbf{R} to be within a trust radius of 0.5. This is necessary since the BFGS yields a good search direction, but sometimes overshoots the step-length. Furthermore, the curvature condition (6.7) of a new BFGS vector pair $\{\mathbf{y}_i, \mathbf{z}_i\}$ can be violated. To maintain the positive definite form of the BFGS Hessian, a new pair is only added if the curvature condition is fulfilled. We found it also helpful to reset the BFGS optimization if the energy is increasing or if there is a large change in the density. This is often related to a swap between an active orbital with an inactive or a virtual orbital, which results in a strong change in the energy functional, and the extrapolation from old BFGS vectors is no longer helpful. In such cases the energy usually decreases significantly in the subsequent iteration.

If these tricks are considered, we found the L-BFGS acceleration to perform very reliably. As shown in benchmark calculations in chapter 8 the MCSCF convergence is strongly improved in all methods. The additional costs through the L-BFGS acceleration are negligible, since only the storage and scalar products of the BFGS vectors are required. In principle, it

is possible to completely turn off the CI Davidson optimization in the beginning and do the CI optimization similar to the direct-CI example. This could be interesting for huge active spaces, although the convergence usually drops down significantly, and more density evaluations are required. The L-BFGS acceleration is used in the WMK method to improve the micro-iterations and the internal optimization. This defines a new method, denoted in the following as the "QN-Coupled WMK" method. Here, a direct comparison between the QN coupling and the explicit coupling is possible. The L-BFGS acceleration is also vital for approximated orbital optimizations which are presented in the next chapter. Here, the acceleration does not only compensate for the missing orbital-CI coupling, but also improves approximations in the orbital Hessian.

The described L-BFGS acceleration has a very general structure, and applications beyond the MCSCF method are possible as well. It has been used to improve the convergence of the coupled cluster amplitudes by my colleague Qianli Ma [283], where it worked straight out of the box without further adjustments, but showed a convergence slightly slower as the usually used DIIS method [284]. Furthermore, we found several single-reference calculations where the approximated orbital optimization with the L-BFGS acceleration finds a lower energy than the corresponding HF calculation with DIIS. Such an example is also shown in Chapter 8. Although the L-BFGS acceleration appears to be a strong tool for non-linear optimization problems, it is rarely mentioned in the literature [285–287]. Therefore, it would be interesting to try out other applications and examples beyond the MCSCF context.

7 | First-order MCSCF

The calculation of the full orbital Hessian requires the computation of the integrals J_{rs}^{kl} and K_{rs}^{kl} . This computation scales with $O(N^5)$, where N represents the molecule size. This is due to the linear dependency of the number of occupied orbitals N_{occ} and the total number of orbitals N_{MO} on the system size. The scaling originates in the first step in the integral transformation from the AO basis to the MO basis:

$$(\rho\sigma|\mu k) = \sum_{\nu}^{AO} (\rho\sigma|\mu\nu)C_{\nu k}, \quad (7.1)$$

which scales as $O(N_{AO}^4 N_{occ}) = O(N^5)$ where N_{AO} is the number of AO basis functions. The assembly step in density fitting shows a similar scaling: $O(N_{MO}^2 N_{fit} N_{occ}^2) = O(N^5)$. Here, the number of fitting functions N_{fit} is also linearly depending on the molecular size. However, it is also possible to perform the density fitting during the Hessian action calculation, where one index is contracted before the density fitting is performed [174, 176]. This yields formally a scaling of $O(N^4)$ as shown in the following example. The contraction of the J_{rs}^{ij} matrix with the current step $\Delta\mathbf{R}$ occurs during the Hessian action calculation and can be rewritten as:

$$h_{ri,sj}\Delta R_{sj} \rightarrow \sum_{sj} J_{rs}^{ij}\Delta R_{sj} = \sum_{\bar{A}} \sum_j^{cs} (ij|\bar{A}) \left[\sum_s (\bar{A}|rs)\Delta R_{sj} \right]. \quad (7.2)$$

Here, the contraction of $(\bar{A}|rs)$ with ΔR_{sj} scales as $O(N_{fit} N_{orb}^2 N_{cs}) = O(N^4)$, and the assembly shows a scaling of $O(N_{fit} N_{cs}^2 N_{orb}) = O(N^4)$ where N_{cs} is the number of closed-shell orbitals. However, hundreds of Hessian actions are easily required in the MCSCF optimization, and therefore a large pre-factor is the consequence.

All of this makes a second-order orbital optimization nearly impossible for larger molecules with more than 100 atoms. The problem can be solved by introducing approximations into the orbital optimization which destroy the second-order convergence. The discussed MCSCF methods in this chapter are similar to the UC-AH method introduced in Section 4.3, but with the orbital optimization replaced by a cheaper and more approximated treatment.

Without introducing local approximations, the best possible scaling is $O(N^4)$, since this is the scaling of the Fock matrix construction required in the gradient calculation. The presented approximated methods require not much more than the intermediates of the orbital and CI gradient calculation.

We first review the Super-CI method [50, 54, 63–65] which has successfully been used in many applications of MCSCF optimization during in the last decades. It requires considerably more iterations than a second-order optimization, but with a significantly lower computation time per iteration. The Hessian in the Super-CI method can be derived from multireference perturbation theory (MRPT), which is also discussed in the following section.

A new approximated orbital optimization is presented in the second part of this chapter. Here, only the inactive-virtual rotations are approximated by the Super-CI method while the active orbitals are still treated on the second-order level [2]. In the following, this method is called the SO-SCI method, and it is not significantly more expensive than the Super-CI method, but shows a faster convergence as shown for many examples in Chapter 8.

7.1 The Super-CI method

The Super-CI method has been first presented in 1971 by Grein and Chang [54], who also introduced the expression Super-CI. The method is based on the generalized Brillouin theorem in which the Hamiltonian overlap between the optimized MCSCF wavefunction and single excitations vanish.¹ The Super-CI wavefunction $|\Psi_{SCI}\rangle$ is construct from these single excitations [54]:

$$|\Psi_{SCI}\rangle = (1 + \hat{R}) |\Psi\rangle = |\Psi\rangle + \sum_{r>k} R_{rk} |rk\rangle, \quad (7.3)$$

and the singly excited states $|rk\rangle$ are called Brillouin states [50] in the following:

$$|rk\rangle = (\hat{E}_{rk} - \hat{E}_{kr}) |\Psi\rangle. \quad (7.4)$$

The Super-CI wavefunction is a first-order approximation of the exponential transformation of the wavefunction (3.11). The Brillouin states are non-orthogonal, and the non-vanishing

¹Historically, the Super-CI method is also called the Generalized Brillouin Theorem Multiconfiguration (GBT-MC) method in the literature [57–59].

overlap terms $\langle rk|sl\rangle$ read [65]:

$$\langle ti|uj\rangle = 2\delta_{tu}\delta_{ij} - \delta_{ij}D_{tu}, \quad (7.5)$$

$$\langle ai|bj\rangle = 2\delta_{ab}\delta_{ij}, \quad (7.6)$$

$$\langle at|bu\rangle = \delta_{ab}D_{tu}, \quad (7.7)$$

$$\langle tu|vw\rangle = -2[\langle \Psi|\hat{E}_{tu,vw}|\Psi\rangle - \langle \Psi|\hat{E}_{tu,wv}|\Psi\rangle] + (1 - \tau_{tu})(1 - \tau_{vw})\delta_{uv}D_{tv}. \quad (7.8)$$

The evaluation of equation (7.8) is only needed in case of a non-CASSCF optimization. Here, the coupling coefficients are considered in the non-symmetrized form. If natural orbitals are used, the overlap matrix becomes diagonal for the CASSCF wavefunction.

In the beginning of the Super-CI method development, the coefficients R_{rk} have been determined via perturbation theory, where only the diagonal of the Hamiltonian in the Brillouin state basis is required [56]. However, this neglects any orbital coupling, and soon, the Hamiltonian in the full Brillouin state basis has been computed to achieve a more robust convergence [55, 57, 61]. The Super-CI coefficients R_{rk} are determined by solving the secular problem (summation over the indices s and l is implied):

$$\begin{pmatrix} -\epsilon & \langle \Psi|\hat{H}|ls\rangle \\ \langle rk|\hat{H}|\Psi\rangle & \langle rk|\hat{H} - E_0 - \epsilon|sl\rangle \end{pmatrix} \begin{pmatrix} 1 \\ R_{sl} \end{pmatrix} = 0. \quad (7.9)$$

Here, the secular problem is shifted by the MCSCF energy E_0 . The off-diagonal terms are given by the generalized Brillouin theorem in equation (3.13), and they are equal to the gradient times 0.5. Equation (7.9) shows a very close relationship to the similar structured AH matrix (4.5). The only difference is the inclusion of the overlap matrix $\langle rk|sl\rangle$ because of the non-orthogonal Brillouin states. However, the evaluation of the Hamiltonian element $\langle rk|\hat{H} - E_0|sl\rangle$ requires third-order density matrices and the integrals J_{rs}^{kl} and K_{rs}^{kl} . The exact equations can be found in Reference [50] in which the authors also concluded that this Super-CI approach is less favorable than a second-order NR optimization of the orbitals, since the second-order optimization yields a quadratic convergence from the exact same integrals and without the third-order densities.

Nevertheless, Roos et al. [50, 63–65] found a way to reduce the computational costs of the Super-CI method significantly, by approximating the Hamiltonian in the matrix element $\langle rk|\hat{H} - E_0|sl\rangle$ by an effective Hamiltonian:

$$\hat{H}^{\text{eff}} = \hat{F} = \sum_{rs} F_{rs} \hat{E}_{rs} \quad (7.10)$$

which is built from the general Fock matrix F_{rs} (3.16). This approximation can be derived from MRPT introduced in Section 3.6, and we recall the definition of the MRPT zeroth-order Hamiltonian in equation (3.64):

$$\hat{H}^{(0)} = \hat{P}\hat{H}^{\text{eff}}\hat{P} + \hat{Q}\hat{H}^{\text{eff}}\hat{Q}. \quad (7.11)$$

The first-order wavefunction $|\Psi^{(1)}\rangle$ is constructed from the Brillouin states, and the Super-CI wavefunction is reproduced by the wavefunction expansion:

$$|\Psi_{SCI}\rangle = |\Psi^{(0)}\rangle + |\Psi^{(1)}\rangle = |\Psi\rangle + \sum_{r>k} |rk\rangle R_{rk}. \quad (7.12)$$

Thus, the Hylleraas functional (3.62) of the Super-CI wavefunction reads:

$$E^{(2)} = 2 \sum_{r>k} R_{rk} \langle rk|\hat{H}|\Psi\rangle + \sum_{\substack{r>k \\ s>l}} R_{rk} \langle rk|\hat{H}^{\text{eff}} - E^{(0)}|sl\rangle R_{sl} = \mathbf{x}^T \mathbf{g} + \frac{1}{2} \mathbf{x}^T \mathbf{h}^{\text{SCI}} \mathbf{x}, \quad (7.13)$$

where \mathbf{x} represents again the non-redundant rotation parameters R_{rk} . The total energy $E_0 + E^{(2)}$ is equivalent to the second-order expansion of the energy in which the orbital Hessian is replaced by the Super-CI Hessian:

$$h_{rk,sl}^{\text{SCI}} = 2 \langle rk|\hat{H}^{\text{eff}} - E^{(0)}|sl\rangle. \quad (7.14)$$

The minimization of the Hylleraas functional can be accomplished by the AH method. In practice, the convergence is considerably accelerated by orthogonalizing the Brillouin states as usually done in MRPT [96], which can be achieved by the Cholesky decomposition of the overlap matrix:

$$O_{rk,sl} = \langle rk|sl\rangle \rightarrow \mathbf{L}\mathbf{L}^T = \mathbf{O} \rightarrow |\widetilde{rk}\rangle = \sum_{r>k} [\mathbf{L}^{-1}]_{rk,rk} \widetilde{r} |rk\rangle. \quad (7.15)$$

Since this is a linear transformation, the orthogonalization can be moved outside the gradient and Hessian evaluation, and the generalized eigenvalue problem in equation (7.9) is reproduced with the matrix element $\langle rk|\hat{H} - E_0|sl\rangle$ replaced by the Super-CI Hessian. Because of the close relationship with the AH method, this resembles a NR orbital optimization with an approximated orbital Hessian.

The evaluated terms of the Super-CI Hessian are presented in Figure 7.1. Here, the terms including active-active rotations for non-CASSCF optimizations are derived under the approx-

$$h_{rk,sl}^{\text{SCI}} = \delta_{rs}N_{kl} - \delta_{kl}M_{rs} + D_{kl}F_{rs} + D_{rs}F_{kl} \quad (7.16)$$

with

$$N_{ij} = -2F_{ij}, \quad N_{ti} = N_{it} = -\sum_v^{\text{act}} F_{iv}D_{vt} \quad (7.17)$$

$$N_{tu} = \sum_{vw}^{\text{act}} [D_{tu,vw} - D_{tu}D_{vw}]F_{vw}, \quad N_{ra} = N_{ar} = 0, \quad (7.18)$$

and

$$M_{rs} = N_{rs} + \sum_k^{\text{occ}} D_{rk}F_{ks} + \sum_k^{\text{occ}} F_{rk}D_{ks}. \quad (7.19)$$

Figure 7.1: Evaluated terms of the Super-CI Hessian $h_{rk,sl}^{\text{SCI}}$. The equations are obtained from Reference [65].

imation $(\hat{E}_{tu} - \hat{E}_{ut})|\Psi\rangle \approx \hat{E}_{tu}|\Psi\rangle$ for $t > u$ [65]. The Super-CI Hessian depends only on the one- and two-particle RDMs and the generalized Fock matrix F_{rs} . Parts of the generalized Fock matrix are also needed in the orbital gradient (3.15), and therefore no large overhead is introduced compared to the gradient calculation. Nowadays, the expression Super-CI is exclusively used for the Roos method [64, 65] which is part of the Molcas program [271].

We implemented the Super-CI method in Molpro to be able to make a fair comparison with the other MCSCF methods. In our implementation, the secular problem in equation (7.9) is solved with the P-space Davidson method for the AH matrix. The P-space is determined as usual by selecting the parameters R_{rk} with the largest quotient of the gradient and the diagonal of the Super-CI Hessian. The major difference in the Davidson method is the inclusion of the overlap matrix $O_{rk,sj} = \langle rk|sl\rangle$, which has to be explicitly computed for the P-space rotations. It is then iteratively enlarged for each new Q-space vector. The reduced system of the AH matrix with the overlap matrix reads (the damping parameter λ is omitted for simplicity):

$$\begin{pmatrix} 0 & \bar{g}_{P'}^\top & \bar{g}_\alpha^\top \\ \bar{g}_P & \bar{h}_{PP'} & \bar{h}_{P\alpha'} \\ \bar{g}_\alpha & \bar{h}_{\alpha P'} & \bar{h}_{\alpha\alpha'} \end{pmatrix} \begin{pmatrix} 1 \\ \bar{R}_{P'} \\ \bar{R}_{\alpha'} \end{pmatrix} = \epsilon \begin{pmatrix} 1 & 0 & 0 \\ 0 & \bar{O}_{PP'} & \bar{O}_{P\alpha'} \\ 0 & \bar{O}_{\alpha P'} & \bar{O}_{\alpha\alpha'} \end{pmatrix} \begin{pmatrix} 1 \\ \bar{R}_{P'} \\ \bar{R}_{\alpha'} \end{pmatrix}. \quad (7.20)$$

The reduced overlap matrix $\bar{\mathbf{O}}$ is constructed as the reduced matrix $\bar{\mathbf{H}}$ in equation (4.8). The general eigenvalue equation is solved by calculating the Cholesky decomposition of the overlap matrix first ($\mathbf{LL}^\top = \bar{\mathbf{O}}$). Afterwards, the reduced AH matrix is multiplied with the inverse lower triangular matrix \mathbf{L}^{-1} from the left and right hand side, and the usual eigenvalue problem

is obtained. However, the overlap matrix can become singular if natural orbitals are exactly doubly- or non-occupied. Rotations with these orbitals are redundant and should be removed from the optimization beforehand, since otherwise the Cholesky decomposition fails. In the beginning of each orbital optimization, the one-particle RDM is diagonalized and searched for eigenvalues close to 0 or 2.² The associated rotations are then removed from the current optimization to avoid the singularities in the overlap matrix. This procedure solves most of the numerical problems, but still, a slow convergence might occur in case of occupation numbers very close to zero or two. The second-order optimization does not need the overlap matrix, and it is in our experience less vulnerable to nearly redundant rotations.

Each iteration in the Super-CI method starts with the computation of the closed-shell Fock matrix \mathbf{F}^c and the integrals $(tu|vw)$, which are both needed in the CI optimization. The thresholds in the CI optimization are the same as is in the UC-AH method. Subsequently, the RDMs, the active part of the Fock matrix, as well as the gradient g_{rk} are computed. After determining the parameters R_{rk} , the orbitals are transformed with the unitary transformation $\mathbf{U}(\mathbf{R})$ as done in Reference [65]. However, the Super-CI method as described so far is not very robust and sometimes starts to oscillate. This is solved by adding a level-shift to the Super-CI Hessian, which is automatically adjusted depending on the diagonal of the Hessian [271]. This damps the update and avoids oscillations. However, even with an adequate damping, the convergence can become extremely slow, and a convergence acceleration as presented in Section 6.2 is vital for a good convergence. The acceleration does not only include the missing orbital-CI coupling, but also counters approximations in the Super-CI Hessian. The L-BFGS acceleration is implemented as shown in Figure 6.3, where the orbital optimization is replaced by the Super-CI method. However, even the accelerated Super-CI method can show a slow convergence, and sometimes around hundred Fock matrix evaluations are necessary.

The presented derivation is only possible for the single-state case, since the formulation of a state-averaged Super-CI wavefunction is not possible. In the early days of the Super-CI development, excited states have been also treated with a Super-CI saddle point optimization [55, 58, 59], but today, state-averaged optimizations are more common. Nevertheless, a working state-averaged Super-CI can be directly obtained by replacing all RDMs by the state-averaged ones. This does not affect the convergence, and the state-averaged case performs similarly to the individual state optimization.

The derivation of the Super-CI method with MRPT opens a path to further approximating orbital optimization methods, based on the different choices of the zeroth-order Hamiltonian

²Thresholds are 10^{-4} for the eigenvalue 2 and 10^{-6} for the eigenvalue 0.

$\hat{H}^{(0)}$ in MRPT. Angeli et al. [264, 288] derived an alternative Super-CI optimization using the the Dyall Hamiltonian \hat{H}_D [247] introduced in equation (3.67). However, it neglects the coupling between all three rotation types R_{ai} , R_{ti} , and R_{at} , since the Hessian becomes block diagonal in the Brillouin basis. We did not implement the Angeli Super-CI method, since we developed another approach with a more accurate treatment of the active rotations. Nevertheless, a direct comparison of both Super-CI methods would be an interesting project, since no comparison has been published yet.

7.2 The SO-SCI method

In this section, we present a new approximated orbital optimization (denoted as the SO-SCI method) in order to improve the convergence of the Super-CI method [2]. This new method combines the second-order optimization of the active orbitals with the Super-CI optimization of the inactive-virtual rotations. The calculation of the general Fock matrix in the Super-CI method requires the two-electron integrals J_{rs}^{tu} and K_{rs}^{tu} . Fortunately, these integrals can also be used to construct the Hessian matrix of the active orbitals. In case of density fitting, the density fitting intermediates in the Super-CI method [289] can be reassembled to generate the integrals \mathbf{J}^{tu} and \mathbf{K}^{tu} [2]. The additional assembly step does not introduce a large computational overhead, and it is usually compensated for by a faster convergence. Furthermore, the optimization of the active orbitals is expected to be more difficult, since they capture the strong correlation and interact with the CI optimization. For example, swaps between active and non-active orbitals are more likely, especially if the choice of the active orbitals is not ideal from the beginning. The optimization of the inactive-virtual rotations is usually less challenging, since they are energetically more separated.

The SO-SCI method is derived by splitting operator \hat{R} in equation (3.11) into two separate operators. We refer to rotations with active orbitals as active rotations, and the operator including them is denoted as \hat{A} . The remaining closed-virtual rotations are called inactive rotations with the associated operator \hat{C} :

$$\hat{A} = \sum_t^{\text{act}} \left[\sum_a^{\text{vrt}} R_{at}^A (\hat{E}_{at} - \hat{E}_{ti}) + \sum_i^{\text{cs}} R_{ti}^A (\hat{E}_{ti} - \hat{E}_{it}) + \sum_{t>u}^{\text{act}} R_{tu}^A (\hat{E}_{tu} - \hat{E}_{ut}) \right], \quad (7.21)$$

$$\hat{C} = \sum_{ai} R_{ai}^C (\hat{E}_{ai} - \hat{E}_{ia}). \quad (7.22)$$

The sum with rotation parameters R_{tu}^A disappears in case of CASSCF wavefunction. We now

separate the rotations of the inactive rotations from the rotations with active orbitals:

$$|\tilde{\Psi}\rangle = \exp(\hat{A}) \exp(\hat{C}) |\Psi\rangle. \quad (7.23)$$

Since \hat{A} and \hat{C} do not commute, equation (7.23) should be considered as an Ansatz, and the orbital transformation in equation (3.9) has to be adjusted accordingly:

$$\mathbf{U} = \exp(\mathbf{R}^C) \exp(\mathbf{R}^A). \quad (7.24)$$

Other separations of \hat{A} and \hat{C} are also possible, and they are discussed in Section 7.2.1. We have chosen this approach to reproduce the Super-CI Hessian for all terms with inactive rotations. In contrast to the Super-CI method, we do not terminate the exponential series. Instead, it is important that the exponential series is kept, since otherwise the active Hessian cannot be reproduced. Next, the energy is expanded with help of the BCH formula as done before in Section 3.2:

$$E(\mathbf{R}^A, \mathbf{R}^C) = \langle \Psi | \hat{H} | \Psi \rangle + \langle \Psi | [\hat{H}, \hat{C}] | \Psi \rangle + \langle \Psi | [\hat{H}, \hat{A}] | \Psi \rangle + \langle \Psi | [[\hat{H}, \hat{A}], \hat{C}] | \Psi \rangle + \\ + \frac{1}{2} \left[\langle \Psi | [[\hat{H}, \hat{A}], \hat{A}] | \Psi \rangle + \langle \Psi | [[\hat{H}, \hat{C}], \hat{C}] | \Psi \rangle \right] + \dots \quad (7.25)$$

$$= E_0 + \mathbf{g}^T \mathbf{x} + \frac{1}{2} \mathbf{x}^T \mathbf{h} \mathbf{x} + \dots \quad (7.26)$$

Again, \mathbf{x} includes the non-redundant parameters of \mathbf{R}^A and \mathbf{R}^C . The orbital gradient is exactly reproduced, since the transformation Ansatz only affects higher-order terms. The double commutator $\langle 0 | [[\hat{H}, \hat{A}], \hat{A}] | 0 \rangle$ reproduces the Hessian of the active rotations, and it can be evaluated without approximations from the integrals \mathbf{J}^{tu} and \mathbf{K}^{tu} . The evaluated Hessian equation has been already presented in equation (3.22). The terms $\langle 0 | [[\hat{H}, \hat{C}], \hat{C}] | 0 \rangle$ and $\langle 0 | [[\hat{H}, \hat{A}], \hat{C}] | 0 \rangle$ are the Hessian blocks including inactive rotations. However, the computation of the exact Hessian parts arising from \hat{C} require the computation of the integrals \mathbf{J}^{ki} , \mathbf{K}^{ki} , and the scaling of the second-order optimization would be reproduced. To avoid the computation of these integrals, the Hamiltonian operator in these two double commutators is replaced by the effective Hamiltonian \hat{H}^{eff} from the Super-CI method (7.10):

$$\frac{1}{2} \mathbf{x}^T \mathbf{h} \mathbf{x} \approx \frac{1}{2} \mathbf{x}^T \mathbf{h}^{\text{eff}} \mathbf{x} = \frac{1}{2} \langle \Psi | [[\hat{H}, \hat{A}], \hat{A}] | \Psi \rangle \\ + \frac{1}{2} \langle \Psi | [[\hat{H}^{\text{eff}}, \hat{C}], \hat{C}] | \Psi \rangle + \langle \Psi | [[\hat{H}^{\text{eff}}, \hat{A}], \hat{C}] | \Psi \rangle. \quad (7.27)$$

The evaluation of the commutators involving the Hamiltonian \hat{H}^{eff} can be done with the commutator relation given in equation (2.35). The cumbersome evaluation of these commutator terms has been automatically derived with a Mathematica [290] script. One finds, that the evaluated approximate Hessian terms $h_{rk,sl}^{\text{eff}}$ with at least one inactive index are equal to the Super-CI Hessian shown in Figure 7.1:

$$h_{ai,bj}^{\text{eff}} = h_{ai,bj}^{\text{SCI}}, \quad h_{ai,bu}^{\text{eff}} = h_{ai,bu}^{\text{SCI}}, \quad h_{ai,uj}^{\text{eff}} = h_{ai,uj}^{\text{SCI}}, \quad \text{and} \quad h_{ai,tu}^{\text{eff}} = h_{ai,tu}^{\text{SCI}} = 0. \quad (7.28)$$

However, this is exclusively true for the double commutators that contain \hat{C} , and the active part in the Super-CI Hessian is not reproduced if the Hamiltonian in $\langle \Psi | [[\hat{H}, \hat{A}], \hat{A}] | \Psi \rangle$ is replaced by the effective Hamiltonian.

The rotational parameters \mathbf{R}^A and \mathbf{R}^C are obtained from the AH matrix diagonalized with the P-space Davidson method. In the AH matrix, the exact Hessian is used for all blocks with two active rotations, while the remaining blocks are given by the Super-CI Hessian. As in the Super-CI method, the overlap matrix of the inactive-virtual rotations (7.6) is taken into account since it improves convergence. In contrast to the WMK method, the Hessian is not computed as shown in equation (3.22), since the construction of the G_{rs}^{tu} matrix can be avoided. Instead, the Hessian matrix is stored in a four dimensional tensor $H_{rs}^{tu} = h_{rt,su}$ to enable a faster computation, since it can be directly evaluated from the integrals. Here, the most time consuming step is the contraction with the two-electron RDM:

$$H_{rs}^{tu} \leftarrow \sum_{vw}^{\text{act}} [J_{rs}^{vw} D_{tu,vw} + 2K_{rs}^{vw} D_{tv,uw}] \quad (7.29)$$

which scales as $O(N_{\text{act}}^4 N_{\text{orb}}^2)$. This is a disadvantage of the SO-SCI method compared to the Super-CI method in which the evaluation of the Super-CI Hessian matrix is trivial. However, the computation of H_{rs}^{tu} can be done very efficiently by splitting rs into blocks and evaluate the sum in equation (7.29) as a matrix multiplication over the index pairs vw and tu . The blocks in rs are chosen to be central processing unit (CPU) cache efficient, and the computation of the Hessian matrix becomes negligible even for a large number of active orbitals. Also, the parallelization over the blocks is trivial. This method is also adapted in the new WMK implementation to solve a similar performance issue in the construction of the G_{rs}^{tu} matrix.

The MCSCF optimization of the SO-SCI method is very similar to the L-BFGS accelerated UC-AH and Super-CI method. The CI optimization is exactly the same in all three methods, and the only differences are the orbital Hessian and the orbital transformation (7.24). As in the

Super-CI method, the presented derivation only works for the single-state case, but replacing the density by the state-averaged RDMs works here as well.

7.2.1 Other wavefunction transformation approaches

The presented separation of the active and inactive rotations (7.23) is only one possible approach, and it was chosen to reproduce the Super-CI Hessian for the inactive rotations. However, there are two other possible separations which are briefly discussed in this section. The Ansatz in Equation 7.23 is labelled as $|\tilde{\Psi}_1\rangle$ in the following, and the two other separations are:

$$|\tilde{\Psi}_2\rangle = \exp(\hat{C}) \exp(\hat{A}) |\Psi\rangle \quad \text{and} \quad |\tilde{\Psi}_3\rangle = \exp(\hat{C} + \hat{A}) |\Psi\rangle = \exp(\hat{R}) |\Psi\rangle. \quad (7.30)$$

The transformation $|\tilde{\Psi}_3\rangle$ is similar to the original transformation with $\exp(\hat{R})$. The corresponding orbital transformations read:

$$\mathbf{U}_2 = \exp(\mathbf{R}^A) \exp(\mathbf{C}^A) \quad \text{and} \quad \mathbf{U}_3 = \exp(\mathbf{R}^A + \mathbf{C}^A). \quad (7.31)$$

The derivation follows the exact same path as described in Section 7.2. The major difference is located in the BCH expansion in equation (7.25), where the double commutators including both \hat{C} and \hat{A} are different:

$$|\tilde{\Psi}_1\rangle \rightarrow \langle \Psi | [[\hat{H}, \hat{A}], \hat{C}] | \Psi \rangle, \quad (7.32)$$

$$|\tilde{\Psi}_2\rangle \rightarrow \langle \Psi | [[\hat{H}, \hat{C}], \hat{A}] | \Psi \rangle, \quad (7.33)$$

$$|\tilde{\Psi}_3\rangle \rightarrow \frac{1}{2} \left[\langle \Psi | [[\hat{H}, \hat{C}], \hat{A}] | \Psi \rangle + \langle \Psi | [[\hat{H}, \hat{A}], \hat{C}] | \Psi \rangle \right]. \quad (7.34)$$

Therefore, the Super-CI Hessian for the inactive sub-block $h_{ai,bj}^{\text{eff}}$ is reproduced in all approaches. However, the Hessian blocks which couple the active and inactive rotations are different (summation over repeated indices implied):

$$|\tilde{\Psi}_1\rangle \rightarrow h_{ai,bu}^{\text{eff}} = -2\delta_{ab} D_{uv} F_{vi} \quad \text{and} \quad h_{ai,uj}^{\text{eff}} = \delta_{ij} [4F_{au} - 2F_{av} D_{vu}], \quad (7.35)$$

$$|\tilde{\Psi}_2\rangle \rightarrow h_{ai,bu}^{\text{eff}} = -4\delta_{ab} F_{ui} \quad \text{and} \quad h_{ai,uj}^{\text{eff}} = 4\delta_{ij} F_{au}, \quad (7.36)$$

$$|\tilde{\Psi}_3\rangle \rightarrow h_{ai,bu}^{\text{eff}} = -\delta_{ab} [D_{uv} F_{vi} + 2F_{ui}] \quad \text{and} \quad h_{ai,uj}^{\text{eff}} = \delta_{ij} [4F_{au} - F_{av} D_{vu}]. \quad (7.37)$$

All three approaches are implemented into the SO-SCI program, and they can be activated by an additional option.

Table 7.1: Number of MCSCF iterations for the SO-SCI transformation Ansatz $|\tilde{\Psi}_1\rangle$, $|\tilde{\Psi}_2\rangle$ and $|\tilde{\Psi}_3\rangle$.

System	active space	states	Ansatz $ \tilde{\Psi}_1\rangle$	Ansatz $ \tilde{\Psi}_2\rangle$	Ansatz $ \tilde{\Psi}_3\rangle$
$[\text{FeCo}[\text{No}]_3]^-$	CAS(10,8)	state-averaged	23	23	20
CrO_3	CAS(10,10)	$^1\text{A}_2$	26	23	23
Co_2O complex	CAS(14,10)	^1A	34	33	35
Co_2O complex	CAS(14,10)	^3A	49	55	53
Co_2O complex	CAS(14,14)	^1A	32	33	34
Co_2O complex	CAS(14,14)	^3A	36	33	33

A comparison for different systems is shown in Table 7.1. In many systems, the SO-SCI convergence is exactly equal in all three approaches, and only systems with varying numbers are shown. More details about the calculations can be found in Section 4.4 and 5.2.1 for $[\text{FeCo}[\text{No}]_3]^-$ and CrO_3 respectively. The Co_2O complex is discussed in detail in Section 8.4 in the next chapter. The largest variation is found for the difficult triplet calculation of the Co_2O complex with an active space of CAS(14,10). However, the convergence in all three approaches is still very similar, and we have chosen approach $|\tilde{\Psi}_1\rangle$ as the default, since the Super-CI Hessian is reproduced.

7.2.2 Start with the WMK method

In order to further improve the convergence of the SO-SCI method, we implemented an option in which the active-virtual rotations are optimized with the WMK method in the beginning, while all other rotations are treated with the SO-SCI method [2]. This is done in the first few iterations, until the total step of in the WMK optimization becomes lower than 0.1. The WMK optimization is possible, since the energy expansion $E^{(2)}(\mathbf{T})$ can be built from the integrals \mathbf{J}^{tu} and \mathbf{K}^{tu} if the optimization is restricted to active-virtual rotations. Adding the optimization of the inactive-active rotations is only possible with approximations and unfortunately leads to an unstable convergence. The optimization of the energy $E^{(2)}(\mathbf{T})$ is done as in the WMK method with a two-step optimization including the CI optimization. This corresponds to a WMK optimization with frozen closed-shell orbitals. Subsequently, the remaining orbital-rotations are optimized with the SO-SCI method starting from the updated RDMs. However, the integrals and the Fock matrix are not updated to avoid the expensive recomputation. We therefore neglect the coupling between the virtual-active and all other rotations in these first

iterations. Calculations show that convergence is only improved for very large active-virtual rotations, and even then the savings are small. Often, the additional CI optimization in the WMK method cannot be compensated for by the reduction of the MCSCF iterations.

An example, where the optimization with the WMK method makes a difference, is the optimization of Rydberg orbitals, which is shown in the benchmark chapter in Section 8.5 for Pyrrole and Furan. In our implementation, the start with the WMK method can be activated by an extra option, but it is not set as the default.

8 | Benchmark calculations

In this chapter, benchmark calculations with all introduced MCSCF methods are presented to discuss the convergence properties and the efficiency of the methods. The MCSCF optimization is iterated until the orbital gradient and CI residual are lower than 10^{-5} . Additionally, we check the energy change of each particular state in every MCSCF iteration. Here, we use a convergence threshold of 10^{-8} Hartree for the first-order methods in which the convergence is checked after the CI optimization. The second-order MCSCF allows a less strict criterion because of the second-order convergence, and the energy change of each state has to be less than 10^{-6} Hartree. Here, the convergence is verified after the internal optimization.

We begin this chapter with the starting guess generation based on the Automated Construction of Molecular Active Space from Atomic Valence Orbitals (AVAS) procedure [164], which is utilized in almost all calculations. The first benchmark computes the first π - π^* excitations of 21 simple aromatic systems [188], and these molecules are small enough to allow a comparison of all presented MCSCF methods. Afterwards, the convergence difficulties of the uncoupled optimization are illustrated for the strongly coupled $[(\text{NH}_3)_3\text{Cu}]_2\text{O}_2^{2+}$ isomerization [291]. Here, a strong improvement through the explicit and QN couplings can be achieved. The efficiency of the first-order MCSCF is demonstrated for three larger transition metal complexes with up to 231 atoms [187, 292], where single-reference calculations and a comparison with the HF method are presented as well. Furthermore, we investigate the effect of the WMK optimization at the beginning of the SO-SCI method (see Section 7.2.2) for the 3s and 3p Rydberg orbitals of Furan and Pyrrole. The final two examples also include an application of MRPT. We performed multireference calculations of a catalyzed rearrangement of two vinylcyclopropane species to the cyclopentene versions [293]. This includes a huge CAS(18,16) active space covering all orbitals involved in the reaction. The last example is a RASSCF study of the first electronic excitation in Mg-porphyrin in which the results are also compared with experimental values.

We have already published similar calculations as presented in Section 8.2, 8.3, and 8.4 (see [1, 2, 190]). However, adjustments in thresholds and other minor improvements have been made in the meantime so that iterations and computation time can vary slightly. Nevertheless,

the observations and conclusions made in these publications are not affected by the recalculations.

The calculations are run in parallel using 20 processes on workstations equipped with either 2x12 Intel® Xeon® E5-2650 v4 CPUs at 2.20GHz or 2x10 Intel® Xeon® E5-2660 v3 CPUs at 2.60 GHz. If not noted otherwise, the calculations are carried out using density fitting in which Molpro's default JK fitting basis have been used for the MCSCF. The speedup through parallelization is discussed at the end of this chapter.

8.1 Starting guesses

A good starting guess is very important for a successful MCSCF optimization. In particular, the active orbitals should have the qualitatively correct character in order to avoid the convergence into unwanted solutions and local minima. A simple but common construction of the starting orbitals is achieved by hand-picking orbitals from a previous HF or DFT solution. This might be straightforward for small molecules, but in case of larger systems, the amount of orbitals complicates a manual selection and hence cumbers the process.

This can be avoided by using the Automated Construction of Molecular Active Space from Atomic Valence Orbitals (AVAS) method developed by Knizia et al. [164]. The AVAS procedure rotates the orbitals of a previous (nearly) converged single-reference solution such that the overlap with a predefined target space of atomic orbitals is maximized. This target space is chosen to describe the strongly correlated orbitals, for example the 3d orbitals of a transition metal. The rotations are determined by calculating the overlap matrix of the occupied orbitals with a projection operator built from the target orbitals. A diagonalization of this overlap matrix yields a unitary transformation which is then used to rotate the occupied orbitals. The eigenvalues correlate with the overlap of the target orbitals, and orbitals with eigenvalues larger than a user-defined AVAS threshold are added to the active space. This is also done in a separated step for the virtual orbitals such that closed-shell and virtual orbitals are not mixed. Open-shell orbitals can be included in the closed-shell procedure, or they are simply added to the active space. Furthermore, AVAS also automatically determines the number of electrons in the active space, since the electrons are obtained by the number of selected closed-shell and open-shell orbitals.

The AVAS procedure avoids the cumbersome manual selection of orbitals as it automatically detects the orbitals similar to the target space. However, we found that a previous HF or DFT optimization is not needed for generating a starting guess with qualitatively correct ac-

tive orbitals. Instead, we use orbitals from an atomic density guess which is constructed from a minimal basis of atomic orbitals and pre-optimized fractional occupation numbers of each atomic orbital [222]. A Fock matrix is computed from this density guess, and the final orbitals are obtained from the diagonalization of this Fock matrix. Afterwards, these orbitals are used in the AVAS procedure to construct the active space and the starting orbitals for the MCSCF optimization. This becomes especially important for large molecules, where our fastest MCSCF methods are only slightly more expensive than the HF calculations (if the active space is small). Furthermore, in some open-shell cases the standard Hartree-Fock procedure sometimes fails to converge.

The described procedure is obviously not a black-box method, since the AVAS target orbitals have to be manually selected by chemical intuition. Often, the valence orbitals of specific atoms are a good starting point, for example the two atoms in a bond breaking scenario. The selection of the target orbitals still requires some experiments, but nevertheless, the described procedure considerably simplifies the active space construction. AVAS may generate more active orbitals than target functions, which is often very useful to detect bonding orbitals. For example, AVAS is capable of adding the bonding and anti-bonding orbitals with a 3d orbital automatically, although only the 3d orbital is put into the target space [164]. The number of selected orbitals can be manually adjusted by changing the AVAS threshold. In our experience, a threshold of 0.3 - 0.5 often yields the desired solution.

8.2 Aromatic systems

In this benchmark calculations, the lowest π - π^* excitation for 21 aromatic systems are computed with a state-averaged CASSCF. This benchmark set has been introduced by Menezes et al. to demonstrate the accuracy the PNO-CASPT2 method [188]. The geometries are obtained from Reference [188] which also provides an overview of the molecules and the various active spaces. The active space includes all π orbitals of the aromatic system and covers various sizes from CAS(6,6) (Pyridine) to CAS(12,12) (Biphenyl). The size of the molecules shows a range between 24 occupied orbitals (Pyridine) and 58 occupied orbitals (Tryptophan). The reference active spaces of Niacinamide, Niacin and Picolinic-Acid are adjusted by removing a almost doubly occupied orbital yielding CAS(8,8) instead of a CAS(10,9) active space for all three molecules. The calculations are performed with the aug-cc-pVDZ (avdz), aug-cc-pVTZ (avtz), and the aug-cc-pVQZ (avqz) basis sets [282]. The active space and the starting guesses are generated with AVAS and the 2p orbitals perpendicular to the aromatic ring. Since these

Table 8.1: Results of the second-order MCSCF for the aromatics benchmark set [188]. The table shows the total number of macro-iterations, orbital optimizations in the micro-iterations, CI work (**Hc**, RDM, and transition density matrix evaluations), and the computation time in minutes. All numbers are summed over the 21 calculations.

Method	avdz				avtz				avqz			
	Mac	Orb	CI	Time	Mac	Orb	CI	Time	Mac	Orb	CI	Time
WMK (old impl.)	77	858	6092	214.5	78	882	6212	1599.1	78	884	6213	6649.6
Uncoupled (CI)	77	476	5288	16.6	77	479	5324	80.5	77	478	5324	312.9
Uncoupled (Orb)	74	465	5572	15.2	75	465	5568	71.1	75	466	5568	282.5
Coupled (0)	74	419	12182	17.5	76	435	12642	78.9	75	428	12488	297.9
Coupled (1)	71	408	14881	18.1	74	412	14864	76.2	74	413	14972	292.2
Coupled (auto)	72	395	20624	18.4	73	405	21062	77.9	74	408	21291	293.9
QN-Coupled	72	450	5276	14.6	74	449	5230	69.9	73	449	5212	279.6

are rather small systems, we can compare all the various presented MCSCF methods. The systems are not posing any challenge for the convergence, and the discussion is limited on the results summed over all 21 calculations. However, many characteristics of the different MCSCF methods are already observable for such simple systems.

The results of the second-order WMK method with the different micro-iteration solvers are presented in Table 8.1. In addition to the macro-iterations and computation time, the number of orbital optimizations with the AH method and the CI work is shown. Here, the CI work refers to the sum over all **Hc**, RDM and transition density matrix evaluations which all require roughly the same computation time. Additionally, the results of the old WMK implementation [21, 92, 93] are presented for comparison, where the same improved density fitted and parallelized CI routines are used as in the modern program. The large computation times in the old implementation are explained by a heavier disk usage and by the non-parallelized orbital optimization and internal transformation.

All methods show an average convergence of only 3-4 macro-iterations. The Uncoupled (CI) algorithm follows the same optimization strategy as the old implementation, which is also reflected in a similar number of macro-iterations. However, the convergence of the micro-iterations is strongly improved by the introduction of the rotational P-space. This nearly halves the number of required AH calculations, and the CI work is also lowered through the faster convergence. The increased number of CI optimization steps in the Uncoupled (Orb) algorithm reduces the number of AH calculations further and also yields less macro-iterations. The

coupling with the reduced CI space in Coupled (0) has no strong impact on these weakly coupled systems. However, the computation time increases, since the CI work is doubled through the calculation of the transition density matrices. Adding more expansion vectors decreases the number of macro-iterations, but the additional CI work cannot be compensated for, and the computation time further increases. The last row in Table 8.1 shows the results of the L-BFGS accelerated micro-iterations in the QN-Coupled method. Here, the number of macro-iterations is very similar to the Coupled (auto) algorithm but without introducing any further CI work. Moreover, the QN-Coupling exhibits also the lowest number of CI work, since less macro-iterations are required compared to the uncoupled methods. This yields the lowest computation time of all second-order methods, although the differences are not strongly pronounced for these simple systems. The differences between the methods become more visible for a strong orbital-CI coupling as shown in Section 8.3.

Table 8.2 shows the number of iterations and computation time of the first-order methods. The SO-SCI method requires less than half of the iterations than the Super-CI method, regardless of the L-BFGS acceleration. The number of iterations is further reduced by the UC-AH method, but the computation time is about three to five times higher than in the SO-SCI method due to the more expensive integral evaluations. If the L-BFGS acceleration is activated, the number of iterations and timings of the Super-CI and the SO-SCI method are more than halved. The improvements in the UC-AH method are less significant, indicating

Table 8.2: Results of the first-order MCSCF for the aromatics benchmark set [188]. The total number of MCSCF iterations and the total computation times in minutes are presented, and all numbers are summed over the 21 calculations.

Method	avdz		avtz		avqz	
	Iter.	Time [min]	Iter.	Time [min]	Iter.	Time [min]
Without L-BFGS acceleration:						
Super-CI	1307	22.8	1329	85.4	1342	346.7
UC-AH	213	16.4	217	88.8	217	395.6
SO-SCI	564	9.9	592	39.6	596	163.4
With L-BFGS acceleration:						
Super-CI	510	9.1	518	32.7	524	131.8
UC-AH	168	13.8	166	71.8	169	332.0
SO-SCI	228	4.1	235	15.4	235	62.4

that the L-BFGS procedure compensates not only for the missing orbital-CI coupling, but also for some of the approximations in the Super-CI and the SO-SCI orbital optimizations. Therefore, the L-BFGS is important for achieving a robust convergence, and it is enabled by default unless otherwise noted. The computation time of the SO-SCI method is considerably lower compared to all other optimization methods including the second-order MCSCF. The computation of all 21 systems with the large avqz basis set takes only one hour with the SO-SCI method, which is 100 times faster than the old WMK implementation.

8.3 $[(\text{NH}_3)_3\text{Cu}]_2\text{O}_2^{2+}$ isomerization

This section discusses an example of a strongly coupled system. The example is taken from a study of Cramer et al. [291] and demonstrates the isomerization of the $[(\text{NH}_3)_3\text{Cu}]_2\text{O}_2^{2+}$ complex [294] from the bis(μ -oxo) to the μ - η^2 : η^2 peroxo structure. The system has been heavily investigated on the theoretical level, since studies showed a poor performance of the CASPT2 method [291, 295, 296]. The disagreement of the MRPT has been solved by using a RASPT2 approach [297] including the Cu 3d-4d correlation in the reference wavefunction. In the meantime, DMRG calculations [298–300] and DMRG-CASPT2 [301] results are also available.

We carried out similar CASSCF calculations as described in Reference [291], where an active space of CAS(16,14) has been presented. The calculations are performed with the aug-cc-pVTZ basis set [282] and the C_{2h} symmetry, where O_2 lies on the z -axis, and the Cu atoms are displaced in y -direction. The benchmark includes six CASSCF calculations of the 1A_g ground state along an isomerization path from the bis(μ -oxo) ($F=0$) to the peroxo ($F=100$) structure. The structures are obtained from the Supporting Information of Reference [291] in which also more details on the active space can be found. We started the calculations at the bis(μ -oxo) structure, where the AVAS starting guess is generated from the 2s, 3s, 2p, and 3p orbitals of the oxygen atoms, and the $3d_{yz}$ orbitals of the Cu atoms. The result is a CAS(18,19) active space ($4a_g, 5a_u, 5b_u, 5b_g$), and the orbitals of the CAS(16,14) active space are obtained by removing the $4a_g, 4a_u, 5a_u, 5b_u,$ and $5b_g$ active orbitals.

All subsequent calculations along the reaction path start from the final orbitals of the previous structure. However, despite these apparently good starting orbitals, the convergence slows down dramatically along the isomerization path. We found that this is due to qualitative changes of the weakly occupied $23a_g$ and $13b_g$ orbitals which are localized at the O-O bond. Both orbitals and the structure of the $[(\text{NH}_3)_3\text{Cu}]_2\text{O}_2^{2+}$ complex are shown in Figure 8.1 for

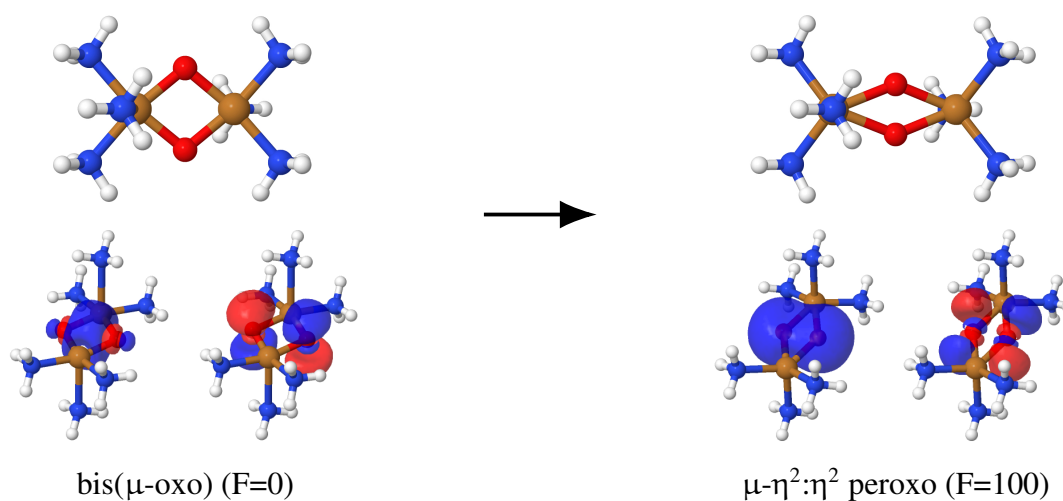


Figure 8.1: The structure of the $[(\text{NH}_3)_3\text{Cu}]_2\text{O}_2^+$ complex [291] and the $23a_g$ (left) and $13b_g$ (right) orbital for F=0 and F=100.

F=0 and F=100. The $23a_g$ orbital changes its character from a 3p sigma bonding orbital at F=0 to the 3s sigma bonding orbital at F=100, while the $13b_g$ orbital rotates from the $3p_x \pi^*$ at F=0 to the $3p_y \pi^*$ orbital at F=100. The strongest changes of the orbitals are observed in the range F=60-100. The rotation of the $13b_g$ orbital induces a strong coupling between the CI coefficients and the orbitals leading to an extremely slow convergence if no treatment of the coupling is included. The strong coupling and the change of the orbitals can be removed by adding the missing a_g and b_g orbital to the active space resulting in a CAS(16,16) space.

We first discuss the results of the first-order methods which are shown in Table 8.3. Without the L-BFGS acceleration, the number of iterations increases drastically at F=60-100 for all first-order methods, and hundreds of iterations are required to fulfill the convergence criteria. The slow convergence can be clearly attributed to the absence of the orbital-CI coupling, since the UC-AH method with the exact second-order orbital optimization shows a similar performance. Also, the CI optimization in each iteration convergences relatively fast, so we can conclude that the difficulties are caused by the two-step optimization. When the L-BFGS acceleration is switched on, the convergence is massively improved, and maximal 20 iterations are required for the SO-SCI and the UC-AH method. The Super-CI convergences slightly slower but still within an acceptable speed. A plot of the energy convergence at the most difficult structure F=80 is presented in Figure 8.2. The dashed lines show the extremely slow linear decay of the uncoupled optimization. The results with the L-BFGS acceleration are indicated by the solid lines. The BFGS treatment starts at iteration number four, however, a

Table 8.3: Number of first-order MCSCF iterations of the isomerization of $[(\text{NH}_3)_3\text{Cu}]_2\text{O}_2^{2+}$ from the bis(μ -oxo) to the peroxy structure [294] with an active space of CAS(16,14) and CAS(16,16). Also, the total computation times summed over all six isomerization steps are presented in minutes.

CAS(16,14)							
F	without L-BFGS			with L-BFGS			Energy [Hartree]
	SCI	SO-SCI	UC-AH	SCI	SO-SCI	UC-AH	
0	51	46	25	20	16	14	-3764.853 570
20	40	42	14	17	12	11	-3764.868 411
40	54	67	25	16	14	12	-3764.880 120
60	209	179	140	23	17	15	-3764.898 386
80	418	285	283	26	20	18	-3764.912 442
100	239	184	162	23	15	14	-3764.906 682
Sum	1011	803	649	125	94	84	
Time	131.0	107.1	556.6	18.0	13.9	77.0	
CAS(16,16)							
F	without L-BFGS			with L-BFGS			Energy [Hartree]
	SCI	SO-SCI	UC-AH	SCI	SO-SCI	UC-AH	
0	52	25 ^{a)}	14	17	13	10	-3764.906 346
20	36	21 ^{a)}	9	13	9	6	-3764.924 469
40	56	29 ^{a)}	9	14	9	7	-3764.940 779
60	73	35 ^{a)}	9	15	9	7	-3764.960 163
80	80	16 ^{a)}	10	15	9	8	-3764.973 119
100	40	30 ^{a)}	12	17	10	8	-3764.966 311
Sum	337	156	63	91	59	46	
Time	325.5	129.9	112.4	89.5	58.7	86.5	

^{a)} Additional level-shift of 0.3 for the inactive-virtual rotations.

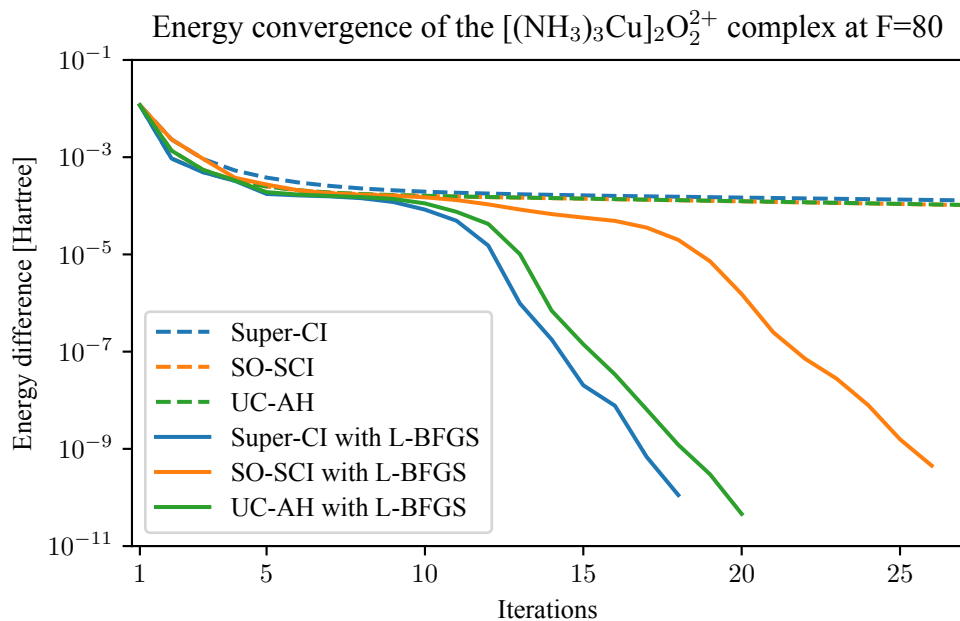


Figure 8.2: Energy convergence of the first-order MCSCF methods for the CAS(16,14) calculation of the $[(\text{NH}_3)_3\text{Cu}]_2\text{O}_2^{2+}$ complex at $F=80$. Results are shown with and without the L-BFGS convergence.

strong difference is first identified at iteration ten after collecting several BFGS vectors. Then, a rapid linear convergence of all accelerated methods can be observed.

In case of the CAS(16,16) active space, the UC-AH method does not depend heavily on the L-BFGS acceleration to show a robust convergence, indicating that the orbital-CI coupling is much weaker. Here, the effect on the Super-CI and the SO-SCI method is more dominant, since the approximated orbital optimization is improved in addition to the orbital-CI coupling. The convergence of the not accelerated SO-SCI is strongly enhanced by an extra level-shift for the inactive-virtual rotations in the orbital Hessian, but this is not required in the accelerated version. In case of the Super-CI optimization, the additional shift yields no change, since a level-shifting procedure is already included in the Super-CI. The accelerated SO-SCI method shows a significant lower number of iterations than the Super-CI method, and it again achieves the lowest computation time of all (first-order) methods.

The convergence difficulties of the CAS(16,14) active space are also visible in the second-order MCSCF. Table 8.4 shows the convergence of the macro-iterations at each isomerization step. Additionally, the number of AH optimizations, the CI work as defined in the previous section, and the computation times are also available with the results summed over all six

Table 8.4: Number of second-order MCSCF iterations of the isomerization of $[(\text{NH}_3)_3\text{Cu}]_2\text{O}_2^{2+}$ from the bis(μ -oxo) to the peroxo structure [294] with an active space of CAS(16,14) and CAS(16,16). Also, the number of AH optimziations, the CI work, and the total computation times in minutes summed over all six isomerization steps are presented.

Method	macro-iterations at F =						summed over all F			
	0	20	40	60	80	100	Macro	Orb	CI	Time [min]
CAS(16,14)										
WMK (old impl.)	7	4	7	36	40	40	134	1613	5246	813.6
Uncoupled (CI)	6	3	3	6	11	7	36	1004	3737	76.7
Uncoupled (Orb)	5	3	3	5	9	6	31	910	4238	71.0
Coupled (0)	5	3	3	4	5	4	24	550	5169	63.8
Coupled (1)	5	3	3	3	4	3	21	330	4276	52.6
Coupled (auto)	5	3	3	3	3	3	20	146	3084	43.8
QN-Coupled	5	3	3	3	4	3	21	245	1336	38.5
CAS(16,16)										
WMK (old impl.)	6	3	4	3	3	4	23	309	1089	402.5
Uncoupled (CI)	5	3	3	3	3	3	20	213	1156	168.5
Uncoupled (Orb)	5	2	3	3	2	3	18	163	1071	146.6
Coupled (0)	5	2	3	3	2	2	17	123	1625	201.0
Coupled (1)	5	2	3	3	2	2	17	120	1888	225.1
Coupled (auto)	5	2	3	3	2	2	17	122	2395	280.7
QN-Coupled	5	2	3	3	2	2	17	139	916	137.6

isomerization steps. The old implementation hardly reaches convergence at F=60-100, and the optimization is aborted after reaching the limit of 40 macro-iterations. The new uncoupled implementations are able to find a solution, but many macro-iterations are required due to the slow convergence of the micro-iterations. When the explicit coupling is activated, the convergence is significantly improved. Here, additional expansion vectors further decrease the number of the micro-iterations, and the increased CI work can be compensated for by a lower number of micro- and macro-iterations. As a result, the coupled methods provide a faster computation time than the uncoupled optimization. However, the performance of the L-BFGS accelerated QN-coupled method is very similar without performing additional CI evaluations yielding the fastest computation time in the second-order MCSCF. Nevertheless, the SO-SCI time of 14 minutes cannot be undercut, since more CI optimization steps are necessary to reach the second-order convergence.

The optimization with the CAS(16,16) active space is not challenging at all, and the conclusions are very similar to the previously discussed benchmark of the aromatic systems in Section 8.2. The explicit coupled methods improve the convergence, but cannot compensate for the additional CI work. The QN-Coupling shows a comparable convergence as the explicit coupled methods and yields again the fastest second-order computation time. Here, significantly less CI evaluations than in the Uncoupled (CI) optimization are required.

This example clearly shows that it is not necessary to compute the expensive coupling terms to overcome the convergence difficulties of a strongly coupled scenario. In the end, a comparable convergence can be accomplished with the considerable cheaper L-BFGS acceleration. Furthermore, the L-BFGS acceleration also improves convergence for weakly coupled systems without introducing any computational overhead, and therefore the QN-Coupled method is from now on the default in our second-order MCSCF.

8.4 Large transition metal clusters

The next benchmark demonstrates the performance for three large transition metal clusters. The structures of all three complexes are shown in Figure 8.3, and the largest system is the nickel complex with 231 atoms and 826 electrons. The iron and the nickel complex are obtained from Guo et al. [187], and they have also been used to benchmark local PNO-NEVPT2 and PNO-CASPT2 methods [187–189]. Here, the preceding CASSCF optimization has been identified as a severe bottleneck and enormous MCSCF computation times have been reported. The third complex is the $\text{Co}_2\text{ON}_4\text{C}_{70}\text{H}_{106}$ complex (in the following Co_2O complex) from

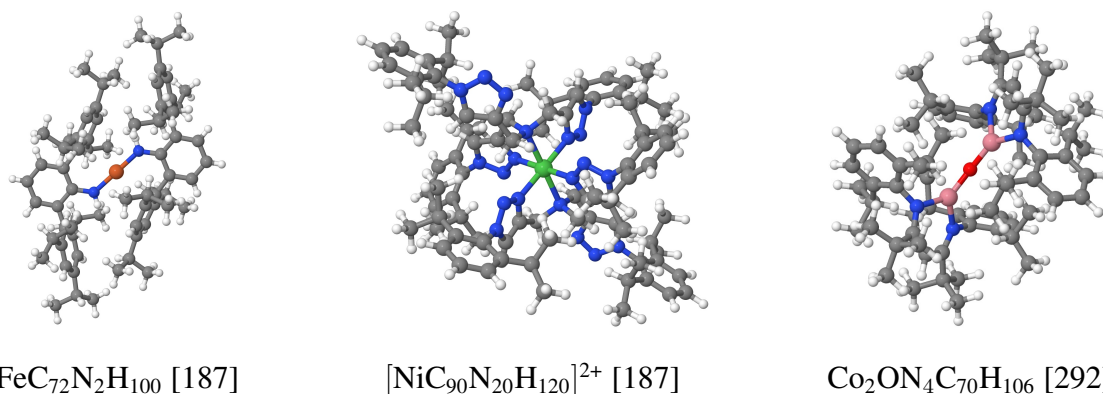


Figure 8.3: Structures of the transition metal complexes for the calculations in Section 8.4.

Roy et al. [292] which shows an extremely strong multireference character for the two lowest states. All three complexes contain too many occupied orbitals for a second-order orbital optimization, and only calculations with the Super-CI and the SO-SCI method are possible. The iron complex has C_i symmetry, while the other two complexes are optimized without any symmetry treatment. Additionally, we carried out single-determinant calculations for the single-reference states of all three clusters. The convergence and the timings are compared with the ROHF method, which is discussed in Section 8.4.1. All calculations are done with both the def2-tzvp and the def2-tzvpvpp bases [213] using 20 processes on a single workstation with 2 x 10 Intel® Xeon® CPU E5-2660 v3 processors at 2.60 GHz and 512 GB memory.

We begin the discussion with the CASSCF calculations of the iron and the nickel complexes. In Reference [187], the active space includes only the 3d orbitals of the transition metal, resulting in a CAS(6,5) for the iron complex, and a CAS(8,5) for the nickel complex. However, the quintet state of the iron complex and the triplet state of the nickel complex are strongly dominated by the high-spin determinant such that some active orbitals are nearly doubly occupied. This leads to convergence problems for all methods, as already observed for the nickel complex in Reference [302]. In order to circumvent this problem, we did a double-d-shell calculation and added the five 4d orbitals into the active space. This results in CAS(6,10) active space for the iron complex and a CAS(8,10) for the nickel complex. The number of Super-CI and SO-SCI iterations for both complexes are shown in Table 8.5. The SO-SCI method shows the lowest computation time and the smallest number of iterations in all calculations, even though the Super-CI already performs to satisfaction. The computation time of SO-SCI with def2-tzvp is less than 7 hours, and compared to the reported calculation time of around 3 days for the PNO-NEVPT2 method [187] or up to 9.5 hours for the PNO-CASPT2 method [189] (both with the def2-tzvp basis), our CASSCF is no longer a bottleneck for the

Table 8.5: Number of MCSCF iterations, timings (in hours) and energies (in Hartree) for the CASSCF calculations of the iron and the nickel complex [187]. The number of basis functions is also shown in parenthesis.

Basis	State	Super-CI		SO-SCI		Energy
		It.	Time [h]	It.	Time [h]	
$\text{FeC}_{72}\text{N}_2\text{H}_{100}$						
def2-tzvp (2939)	$^3\text{A}_g$	23	2.2	20	1.8	-4156.154 789
	$^5\text{A}_g$	39	3.6	33	2.9	-4156.227 647
def2-tzvpp (3785)	$^3\text{A}_g$	25	3.4	21	2.8	-4156.206 566
	$^5\text{A}_g$	40	5.3	37	4.9	-4156.279 034
$[\text{NiC}_{90}\text{N}_{20}\text{H}_{120}]^{2+}$						
def2-tzvp (4175)	^1A	23	7.6	19	6.5	-6074.846 689
	^3A	25	8.3	17	5.9	-6074.923 467
def2-tzvpp (5154)	^1A	22	10.4	19	9.5	-6074.890 582
	^3A	26	12.2	17	8.6	-6074.966 405

subsequent treatments.

Next is the cobalt complex, where we used the DFT optimized geometry from Reference [292]. We tried to reproduce the CAS(20,13) active space of Reference [292], including the 3d orbitals of the two cobalt atoms and the 2p orbitals of oxygen. Although the AVAS starting guess of the 2p oxygen orbitals is reasonable, the 2p oxygen orbitals are rotated out in the CASSCF optimization, and the 3p orbitals of one of the cobalt atoms become active. Obviously, the 3p orbitals of cobalt yield a lower energy through dynamic correlation, even though the final 3p orbitals are also almost doubly occupied. This indicates that the three 2p orbitals of oxygen can be safely removed from the active space without changing the qualitative description of the molecule. The final CAS(14,10) active space reproduces the 3d orbitals of Reference [292]. However, we included the 2p oxygen orbitals in the AVAS starting guess generation, since this visually improved the starting orbitals. In addition, we did calculations with an increased active space of CAS(14,14) in which we added the four 4d orbitals associated with the four strongest occupied 3d orbitals. The starting guess of this active space is generated by adding the $4d_{z^2}$ and $4d_{xy}$ orbital in AVAS.

The computation time and the number of iterations of the cobalt complex are shown in Table 8.6. The cobalt complex is a rather difficult system with a large number of CFs contributing

Table 8.6: Number of MCSCF iterations, timings (in hours) and energies (in Hartree) for the CASSCF calculation of the cobalt complex with CAS(14,10) and CAS(14,14). The number of basis functions are displayed in parenthesis.

Basis	State	Super-CI		SO-SCI		Energy
		It.	Time [h]	It.	Time [h]	
CAS(14,10)						
def2-tzvp (3051)	¹ A	54	6.4	34	4.1	-5768.857 959
	³ A	86	10.2	49	5.9	-5768.857 641
def2-tzvpp (3937)	¹ A	51	9.0	35	6.5	-5768.898 833
	³ A	86	15.2	48	8.9	-5768.898 515
CAS(14,14)						
def2-tzvp (3051)	¹ A	39	5.1	34	4.9	-5768.941 538
	³ A	40	5.2	32	4.6	-5768.940 887
def2-tzvpp (3937)	¹ A	40	7.7	34	7.7	-5768.982 734
	³ A	40	7.7	35	7.9	-5768.982 084

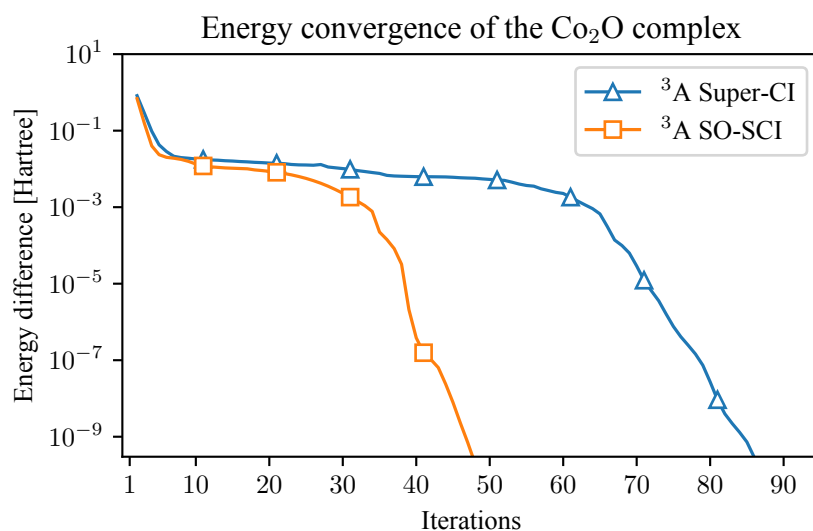


Figure 8.4: Energy convergence of the triplet calculation of the cobalt complex with def2-tzvp and CAS(14,10). Shown is the difference to the converged energy in Table 8.6.

on a similar level. The convergence of the Super-CI methods slows down drastically for the CAS(14,10) active space, and over 80 iterations are required in the triplet state calculation. The energy convergence of the slowly converging triplet state is also shown in Figure 8.4. In the beginning, the convergence of both methods is similar, but the Super-CI decelerates considerably between iteration 10 and 55. The plateau in the energy difference is due to the semi-logarithmic plot, and the energy change in each iteration is still more than 0.1 milli-Hartree. The energy decay in the SO-SCI also diminishes after iteration 10, but the method manages to escape this slow zone considerably faster and finishes in 49 iterations. If the 4d orbitals are added, the convergence is strongly improved. In case of the larger def2-tzvp basis, the timings between the SO-SCI and the Super-CI method are comparable. Here, the evaluation of the \mathbf{J}^{tu} and \mathbf{K}^{tu} matrices becomes noticeable, since a larger number of active orbitals is included. The Super-CI shows even a slightly faster computation time for the triplet state.

8.4.1 Single-reference calculations

We also carried out single-reference calculations for all three complexes. The multireference character of the triplet and quintet state in the iron complex is not strongly pronounced. Here, the open-shell determinant in the CASSCF calculation shows a CI coefficient of 0.953 for the triplet state and 0.992 for the quintet state, and a single-reference treatment is justified. The same applies for the triplet state in the nickel complex and the septet of the cobalt complex with leading CI coefficients of 0.989 and 0.967, respectively. Therefore, we did single-determinant calculations with a CAS(2,2) (triplet), CAS(4,4) (quintet) and CAS(6,6) (septet) active space, which is equivalent to a ROHF calculation. The number of iterations and the computation times are shown in Table 8.7. Results from the ROHF calculations with the ROHF program in Molpro [190] are presented as well. All calculations are started from the atomic density guess since this is also the starting guess in the ROHF program.

In case of the iron complex, we are not able to converge into the correct minimum with the HF program, and the obtained solution yields a significantly higher energy than the MCSCF calculations. Various level-shifts and experiments with Molpro's second RHF program [222] could not fix the problem. The difference to the SO-SCI energy is 29.1 milli-Hartree for the triplet and 1.2 milli-Hartree for the quintet, and it is therefore significant. Comparing the final orbitals shows that the ROHF program finds the wrong 3d open-shell orbitals. We can be sure about the correct 3d orbitals because we know the results of the CAS(6,10) calculation capturing all 3d orbitals. The Super-CI was able to find the correct minimum, but requires a

Table 8.7: Number of iterations (Iter.) and computation times (in hours) of the single-determinant calculations of the large transition metal clusters.

Basis	State	ROHF		Super-CI		SO-SCI		Energy
		Iter.	Time [h]	Iter.	Time [h]	Iter.	Time [h]	
$\text{FeC}_{72}\text{N}_2\text{H}_{100}$								
def2-tzvp	$^3\text{A}_g$	a)		98	8.8	42	3.4	-4156.068 370
(2939)	$^5\text{A}_g$	a)		81	7.3	28	2.3	-4156.160 091
def2-tzvpp	$^3\text{A}_g$	a)		98	12.6	42	5.0	-4156.120 185
(3785)	$^5\text{A}_g$	a)		82	10.6	28	3.4	-4156.211 440
$[\text{NiC}_{90}\text{N}_{20}\text{H}_{120}]^{2+}$								
def2-tzvp	^3A	26	7.3	28	9.1	16	5.0	-6074.798 901
def2-tzvpp	^3A	26	10.1	27	12.6	16	7.2	-6074.841 763
$\text{Co}_2\text{ON}_4\text{C}_{70}\text{H}_{106}$								
def2-tzvp	^7A	68	6.2	86	10.1	27	3.1	-5768.851 186
def2-tzvpp	^7A	67	9.1	87	15.2	29	5.1	-5768.892 008

a) No convergence into the right solution.

massive number of iterations while the SO-SCI method shows a nice and fast convergence into the correct solution.

In case of the nickel and the cobalt complexes, the Hartree-Fock yields the same solution but requires almost twice as many iterations as the SO-SCI program. Although the computation time per iteration is faster in the Hartree-Fock program, the SO-SCI method shows the lowest total computation time. The Super-CI method requires a higher number of iterations than Hartree-Fock (especially for the cobalt complex) and offers no advantage over the Hartree-Fock method. Therefore, the new SO-SCI method is strongly recommended for open-shell calculations. In the meantime, similar observations have been also reported by other colleagues in our institute, where the SO-SCI method is now routinely used for open-shell calculations.

8.5 Rydberg orbitals

This example demonstrates the effect of the WMK optimization at the beginning of the SO-SCI method (see Section 7.2.2) for the Rydberg orbitals of Furan and Pyrrole. Rydberg orbitals are chosen in this benchmark because the optimization has to rotate them into the active space, leading to large active-virtual rotations. The base active space without any Rydberg orbitals is a CAS(6,5) built from the five π orbitals of the systems. AVAS is not needed in these examples, since the atomic density guess already yields a suitable approximation of the five π orbitals. The 3s and the three 3p Rydberg orbitals are captured in a CAS(6,9) active space. All Rydberg orbitals are optimized together in a state-averaged calculation with C_{2v} symmetry, and the optimization includes the ground state (1^1A_1) as well as the four Rydberg states describing the excitations into the Rydberg orbitals: 2^1A_2 for 3s, and $1^1B_1, 1^1B_2$, and 2^1A_2 for the three 3p Rydberg orbitals.

In order to describe the extremely diffuse character of the Rydberg orbitals qualitatively, we used the d-aug-cc-pVTZ basis [303]. Here, density fitting was disabled due to the lack of a fitting basis. The structures are obtained from experimental data in Reference [304] and [305]. These calculations do not aim to be very accurate, since additional basis functions, single-state calculations, and a post CASSCF treatment are missing. More precise results for the Rydberg excitations of these molecules can for example be found in the work of Chrisitansen et al. [306, 307].

Table 8.8 shows the number of iterations and the computation time of the CAS(6,5) and the CAS(6,9) active space. The optimization of the active-virtual orbitals with the WMK method in the beginning is denoted as "SO-SCI (WMK)". In case of the Rydberg orbitals, the extra optimization reduces the number of iterations considerably compared to the SO-SCI method. However, one reason for the slow convergence of the SO-SCI method is a premature start of the L-BFGS acceleration in which the step restriction in the L-BFGS strongly damps the optimization in the beginning. Therefore, we did additional calculations, where the L-BFGS acceleration is not started until the step is lower than 0.1. This brings the number of iterations closer to SO-SCI (WMK) for Furan, but a difference is still visible in case of Pyrrole. The slow convergence of the Super-CI method is not connected to the L-BFGS acceleration, and it is therefore caused by the approximated treatment of the active rotations. The optimization of the π orbitals is not overly complex, and all methods converge quickly for the CAS(6,5) active space. Here, the additionally start with the WMK optimization has no large effect, but requires additional CI optimizations in the micro-iterations. We observed a similar behavior

Table 8.8: Iterations and computation time for the Furan and Pyrrole calculations. The CAS(6,9) active space includes the 3s and three 3p Rydberg orbitals in addition to the five π orbitals.

Method	Furan				Pyrrole			
	CAS(6,5)		CAS(6,9)		CAS(6,5)		CAS(6,9)	
	Iter.	Time [s]						
Super-CI	10	10	47	71	11	13	52	102
Super-CI ^{a)}	10	10	47	76	11	13	52	102
SO-SCI	10	10	27	43	10	12	21	47
SO-SCI ^{a)}	10	10	16	26	11	14	16	32
SO-SCI (WMK)	8	8	13	22	9	11	11	25
UC-AH	9	33	17	88	9	45	23	145
UC-AH ^{a)}	9	34	16	83	9	47	14	99
WMK (QN-Coupled)	3	14	4	30	3	19	4	39

^{a)} The L-BFGS acceleration is not started until the step is lower than 0.1.

in other cases where the active orbitals are qualitatively correct in the beginning. However, the computational overhead from the extra WMK optimization might become significant for larger active spaces, and therefore the start with the WMK optimization is implemented only as an option.

8.6 The Ni(NHC) catalyzed rearrangement

This section presents CASSCF calculations of the catalyzed rearrangement of a vinylcyclopropane (VCP) species to the cyclopentene versions. The reaction is obtained from the work of Zens et al. [293] in which the rearrangement of several VCPs with different catalysts have been investigated experimentally. Additionally, a first computational analysis at the DFT level is also presented in Reference [293] by Florian Bauer from our institute with whom we collaborated for this project. Throughout this section, we use the same labelling as in Reference [293]. Our discussion is limited to the rearrangement of the endo-8b and endo-8c species which are displayed on the left hand side in Figure 8.5. The only structural difference between the two species is the position of the methyl group. A yield of 38% has been found for the endo-8c structure while the endo-8b species shows no rearrangement. The question why a rearrangement is only observed with the endo-8c structure is the main interest in the theoret-

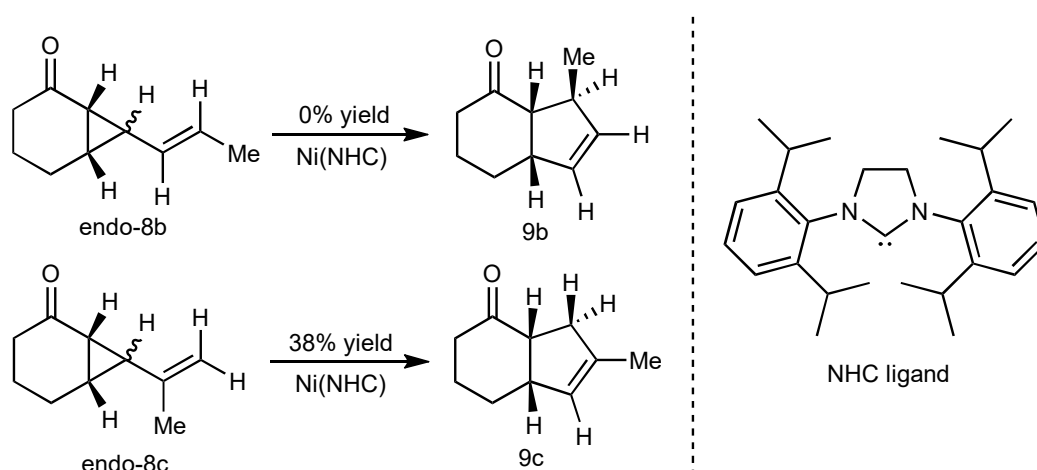


Figure 8.5: The left hand side shows the rearrangements and the yields from the endo-8c and endo-8b reactants to the 9b and 9c products. The NHC ligand which forms the catalyst together with nickel is presented on the right hand side. The structures are reproduced from Reference [293].

ical investigation. The catalyst used in the reaction is formed by Nickel and a N-heterocyclic carbene (NHC) ligand. The structure of the ligand is shown in Figure 8.5 on the right hand side. The formation of the catalyst from a $\text{Ni}(\text{COD})_2$ compound and a imidazolium salt has been investigated in detail in Reference [293] and is not discussed here. The reaction takes place at 120 °C in a solution of toluene.

A possible mechanism of the catalyzed rearrangement has been already presented in Reference [293], and the reaction cycle of the endo-8c rearrangement is displayed in Figure 8.6. The seven intermediate (INT) and transition state (TS) structures have been optimized by Bauer at the DFT level and are obtained from the Supplementary Information of Reference [293]. The absorption of the reactant and the separation of the product have been neglected in this cycle. Calculations with the B3LYP-D3 DFT functional [7] and a subsequent correction with B2PLYP [308] have been presented in Reference [293]. Solvent effects of the toluene were treated with COSMO [309]. Additionally, zero-point energy corrections have been obtained from the harmonic approximation and B3LYP-D3 calculations. The contrary yields of the two species has been explained by different overall reaction barrier heights. However, after the publication, Bauer has done explicitly correlated PNO-CCSD(T)-F12 [310] calculations to obtain more accurate results. These agreed more with the B3LYP-D3 results implying that the B2PLYP correction is most likely systematically wrong. Furthermore, the energies of the F12a and F12b approximations in the PNO-CCSD(T)-F12 varied strongly (up to 20 kJ/mol)

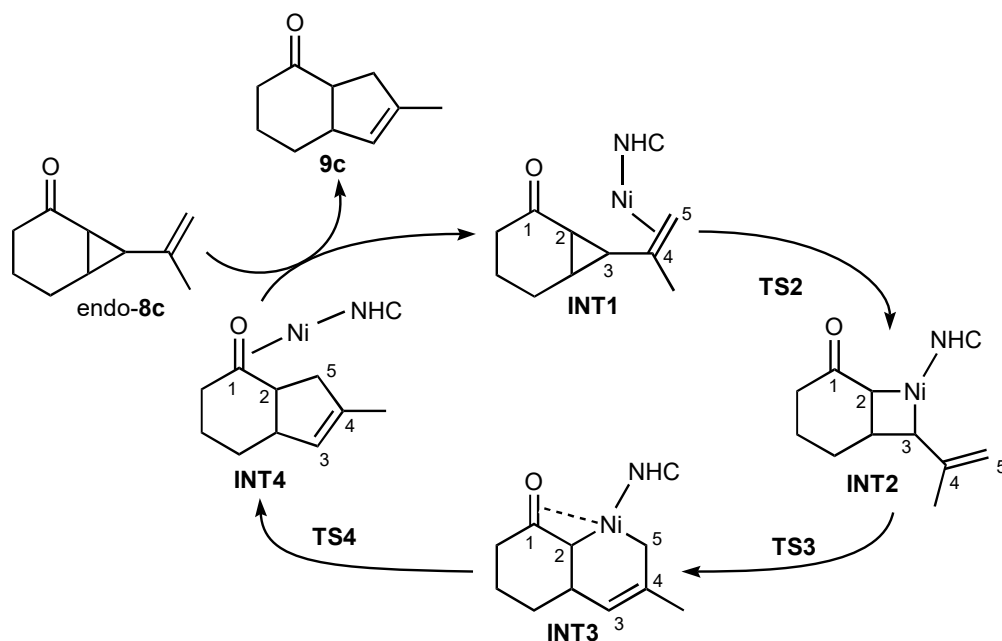


Figure 8.6: Reaction cycle of the endo-8c rearrangement. The carbon atoms forming bonding and anti-bonding orbitals with nickel are additionally labelled by numbers. The structures and the reaction cycle are reproduced from Reference [293].

indicating that this might be a multireference case. In order to investigate the strength of the multireference character, we did CASSCF calculations for the whole reaction cycle.

CASSCF calculations along reaction paths are particularly challenging due to the fact that the multireference character of the wavefunction and the active orbitals can strongly vary for the different geometries. However, the active space should contain the same set of orbitals in all calculations, since otherwise the correlation contribution in the CAS wavefunction strongly changes and the energies are not comparable. The construction of the active space was a cumbersome process despite the AVAS tool. It was helpful to interpolate between the structures such that an active space could be propagated through the reaction without heavy changes in the calculations. However, the finally obtained active space is robust enough to be passed through the reaction without the interpolation.

Along the reaction, the $3d_{xz}$ orbital of nickel (with the imidazole oriented in the xz plane) forms bonding and anti-bonding orbitals with the surrounding oxygen and the carbon atoms labeled by 1 to 5 in Figure 8.6. Each involved atom participates in this bond with one of the three $2p$ orbitals, and this interaction with nickel shows a considerable multireference character. Furthermore, the sigma bond breaking between carbon atoms 2 and 3 in TS2 and

the sigma bond forming of carbon atoms 2 and 5 in TS4 also feature a weak multireference contribution. Here, the sigma orbitals are formed by the same 2p orbitals which interact with nickel in the other structures, and therefore no additional orbitals are required in the active space. The resulting seven natural active orbitals are shown in Figure 8.7 for the INT1, the TS3 and the INT4 state together with the sigma bond between nickel and the NHC ligand. In the initial structure INT1, the MOs 161 and 164 are the π and π^* orbital of oxygen and carbon atom 1. These two orbitals interact with nickel in the INT4 state, which can be seen in the MOs 155, 162, and 163 in INT4. The sigma bond of carbon atoms 2 and 3 in INT1 (MO 156 and 169) is broken, and the involved 2p orbital of carbon atom 3 forms first a sigma bond with nickel (154 in TS3) and later a π and π^* orbital (MO 161 and 164 in INT4) with carbon atom 4. The π and π^* orbital of carbon atoms 4 and 5 interact first with nickel in INT1 (MO 155, 162, and 163). In TS3, the carbon atom 2 is also involved in this interaction (MO 161, 162, 163 and 164), and in structure INT4, the carbon atoms 2 and 5 form a new sigma bond shown in the MOs 156 and 164 in Figure 8.7.

The four remaining 3d orbitals of nickel hardly exhibit any interaction with the ligands and are basically isolated in the reaction. However, excitations into the 4d orbitals can yield a significant energy lowering through dynamic correlation, and they rotate into the active space for some structures. We hence added all 3d orbitals of nickel as well as the four 4d orbitals associated with the isolated 3d orbitals. In total, this yields a CAS(16,15) space, and first calculations of the endo-8c rearrangement confirmed the multireference character.

We begin the calculations at the last intermediate structure, since INT4 is better oriented for the AVAS program. It is possible to construct a CAS(14,13) with AVAS, and the remaining two 2p orbitals are rotated in manually in a subsequent calculation. From here, the reaction is calculated backwards, where the previous orbitals are reused as the starting guess. All calculations are performed with the def2-tzvp basis [213] which has also been used in Reference [293]. Since nearly 100 atoms are involved in the reaction, we can only use the first-order methods. As a benchmark, we did the CAS(16,15) optimization with the Super-CI and the SO-SCI method. Here, the Super-CI method requires about 50% more iterations than the SO-SCI method while showing a similar computation time per iteration. Furthermore, the Super-CI converged into a higher energy in the first CAS(14,13) calculation yielding another set of active orbitals.

However, the CASSCF optimization of the TS3 state rotates MO 154 in Figure 8.7 with the sigma bonding orbital of nickel and the NHC ligand (MO 155). To maintain a consistent active space in all computations, we additionally moved this sigma orbital into the active space. This

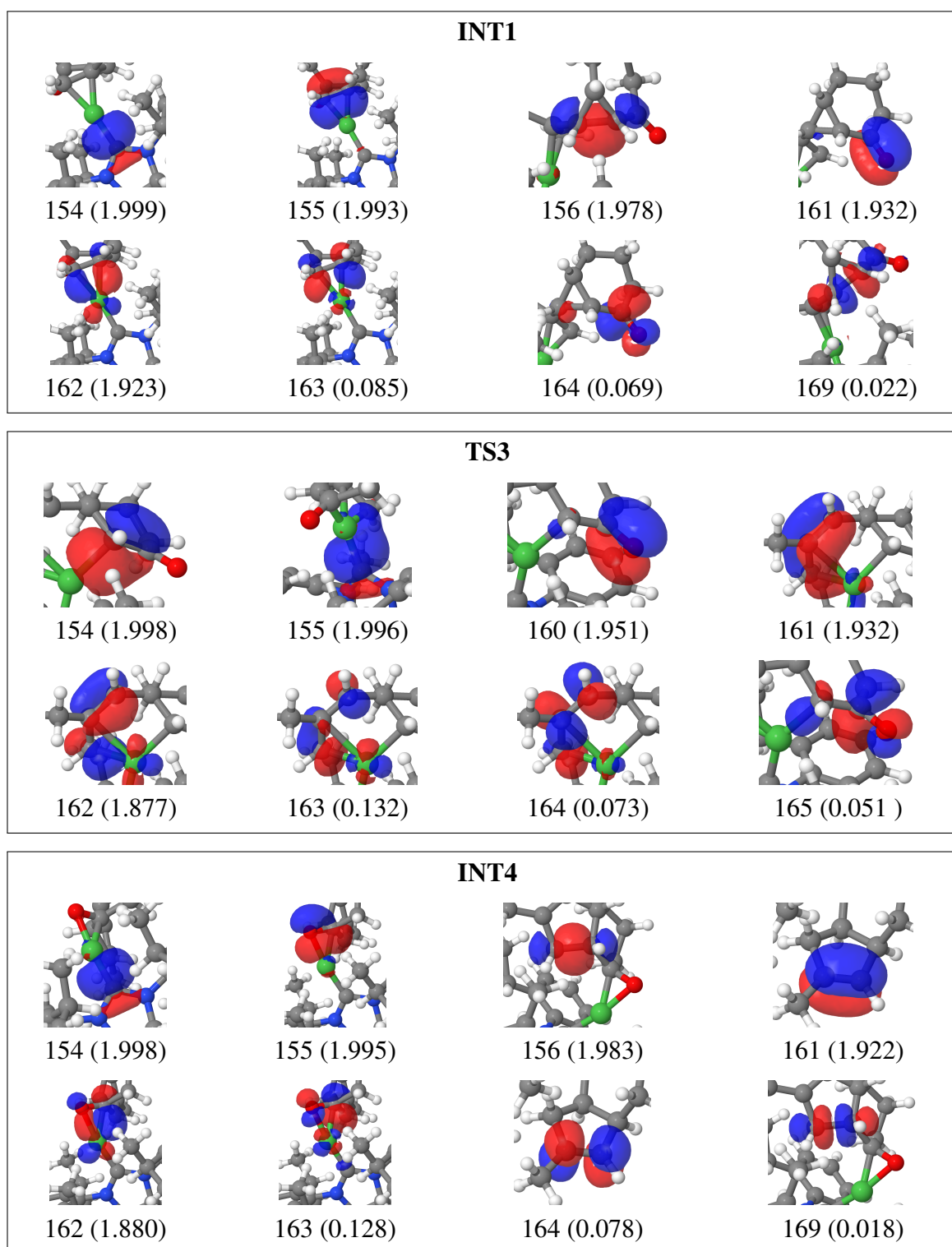


Figure 8.7: The natural active orbitals of the INT1, TS3, and INT4 state of the endo-8c rearrangement. The isolated 3d and 4d orbitals are neglected. Additionally, we display the orbital numbers and natural orbital occupation numbers in parenthesis.

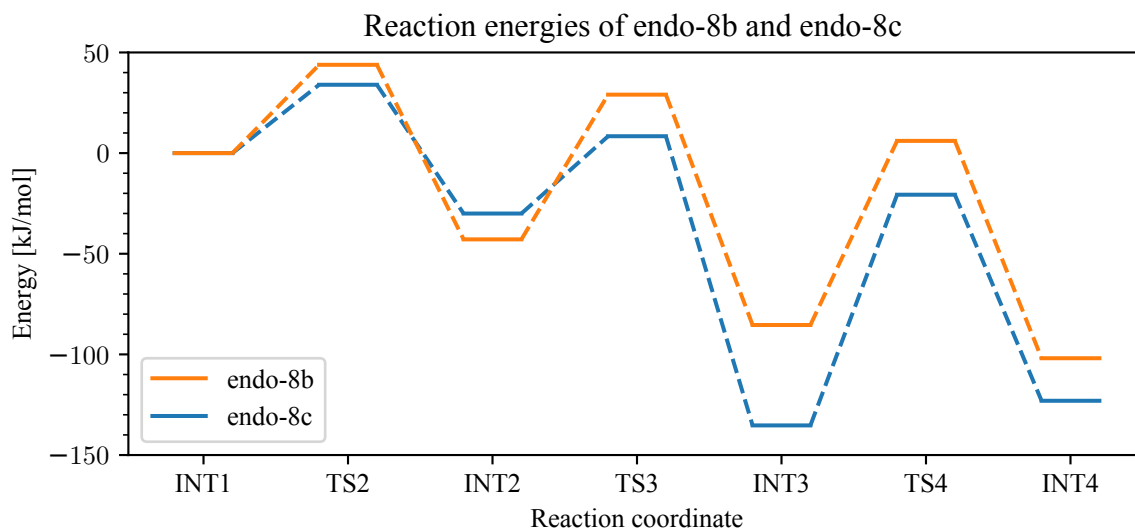


Figure 8.8: Reaction energies calculated with PNO-CASPT2 for the endo-8b and the endo-8c species. The energy is relative to the first intermediate state INT1.

results in a CAS(18,16) that contains all orbitals interacting with nickel at some point. The CI expansion of the CAS(18,16) space includes 130 873 600 determinants, and it is the largest CI presented in this thesis. However, the 3p and 3s outer core orbitals of nickel now rotate easily with almost doubly occupied active orbitals during the optimization yielding a slightly lower energy. To converge into the desired local minimum, we did several CASSCF calculations for each structure, where either the 3p and 3s orbitals or the lowest four active orbitals are frozen. These two MCSCF optimizations are alternated until the energy is fully converged, and the final orbitals are obtained from the calculation with the nickel core orbitals frozen. This procedure is used for both the endo-8b and endo-8c system.

Subsequently, CASPT2 calculations with the PNO-CASPT2 [188, 189] program are performed to obtain the final energies. Here, the outer core orbitals of nickel are included in the correlation, since the swapping with the active orbitals already clarified the importance of correlating these orbitals. The final reaction energies are presented in Figure 8.8, and they strongly deviate from the results in Reference [293]. However, we believe that the PNO-CASPT2 results are more trustworthy, since the clear multireference character of the system is treated appropriately. The highest barrier is extremely similar in both systems, and therefore we cannot reproduce the original statement that explains the different yields by the varying reaction rates. Our calculations do not include any solvent effects since this is not possible with the current implementation. However, we know from the DFT calculations that they are considered neg-

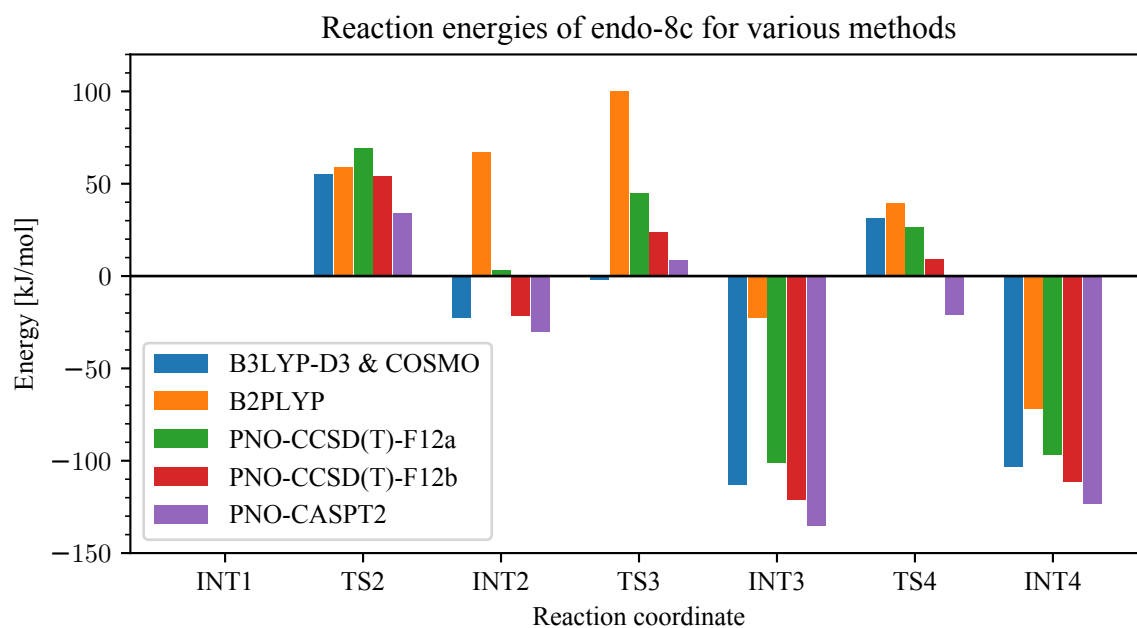


Figure 8.9: The reaction energies of various methods for the endo-8c species. All energies are relative to the corresponding energy of the first intermediate state INT1. The B2PLYP values are obtained from the Supplementary Information in Reference [293], the other single-reference results are provided by Bauer.

ligible for this system. More dominant are the zero-point corrections, which are unfortunately too expensive to be calculated on the PNO-CASPT2 level. Each PNO-CASPT2 calculation requires a computation time of nearly 24 hours using two processes. A parallelization with more processes is not possible because of the huge memory requirements in the CASPT2 program induced by the large active space. Nevertheless, in a first approximation, we can add the zero-point energy corrections provided by Bauer which are calculated using B3LYP-D3. This shifts the first barrier by 16 kJ/mol for endo-8c and 29 kJ/mol for endo-8b, which is significant compared to the PNO-CASPT2 barrier height of 34.0 kJ/mol and 43.9 kJ/mol for endo-8c and endo-8b, respectively. However, the final barrier heights are not large enough to explain why the endo-8b rearrangement is not observed as both barriers still allow a fast reaction according to transition state theory. We can thus conclude that the difference between the endo-8b and the endo-8c rearrangement cannot be found in the reaction mechanism. Another route for investigation could be the absorption of the reactant, since here the outer position of the methane group in endo-8b might inhibit the process.

A comparison of the reaction energies calculated with B3LYP-D3, B2PLYP [293], PNO-

CCSD(T)-F12a,-F12b (all kindly provided by Bauer) and our PNO-CASPT2 values is presented in Figure 8.9 for the endo-8c system. The B2PLYP values strongly deviate from the other results, indicating that these energies are not very reliable. The severe differences between the F12a and F12b energies in the coupled cluster results are visible for all states. The best agreement is found between the PNO-CASPT2 and the PNO-CCSD(T)-F12b with a still a difference between 10 and 30 kJ/mol. The overall picture looks very similar for the endo-8b system.

8.7 RASSCF calculations of Mg-porphyrin

Although CASSCF is probably the most typical application, all presented methods are also capable of running calculations for general MCSCF wavefunctions. This section discusses an example of a RASSCF optimization of the Mg-porphyrin complex. Derivatives of the porphyrin molecule are important in biochemical processes. An example is Fe-porphyrin (also known as heme) which plays an essential role in the oxygen transport in the human metabolism [311]. The Mg-porphyrin complex is serving as a model for the structurally similar chlorophyll molecules required for the photosynthesis in plants [312].

The π system of the free-base porphyrin molecule shows a multireference character [147], and it has been concluded [150, 313, 314] that the inclusion of all 24 π orbitals into the active space is necessary for an accurate description of the porphyrin molecule and its derivatives. In the recent years, numerous calculations of the Fe-porphyrin complex including all π orbitals have been presented with various approximating full-CI solvers [147, 150, 161, 179, 313–316] improving the agreement between theory and experiment.

In this section, we use the RASSCF method (see Chapter 3) to calculate the first vertical

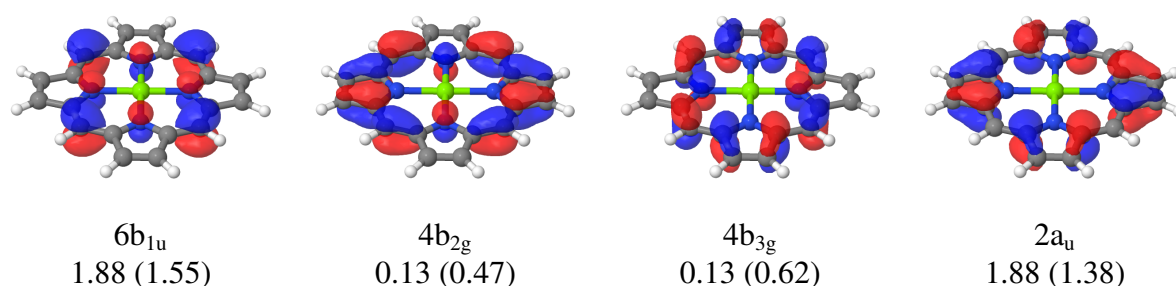


Figure 8.10: The four natural orbitals RAS2 orbitals of Mg-porphyrin. The occupation numbers of the RAS(26,24) calculation are shown for the 1A_g (no parenthesis) and the 1E_u (in parenthesis) state.

excitation energy of the Mg-porphyrin complex including the full π system. We only allow a maximum of two holes in RAS1 and two electrons in RAS3, hence we consider only single and double excitations from RAS1 and into RAS3, respectively. Since the full-CI structure of the wavefunction is destroyed, active-active rotations are additionally included in the orbital optimization.

Recently, occupation numbers of all 24 π orbitals of the free-base porphyrin complex have been presented by Li Manni et al. [147] using the FCIQMC method and a CAS(26,24). The interaction between the magnesium orbitals and the surround π system is considered to be very weak, since all occupied magnesium orbitals are isolated and energetically close to the core orbitals. Therefore, the active space of Mg-porphyrin can be assumed to be similar to the one of free-base porphyrin. In the first three states, there are only four natural orbitals with occupation numbers strongly deviating from two and zero [147]. These four orbitals, also known as the Gouterman orbitals [317], are displayed in Figure 8.10 with the occupation numbers for the ground state (1A_g) and the first excited state (1E_u) of Mg-porphyrin. Mg-porphyrin features a D_{4h} symmetry, but all calculations are carried out in the D_{2h} symmetry for technical reasons with the molecule oriented in the xy plane. The excitation into the first 1E_u state can be then described by the $^1B_{3u}$ state in D_{2h} symmetry [318].

The RAS of Mg-porphyrin is constructed by putting the nearly doubly occupied orbitals into RAS1 (2-5b_{1u}, 1-3b_{2g}, 1-3b_{3g}, 1a_u), the four orbitals with varying occupations into RAS2 (6b_{1u}, 4b_{2g}, 4b_{3g}, 2a_u), and the nearly non-occupied orbitals into RAS3 (7-8b_{1u}, 5-6b_{2g}, 5-6b_{3g}, 3-5a_u). The same RAS space has also been used in other calculations of free-base porphyrin [101] or Mg-porphyrin [318,319]. Unfortunately, no excitation energies on this RASSCF level have been reported in the References [318,319]. Additionally, we run CAS(4,4) calculations with the four RAS2 orbitals in the active space to measure the impact of the missing π orbitals. The structure of the Mg-porphyrin complex is obtained from the Supplementary Information of Reference [147], and all calculations are done with the def2-atzvpp basis set. We have also run calculations with the smaller def2-tzvp basis set, but the results only slightly differ, indicating that the excitation energy is not highly depending on the basis set choice.

Table 8.9 shows the number of iterations and the computation time of the first-order methods and the WMK method with and without the L-BFGS acceleration. In case of the CAS(4,4) active space, the L-BFGS acceleration only improves the Super-CI and the SO-SCI methods, indicating that the orbital-CI coupling is weak in the CAS(4,4) calculations. The SO-SCI calculation without the L-BFGS acceleration requires an additional level-shift of 0.3 for the inactive-active rotations in the orbital Hessian, since otherwise the convergence slows down

Table 8.9: Number of iterations (Iter.) and computation times (in minutes) for the Mg-porphyrin calculation with an active space of CAS(4,4) and RAS(26,24).

Method	CAS(4,4)				RAS(26,24)			
	1A_g		$^1B_{3u}$		1A_g		$^1B_{3u}$	
	Iter.	Time	Iter.	Time	Iter.	Time	Iter.	Time
Without L-BFGS acceleration:								
Super-CI	24	6.9	33	9.4	65	22.2	74	26.2
SO-SCI	19 ^{a)}	4.4 ^{a)}	20 ^{a)}	4.5 ^{a)}	68	32.5	40	19.8
UC-AH	5	19.6	7	26.2	68	276.5	40	165.0
WMK (Unc. (Orb))	3	14.0	3	14.2	4	26.4	4	25.5
With L-BFGS acceleration:								
Super-CI	13	3.9	16	4.7	22	7.9	23	8.4
SO-SCI	11	2.6	12	2.8	22	10.9	17	8.7
UC-AH	5	19.6	6	22.8	20	84.2	16	67.7
WMK (QN-Coupl.)	3	14.0	3	14.2	3	18.5	3	18.8

^{a)} Additional level-shift of 0.3 for the inactive-virtual rotations.

considerably and nearly hundred iterations are required. Again, the level-shift is not needed if the L-BFGS acceleration is activated.

The L-BFGS acceleration becomes more important in the RASSCF optimization, and a strong improvement is visible for all methods. This coincides to the well known observation that the additional active-active rotations increase the orbital-CI coupling through a nearly linear dependency in the variational problem [65]. This linear dependency can be alternatively removed by considering only double excitations in the RAS definition. The convergence of the Super-CI method and the SO-SCI method is very similar in the 1A_g state calculation, but the time per iteration is lower in the Super-CI method. The computation of the active Hessian in the SO-SCI method is still negligible for this large number of active orbitals (7 seconds in total), and the main difference is the assembly of the two-electron integrals required in the SO-SCI method. The WMK method shows its clear advantage over the UC-AH method, in particular in the RASSCF case.

The results of the first vertical excitation energy are presented in Table 8.10. Additionally, results with the MRPT2 method [101] are shown for the CAS(4,4) and RAS(26,24) active space, respectively. The 2p and 2s orbitals of magnesium are included in the MRPT2 treatment, and a level shift of 0.3 is used to avoid problems with intruder states. Furthermore, ex-

Table 8.10: Vertical excitation energy of ${}^1A_g \rightarrow {}^1E_u$ (${}^1B_{3u}$) of Mg-porphyrin.

Method	Active Space	Excitation energy [eV]
MCSCF	CAS(4,4)	3.55
MCSCF	RAS(26,24)	2.89
FCI-QMC [147]	CAS(26,24)	2.50
MRPT2	CAS(4,4)	1.75
MRPT2	RAS(26,24)	2.04
Experiment [320]		2.20
Experiment [321]		2.17

perimental values [320, 321], and the result from the FCIQMC calculation of Li Manni [147] are displayed. The excitation energy of the CAS(4,4) calculation resembles the previously reported 3.59 eV in Reference [318] but deviates strongly from the experiment. The RASSCF improves the results strongly and is already closer to experiment than the largest CASSCF calculation presented in Reference [318] in which an excitation energy of 3.06 eV is obtained for a CAS(15,18). This demonstrates that the inclusion of all π orbitals is crucial. With a CAS(26,24) as achieved by Li Manni et al. [147], the CASSCF result is further improved. The MRPT2 with the CAS(4,4) strongly underestimates the excitation energy, which has also been observed in the work of Rubio et al. [318]. The subsequent MRPT2 treatment with the RAS(26,24) space reproduces the experimental values within the expected accuracy of 0.3 eV for the MRPT [322].

8.8 Computational performance

A serious amount of time was spent to improve the efficiency of the program and especially to achieve a good parallelization. Today, even small computers include numerous CPUs so that parallelization is of key importance for an effective use of modern computers. We therefore rewrote most parts the MCSCF program multi in Molpro [190] in order to improve efficiency and robustness. The first multi implementation is now over 30 years old, and the computational architecture has changed substantially in the meantime. Memory requirements have been more strict at that time. Often, even small data was stored on disk, while today a few megabytes difference in memory is not critical. The unchanged routines from the original implementation are responsible for the input processing and initialization as well as for analyzing and storing the wavefunction information. This simplifies the communication with the

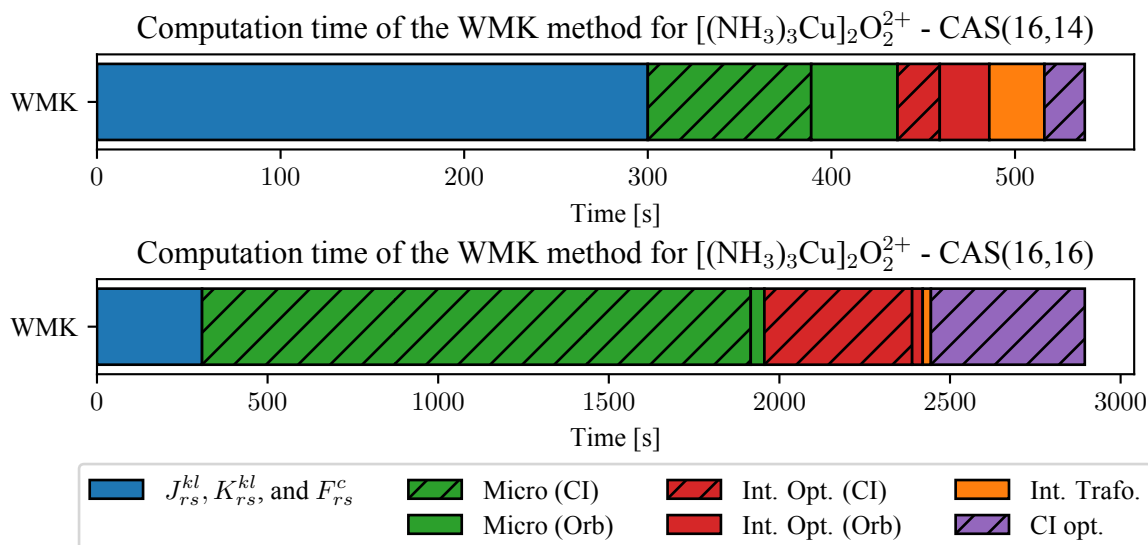


Figure 8.11: Computation times of the QN-coupled WMK optimization of the $[(\text{NH}_3)_3\text{Cu}]_2\text{O}_2^{2+}$ isomerization at $F=0$. The calculations are run with 20 processes.

Molpro environment. The density fitting routines for the integral generation are now based on a very efficient program written by Hans-Joachim Werner. The program has originally been designed for the Hartree Fock program [222] and is adjusted to compute the electron integrals \mathbf{J}^{kl} and \mathbf{K}^{kl} as well. The original determinant and CSF framework is reused [198], but it has been heavily improved through an efficient parallelization implemented by Peter Knowles and Iakov Poliak. However, the Davidson program for the CI optimization has been completely rewritten, since convergence problems in the old implementation are sometimes observed.

A comparison with the old code is possible in the second-order MCSCF, and it is shown in Section 8.2 in Figure 8.1 for the aromatic benchmark set. This version of the old code already includes the modernized density fitting and CI routines, and the large difference in the computation time is achieved by the more efficient and parallelized new program. The largest difference is observed in the construction and contraction of the G_{rs}^{kl} matrices. Here, a blocking of the rs indices yields a massive improvement in the computation time, and a speedup of more than 100 is obtained in the \mathbf{G}^{kl} matrix generation (parallelization included). An example of the distribution of the computation time in the second-order method is presented in Figure 8.11 for the $F=0$ calculation of the $[(\text{NH}_3)_3\text{Cu}]_2\text{O}_2^{2+}$ isomerization with the CAS(16,14) and CAS(16,16) active spaces (see Section 8.3). The results are shown for the QN-Coupled version of the WMK method. In case of the CAS(16,14) more than half of the computation time is spent in the calculation of two-electron integrals followed by the CI optimization in the micro-

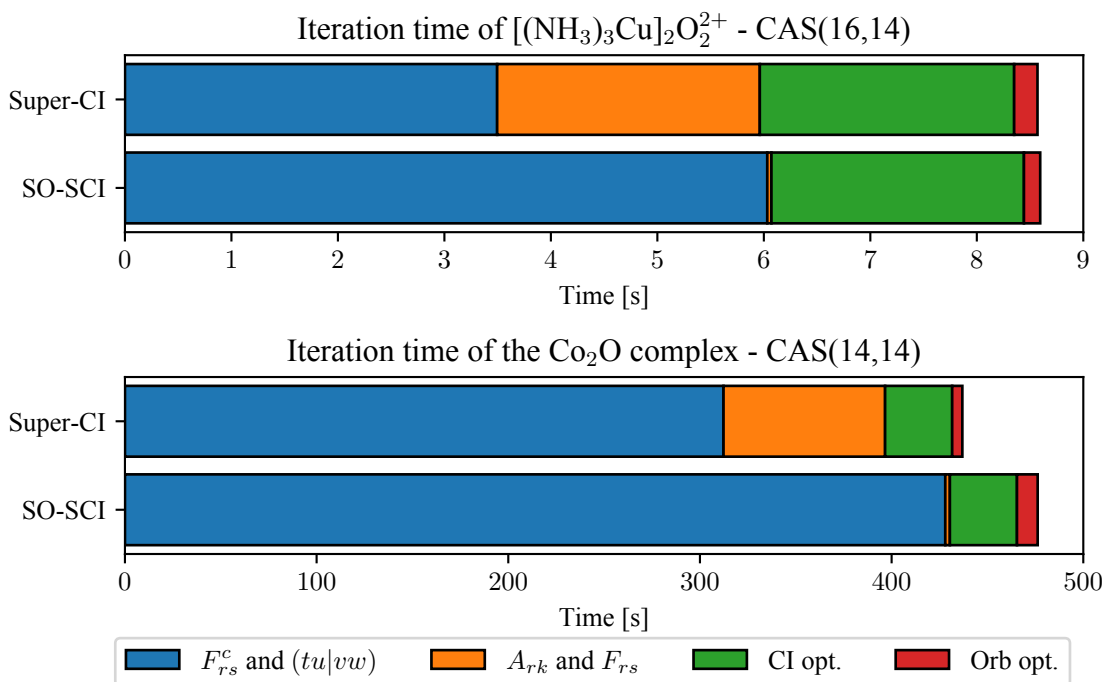


Figure 8.12: Computation time per iteration of the first-order $[(\text{NH}_3)_3\text{Cu}]_2\text{O}_2^{2+}$ CAS(16,14) optimization at $F=0$ and the singlet CAS(14,14) Co_2O complex example. The calculations are run with 20 processes.

iterations and internal optimization. The orbital part in the internal optimization is dominated by the internal transformation. Less than ten percent of the total computation time is required for the second-order orbital optimization. If the active space is increased to CAS(16,16), the CI evaluations dominates the whole optimization, which can be seen on the striped pattern in Figure 8.11.

The computation time of the first-order methods is shown in Figure 8.12 for the same CAS(16,14) example. Here, the time is displayed for a single iteration to enable the comparison between the Super-CI and the SO-SCI method. The different density fitting evaluations of the integral based terms (blue and orange) are clearly visible. In the SO-SCI method, the evaluation of the Coulomb and exchange integrals leads to a larger computation time in the first density fitting routine (blue), but the subsequent calculation of the generalized Fock matrix and the A_{rk} matrix is negligible. In case of the Super-CI method, additional density fitting routines are required in the latter step, but the total computation time is similar in both methods. The time spent on the CI optimization is equal in both methods, since the same thresholds are used

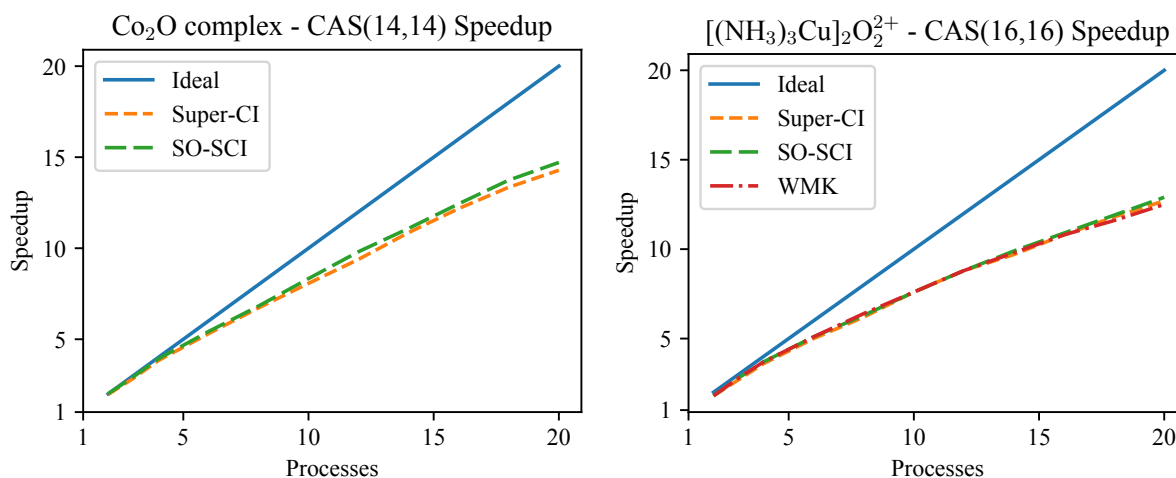


Figure 8.13: Speedup relative to the non-parallel execution for the Co_2O complex on the left hand side, and for the $[(\text{NH}_3)_3\text{Cu}]_2\text{O}_2^{2+}$ example on the right hand side.

in the Davidson method. The orbital optimization in the Super-CI method is slightly longer, since the action of the overlap matrix is noticeable here. However, the picture changes for the second example, which is the singlet CAS(14,14) def2-tzvp optimization of the Co_2O complex presented in Section 8.4. Here, the computation of the \mathbf{J}^{tu} and \mathbf{K}^{tu} integrals takes considerably more time than the density fitting evaluation of all intermediates in the Super-CI method. Also, the orbital optimization in the SO-SCI method takes slightly longer, since a very large Hessian matrix is included. However, in this calculation, the SO-SCI can compensate for the longer iteration time by a faster convergence.

Last, we present speedup curves in Figure 8.13 for the two examples showing the acceleration through parallelization. In case of the large Co_2O complex, the first-order optimization is terminated after 10 iterations to avoid the lengthy single-core computations while this premature abortion hardly affects the speedup. The Co_2O calculations are strongly dominated by the integral evaluation routines. Therefore, the obtained speedups are very similar to the Hartree-Fock program in which a speedup of around 15 has also been reported for 20 processes [222]. In case of the $[(\text{NH}_3)_3\text{Cu}]_2\text{O}_2^{2+}$ calculation, a lower speedup of 12.5 can be obtained in all methods due to the slightly less efficient parallelization in the CI optimization which dominates this example. Here, the marginally better parallelized CSF code has been used. Another very important observation is that the speedup is nearly identical in all methods. Therefore, the discussions and conclusions presented in this chapter are also transferable to non-parallel computations.

9 | Conclusion and Outlook

In this work, we improved the stability of the second-order WMK method, and, furthermore, developed a new first-order MCSCF which allows a robust optimization of large molecules. We first introduced a new micro-iteration optimization for the WMK method where the explicit orbital-CI coupling is included. While this solves the convergence difficulties for strongly coupled cases, the additional CI evaluations introduced by the explicit coupling cannot always be compensated for. A lowering in computation time is only observed for cases with a severe orbital-CI coupling. To improve this unsatisfying result, we developed a second approach in which the coupling is treated on an approximated level with a QN method. Here, the QN-coupling can be implemented in form of a general convergence accelerator based on the L-BFGS optimization. The accelerated WMK method provides a MCSCF convergence as fast as the explicit coupled version but without any additional CI evaluations. The convergence is also improved in more weakly coupled systems, and the QN-coupling is superior to all other implemented and tested optimization strategies in the WMK method. Furthermore, the convergence accelerator has a general structure which allows an usage beyond the MCSCF context. An application in other optimization problems might be an interesting consideration in future method development.

In case of larger molecules, the second-order MCSCF becomes less favorable because of the expensive evaluation of the two-electron integrals required in the orbital Hessian. To perform MCSCF for more than 100 atoms, we developed a first-order method and compared different orbital optimizations. We implemented the Super-CI method of Roos [64, 65] and discussed its connection to MRPT. Furthermore, we presented a new orbital optimization (SO-SCI) in which the active orbitals are still optimized on a second-order level while the remaining inactive-virtual rotations are treated by Super-CI. Here, the two-electron integrals required in the active Hessian can be efficiently computed by an additional assembly of the Super-CI density fitting intermediates, and no large computational overhead compared to the Super-CI method is required.

The convergence of the new SO-SCI method is superior to the Super-CI method, and a significantly lower number of iterations is observed in all our calculations. In combination

with the L-BFGS accelerator, this yields a robust convergence, and less than 50 iterations are observed even for difficult systems. Here, the accelerator does not only include the missing orbital-CI coupling, but also compensates for approximations introduced by the Super-CI. In almost all cases, the SO-SCI method provides the lowest computation time, so we can conclude that the SO-SCI offers an optimal compromise between efficiency and robustness. Much effort was spent on an efficient and parallel implementation, and the largest calculations with 231 atoms and 5154 basis functions required less than 10 hours computation time using 20 processes. Together with the local PNO-CASPT2 method, it is now possible to perform large scale multireference calculations in Molpro [190].

Furthermore, we found that a preceding HF optimization is not required to obtain a proper starting guess for the MCSCF optimization. All our starting guesses are generated using the AVAS procedure [164] based on orbitals of an atomic density guess [222]. If properly used, this yields the qualitatively correct starting orbitals, and our MCSCF methods are robust enough to converge from these guesses. This is especially important in case of the first-order MCSCF in which the pure orbital optimization requires only a slightly higher computation time as the HF.

Furthermore, the SO-SCI method shows a more reliable and even faster convergence of single-determinant open-shell calculations than the usually used ROHF. The application of the SO-SCI method is therefore not only limited to the MCSCF method, but it is also strongly recommended for restricted Hartree-Fock calculations of open-shell systems.

Motivated by the strong performance in the HF case, a future project could be the development of a similarly combined optimization for other orbital optimizers. A first application could be the configuration-averaged Hartree-Fock (CAHF) in which all possible excited states are included. In this case, the state-averaged density is independent of the CI coefficients, since the density can be written as a trace. This allows the separation of the orbital and CI optimization, and the orbital optimization in CAHF is usually done with a conventional ROHF optimization [229]. Here, a strong improvement in the convergence is expected through the SO-SCI method.

Additionally, the integration of approximated CI solvers as for example the FCIQMC or the DMRG method into the first-order MCSCF is straightforward. This is possible, since the orbital optimization depends only on the densities which are usually provided by the approximated CI. The acceleration with the L-BFGS is still possible, since it can work without any knowledge about the CI problem. We already provided for this scenario when writing the first-order MCSCF program such that first results could be achieved relatively quickly.

Acknowledgements

First of all, I would like to express my deep gratitude to Prof. Hans-Joachim Werner, who supported me constantly with his great scientific knowledge and experience, even though it was clear that this project will interfere with his well-earned retirement. I have learned a lot in the last years, not only about the MCSCF theory, and most of its results from our work together.

Furthermore, I would like to offer my special thanks to Prof. Peter Knowles not only for examining the thesis, but also for many helpful discussions and contributions. He also invited and welcomed me several times in Cardiff and did not hesitate to make my stay as pleasant and productive as possible. Also, I want to thank Prof. Joris van Slageren for taking the chair in the examination board.

During the last four years, I met many people who showed their support in various ways, and I would like to sincerely thank all of them. In particular I want to thank my former PhD colleagues Mark Dornbach, Max Schwilk, Christine Krause, and Filipe Menezes for intense discussions and for ensuring such a relaxed atmosphere. Also, I am very grateful to Qianli Ma for his support on efficient parallel programming and to Stefan Jagiella for keeping (not only) the computational infrastructure running. I also thank Florian Bauer for his work on the catalyst reaction, and Iakov Polyak and Marat Sibaev for their work on the CI program and the iterative solver. Moreover, I would like to thank Alexander Denzel and Josh Black for all our institute activities after work.

Furthermore, I wish to thank Prof. Bernard Haasdonk for being my milestone examiner and for his support during my undergraduate studies. I also want to acknowledge the help of Andy May for fixing some and reporting even more of my bugs in the Molpro program. Special thanks should also be given to Josh Kirsopp for making my stays in Cardiff even more enjoyable with many activities and trips on the weekends.

I would also like to thank my friends, especially Jonas, Markus, Nina, Thomas, Philipp, and my sister Hanna for sometimes necessary distraction, and my family for all their everlasting encouragement. Above all, I want to thank Hannah Schrader for her patience and constant support, since this work would have hardly been possible without her.

Bibliography

- [1] D. A. Kreplin, P. J. Knowles, and H.-J. Werner: *Second-order MCSCF optimization revisited. I. Improved algorithms for fast and robust second-order CASSCF convergence*. The Journal of Chemical Physics **150** (19), 194106 (2019)
- [2] D. A. Kreplin, P. J. Knowles, and H.-J. Werner: *MCSCF optimization revisited. II. Combined first- and second-order orbital optimization for large molecules*. The Journal of Chemical Physics **152** (7), 74102 (2020)
- [3] D. R. Hartree: *The Wave Mechanics of an Atom with a Non-Coulomb Central Field. Part I. Theory and Methods*. Mathematical Proceedings of the Cambridge Philosophical Society **24** (1), 89–110 (1928)
- [4] D. R. Hartree: *The Wave Mechanics of an Atom with a Non-Coulomb Central Field. Part II. Some Results and Discussion*. Mathematical Proceedings of the Cambridge Philosophical Society **24** (1), 111–132 (1928)
- [5] R. A. Friesner: *Ab initio quantum chemistry: Methodology and applications*. Proceedings of the National Academy of Sciences of the United States of America **102** (19), 6648–6653 (2005)
- [6] W. Kohn, A. D. Becke, and R. G. Parr: *Density Functional Theory of Electronic Structure*. Journal of Physical Chemistry **100** (31), 12974–12980 (1996)
- [7] S. Grimme: *Density functional theory with London dispersion corrections*. WIREs Computational Molecular Science **1** (2), 211–228 (2011)
- [8] N. Mardirossian and M. Head-Gordon: *Thirty years of density functional theory in computational chemistry: an overview and extensive assessment of 200 density functionals*. Molecular Physics **115** (19), 2315–2372 (2017)
- [9] R. J. Bartlett and M. Musiał: *Coupled-cluster theory in quantum chemistry*. Reviews of Modern Physics **79** (1), 291–352 (2007)
- [10] C. Møller and M. S. Plesset: *Note on an Approximation Treatment for Many-Electron Systems*. Physical Review **46** (7), 618–622 (1934)
- [11] D. Cremer: *Møller-Plesset perturbation theory: from small molecule methods to methods for thousands of atoms*. WIREs Computational Molecular Science **1** (4), 509–530 (2011)

BIBLIOGRAPHY

- [12] C. D. Sherrill and H. F. Schaefer III: *The Configuration Interaction Method: Advances in Highly Correlated Approaches*. *Advances in Quantum Chemistry*, edited by P.-O. Löwdin, J. R. Sabin, M. C. Zerner, and E. Brändas, volume 34, pp. 143–269. Academic Press (1999)
- [13] T. D. Crawford and H. F. Schaefer III: *An Introduction to Coupled Cluster Theory for Computational Chemists*. *Reviews in Computational Chemistry*, volume 14, pp. 33–136 (2000)
- [14] M. W. Schmidt and M. S. Gordon: *The construction and interpretation of MCSCF wavefunctions*. *Annual Review of Physical Chemistry* **49**, 233–266 (1998)
- [15] T. H. Dunning: *Gaussian basis sets for use in correlated molecular calculations. I. The atoms boron through neon and hydrogen*. *The Journal of Chemical Physics* **90** (2), 1007–1023 (1989)
- [16] W. D. Laidig, P. Saxe, and R. J. Bartlett: *The description of N_2 and F_2 potential energy surfaces using multireference coupled cluster theory*. *The Journal of Chemical Physics* **86** (2), 887–907 (1987)
- [17] M. Hanauer and A. Köhn: *Pilot applications of internally contracted multireference coupled cluster theory, and how to choose the cluster operator properly*. *Journal of Chemical Physics* **134** (20), 204111 (2011)
- [18] M. Hanauer and A. Köhn: *Communication: Restoring full size extensivity in internally contracted multireference coupled cluster theory*. *The Journal of Chemical Physics* **137** (13), 131103 (2012)
- [19] M. Hanauer and A. Köhn: *Perturbative treatment of triple excitations in internally contracted multireference coupled cluster theory*. *The Journal of Chemical Physics* **136** (20), 204107 (2012)
- [20] J. Olsen: *The CASSCF Method: A Perspective and Commentary*. *International Journal of Quantum Chemistry* **111** (13), 3267–3272 (2011)
- [21] H.-J. Werner: *Matrix-Formulated Direct Multiconfiguration Self-Consistent Field and Multiconfiguration Reference Configuration-Interaction Methods*. *Advances in Chemical Physics*, volume 69, pp. 1–62. John Wiley & Sons, Inc. (1987)
- [22] R. Shepard: *The Multiconfiguration Self-Consistent Field Method*. *Advances in Chemical Physics*, volume 69, pp. 63–200. John Wiley & Sons, Inc. (1987)
- [23] B. O. Roos: *The Complete Active Space Self-Consistent Field Method and its Applications in Electronic Structure Calculations*. *Advances in Chemical Physics*, volume 69, pp. 399–445. John Wiley & Sons, Inc. (1987)

BIBLIOGRAPHY

- [24] D. R. Hartree, W. Hartree, and B. Swirles: *Self-consistent field, including exchange and superposition of configurations, with some results for oxygen*. Philosophical Transactions of the Royal Society of London. Series A, Mathematical and Physical Sciences **238** (790), 229–247 (1939)
- [25] J. C. Slater: *A Generalized Self-Consistent Field Method*. Physical Review **91** (3), 528–530 (1953)
- [26] P.-O. Löwdin: *Quantum Theory of Many-Particle Systems. II. Study of the Ordinary Hartree-Fock Approximation*. Physical Review **97** (6), 1490–1508 (1955)
- [27] R. McWeeny: *On the basis of orbital theories*. Proceedings of the Royal Society of London. Series A. Mathematical and Physical Sciences **232** (1188), 114–135 (1955)
- [28] T. L. Gilbert: *Optimum-Multiconfiguration Self-Consistent-Field Equations*. The Journal of Chemical Physics **43** (1), S248–S251 (1965)
- [29] G. Das and A. C. Wahl: *Extended Hartree-Fock Wavefunctions: Optimized Valence Configurations for H_2 and Li_2 , Optimized Double Configurations for F_2* . The Journal of Chemical Physics **44** (1), 87–96 (1966)
- [30] A. C. Wahl, P. J. Bertoncini, G. Das, and T. L. Gilbert: *Recent Progress Beyond the Hartree-Fock Method for Diatomic Molecules: The Method of Optimized Valence Configurations*. International Journal of Quantum Chemistry **1** (S1), 123–152 (1967)
- [31] G. Das: *Extended Hartree-Fock Ground-State Wavefunctions for the Lithium Molecule*. The Journal of Chemical Physics **46** (5), 1568–1578 (1967)
- [32] G. Das and A. C. Wahl: *Extended Hartree-Fock Wavefunctions: General Theory of Optimized-Valence Configurations and Its Application to Diatomic Molecules*. The Journal of Chemical Physics **47** (8), 2934–2942 (1967)
- [33] A. C. Wahl and G. Das: *The Method of Optimized Valence Configurations: A Reasonable Application of the Multiconfiguration Self-Consistent-Field Technique to the Quantitative Description of Chemical Bonding*. *Advances in Quantum Chemistry*, edited by P.-O. Löwdin, volume 5, pp. 261–296. Academic Press (1970)
- [34] J. Hinze and C. C. J. Roothaan: *Multi-Configuration Self-Consistent-Field Theory*. Progress of Theoretical Physics Supplement **40**, 37–51 (1967)
- [35] K. K. Docken and J. Hinze: *LiH Potential Curves and Wavefunctions for $X^1\Sigma^+$, $A^1\Sigma^+$, $B^1\Pi$, $^3\Sigma^+$, and $^3\Pi^*$* . The Journal of Chemical Physics **57** (11), 4928–4936 (1972)
- [36] J. Hinze: *MC-SCF. I. The multi-configuration self-consistent-field method*. The Journal of Chemical Physics **59** (12), 6424–6432 (1973)

BIBLIOGRAPHY

- [37] J. Hinze and E. Yurtsever: *An algorithm to solve open and closed-shell and restricted MC-SCF equations*. The Journal of Chemical Physics **70** (7), 3188–3190 (1979)
- [38] V. A. Kuprievich and O. V. Shramko: *Improved Convergence of Self-Consistency Procedures in the MC SCF Theory*. International Journal of Quantum Chemistry **9** (6), 1009–1020 (1975)
- [39] E. Dalgaard and P. Jørgensen: *Optimization of orbitals for multiconfigurational reference states*. The Journal of Chemical Physics **69** (8), 3833–3844 (1978)
- [40] B. Levy: *Multi-Configuration Self-Consistent Wavefunctions of Formaldehyde*. Chemical Physics Letters **4** (1), 17–19 (1969)
- [41] B. Levy: *Molecular MC-SCF calculations*. International Journal of Quantum Chemistry **4** (3), 297–313 (1970)
- [42] V. A. Kuprievich and O. V. Shramko: *The MC SCF Theory: Method of One-Electron Hamiltonian*. International Journal of Quantum Chemistry **6** (2), 327–336 (1972)
- [43] B. Levy: *Multiconfiguration Self-Consistent Wavefunctions for CH₄, C₂H₄ and C₂H₆*. Chemical Physics Letters **18** (1), 59–62 (1973)
- [44] P. D. Dacre, C. J. Watts, G. R. J. Williams, and R. McWeeny: *Molecular MCSCF calculations by direct minimization I. The single excitation MCSCF method*. Molecular Physics **30** (4), 1203–1211 (1975)
- [45] P. D. Dacre and C. J. Watts: *Molecular MCSCF calculations by direct minimization II. Calculations on H₂O using the single excitation MCSCF method*. Molecular Physics **31** (4), 1149–1158 (1976)
- [46] P. D. Dacre and C. J. Watts: *Molecular MCSCF calculations by direct minimization III. Extension of the single excitation MCSCF method to include some double excitations*. Molecular Physics **32** (5), 1437–1449 (1976)
- [47] A. Golebiewski, J. Hinze, and E. Yurtsever: *The orthogonal gradient method. A simple method to solve the closed-shell, open-shell, and multiconfiguration SCF equations*. The Journal of Chemical Physics **70** (3), 1101–1106 (1979)
- [48] J. Hinze: *Developments in the Calculation of Electronic Wavefunctions for Molecules: MCSCF, CI, and Numerical SCF for Molecules*. International Journal of Quantum Chemistry **20** (S15), 69–90 (1981)
- [49] J. Kendrick and I. H. Hillier: *A computational method of performing MC SCF calculations using bonded functions*. Chemical Physics Letters **41** (2), 283–286 (1976)
- [50] P. Siegbahn, A. Heiberg, B. O. Roos, and B. Levy: *A Comparison of the Super-CI and the Newton-Raphson Scheme in the Complete Active Space SCF Method*. Physica Scripta **21** (3-4), 323–327 (1980)

BIBLIOGRAPHY

- [51] P. E. M. Siegbahn, J. Almlöf, A. Heiberg, and B. O. Roos: *The complete active space SCF (CASSCF) method in a Newton-Raphson formulation with application to the HNO molecule*. The Journal of Chemical Physics **74** (4), 2384–2396 (1981)
- [52] B. Levy and G. Berthier: *Generalized Brillouin Theorem for Multiconfigurational SCF Theories*. International Journal of Quantum Chemistry **2** (2), 307–319 (1968)
- [53] B. Levy and G. Berthier: *Generalized Brillouin Theorem for Multiconfigurational SCF Theories*. International Journal of Quantum Chemistry **3** (2), 247 (1969)
- [54] F. Grein and T. C. Chang: *Multiconfiguration Wavefunctions obtained by Application of the Generalized Brillouin Theorem*. Chemical Physics Letters **12** (1), 44–48 (1971)
- [55] F. Grein and A. Banerjee: *Variational Wavefunctions for Low-Lying Excited States*. Chemical Physics Letters **31** (2), 281–285 (1975)
- [56] F. Grein and A. Banerjee: *A Multiconfiguration Method for Excited States of Atoms and Molecules*. International Journal of Quantum Chemistry **9** (S9), 147–154 (1975)
- [57] A. Banerjee and F. Grein: *Convergence Behavior of Some Multiconfiguration Methods*. International Journal of Quantum Chemistry **10** (1), 123–134 (1976)
- [58] W. H. E. Schwarz and T. C. Chang: *Multiconfiguration Wave Functions for Highly Excited States by the Generalized Brillouin Theorem Method*. International Journal of Quantum Chemistry **10** (S10), 91–97 (1976)
- [59] T. C. Chang and W. H. E. Schwarz: *Generalized Brillouin Theorem Multiconfiguration Method for Excited States*. Theoretica Chimica Acta **44** (1), 45–59 (1977)
- [60] K. Ruedenberg and K. R. Sundberg: *MCSCF Studies of Chemical Reactions: Natural Reaction Orbitals and Localized Reaction Orbitals*. *Quantum Science: Methods and Structure. A Tribute to Per-Olov Löwdin*, edited by J.-L. Calais, O. Goscinski, J. Lindenberg, and Y. Öhrn, pp. 505–515. Springer US (1976)
- [61] K. Ruedenberg, L. M. Cheung, and S. T. Elbert: *MCSCF optimization through combined use of natural orbitals and the Brillouin-Levy-Berthier theorem*. International Journal of Quantum Chemistry **16** (5), 1069–1101 (1979)
- [62] L. M. Cheung, K. R. Sundberg, and K. Ruedenberg: *Electronic Rearrangements during Chemical Reactions. II. Planar dissociation of Ethylene*. International Journal of Quantum Chemistry **16** (5), 1103–1139 (1979)
- [63] B. O. Roos, P. R. Taylor, and P. E. M. Siegbahn: *A complete active space SCF method (CASSCF) using a density matrix formulated Super-CI approach*. Chemical Physics **48** (2), 157–173 (1980)

BIBLIOGRAPHY

- [64] B. O. Roos: *The Complete Active Space SCF Method in a Fock-Matrix-Based Super-CI Formulation*. International Journal of Quantum Chemistry **18** (S14), 175–189 (1980)
- [65] P.-Å. Malmqvist, A. Rendell, and B. O. Roos: *The Restricted Active Space Self-Consistent-Field Method, Implemented with a Split Graph Unitary Group Approach*. Journal of Physical Chemistry **94** (14), 5477–5482 (1990)
- [66] J. Paldus: *Group theoretical approach to the configuration interaction and perturbation theory calculations for atomic and molecular systems*. The Journal of Chemical Physics **61** (12), 5321–5330 (1974)
- [67] I. Shavitt: *Graph Theoretical Concepts for the Unitary Group Approach to the Many-Electron Correlation Problem*. International Journal of Quantum Chemistry **12** (S11), 131–148 (1977)
- [68] I. Shavitt: *Matrix Element Evaluation in the Unitary Group Approach to the Electron Correlation Problem*. International Journal of Quantum Chemistry **14** (S12), 5–32 (1978)
- [69] B. R. Brooks and H. F. Schaefer III: *The graphical unitary group approach to the electron correlation problem. Methods and preliminary applications*. The Journal of Chemical Physics **70** (11), 5092–5106 (1979)
- [70] R. Shepard and J. Simons: *Multiconfigurational Wavefunction Optimization Using the Unitary Group Method*. International Journal of Quantum Chemistry **18** (S14), 211–228 (1980)
- [71] J. T. Golab, D. L. Yeager, and P. Jørgensen: *Proper characterization of MC SCF stationary points*. Chemical Physics **78** (2), 175–199 (1983)
- [72] R. N. Camp and H. F. King: *Stable methods for achieving MCSCF convergence*. The Journal of Chemical Physics **77** (6), 3056–3067 (1982)
- [73] R. Shepard, I. Shavitt, and J. Simons: *Comparison of the convergence characteristics of some iterative wave function optimization methods*. The Journal of Chemical Physics **76** (1), 543–557 (1982)
- [74] C. C. J. Roothaan, J. Detrich, and D. G. Hopper: *An Improved MCSCF Method*. International Journal of Quantum Chemistry **16** (S13), 93–101 (1979)
- [75] D. L. Yeager and P. Jørgensen: *Convergency studies of second and approximate second order multiconfigurational Hartree-Fock procedures*. The Journal of Chemical Physics **71** (2), 755–760 (1979)
- [76] B. H. Lengsfeld III: *General second order MCSCF theory: A density matrix directed algorithm*. The Journal of Chemical Physics **73** (1), 382–390 (1980)

BIBLIOGRAPHY

- [77] B. H. Lengsfeld III and B. Liu: *A second order MCSCF method for large CI expansions*. The Journal of Chemical Physics **75** (1), 478–480 (1981)
- [78] B. H. Lengsfeld III: *General second-order MCSCF theory for large CI expansions*. The Journal of Chemical Physics **77** (7), 4073–4083 (1982)
- [79] D. L. Yeager, P. Albertsen, and P. Jørgensen: *Mode damping in multiconfigurational Hartree-Fock procedures*. The Journal of Chemical Physics **73** (6), 2811–2816 (1980)
- [80] D. L. Yeager and P. Jørgensen: *A numerical study of the convergency of second and approximate second-order multiconfiguration Hartree-Fock procedures*. Molecular Physics **39** (3), 587–596 (1980)
- [81] P. Jørgensen, P. Albertsen, and D. L. Yeager: *A method to reduce the number of two electron integral transformations in a second order multiconfigurational Hartree-Fock procedure*. The Journal of Chemical Physics **72** (12), 6466–6473 (1980)
- [82] P. Jørgensen, P. Swanstrøm, and D. L. Yeager: *Guaranteed convergence in ground state multiconfigurational self-consistent field calculations*. The Journal of Chemical Physics **78** (1), 347–356 (1983)
- [83] J. Olsen, P. Jørgensen, and D. L. Yeager: *Multiconfigurational Hartree-Fock studies of avoided curve crossing using the Newton-Raphson technique*. The Journal of Chemical Physics **76** (1), 527–542 (1982)
- [84] J. Olsen, P. Jørgensen, and D. L. Yeager: *Cubic contributions in multiconfigurational self-consistent-field (MCSCF) calculations*. The Journal of Chemical Physics **77** (1), 356–370 (1982)
- [85] J. Olsen, D. L. Yeager, and P. Jørgensen: *Optimization and Characterization of a Multiconfigurational Self-Consistent Field (MCSCF) State*. *Advances in Chemical Physics*, volume 54, pp. 1–176. John Wiley & Sons, Inc. (1983)
- [86] H. J. A. Jensen and H. Ågren: *MC SCF optimization using the direct, restricted step, second-order norm-extended optimization method*. Chemical Physics Letters **110** (2), 140–144 (1984)
- [87] H. J. A. Jensen and P. Jørgensen: *A direct approach to second-order MCSCF calculations using a norm extended optimization scheme*. The Journal of Chemical Physics **80** (3), 1204–1214 (1984)
- [88] H. J. A. Jensen and H. Ågren: *A direct, restricted-step, second-order MC SCF program for large scale ab initio calculations*. Chemical Physics **104** (2), 229–250 (1986)
- [89] H. J. A. Jensen, P. Jørgensen, and H. Ågren: *Efficient optimization of large scale MC-SCF wave functions with a restricted step algorithm*. The Journal of Chemical Physics **87** (1), 451–466 (1987)

BIBLIOGRAPHY

- [90] H.-J. Werner and W. Meyer: *A quadratically convergent multiconfiguration-self-consistent field method with simultaneous optimization of orbitals and CI coefficients*. The Journal of Chemical Physics **73** (5), 2342–2356 (1980)
- [91] H.-J. Werner and W. Meyer: *A quadratically convergent MCSCF method for the simultaneous optimization of several states*. The Journal of Chemical Physics **74** (10), 5794–5801 (1981)
- [92] H.-J. Werner and P. J. Knowles: *A second order multiconfiguration SCF procedure with optimum convergence*. The Journal of Chemical Physics **82** (11), 5053–5063 (1985)
- [93] P. J. Knowles and H.-J. Werner: *An efficient second-order MC SCF method for long configuration expansions*. Chemical Physics Letters **115** (3), 259–267 (1985)
- [94] K. Wolinski, H. L. Sellers, and P. Pulay: *Consistent generalization of the Møller-Plesset partitioning to open-shell and multiconfigurational SCF reference states in many-body perturbation theory*. Chemical Physics Letters **140** (3), 225–231 (1987)
- [95] K. Wolinski and P. Pulay: *Generalized Møller-Plesset perturbation theory: Second order results for two-configuration, open-shell excited singlet, and doublet wave functions*. The Journal of Chemical Physics **90** (7), 3647–3659 (1989)
- [96] K. Andersson, P.-Å. Malmqvist, B. O. Roos, A. J. Sadlej, and K. Wolinski: *Second-order Perturbation Theory with a CASSCF Reference Function*. The Journal of Physical Chemistry **94** (14), 5483–5488 (1990)
- [97] K. Andersson, P.-Å. Malmqvist, and B. O. Roos: *Second-order perturbation theory with a complete active space self-consistent field reference function*. The Journal of Chemical Physics **96** (2), 1218–1226 (1992)
- [98] K. Andersson: *Different forms of the zeroth-order Hamiltonian in second-order perturbation theory with a complete active space self-consistent field reference function*. Theoretica Chimica Acta **91** (1), 31–46 (1995)
- [99] P. Pulay: *A Perspective on the CASPT2 Method*. International Journal of Quantum Chemistry **111** (13), 3273–3279 (2011)
- [100] C. Angeli, R. Cimiraglia, S. Evangelisti, T. Leininger, and J.-P. Malrieu: *Introduction of n -electron valence states for multireference perturbation theory*. The Journal of Chemical Physics **114** (23), 10252–10264 (2001)
- [101] P. Celani and H.-J. Werner: *Multireference perturbation theory for large restricted and selected active space reference wave functions*. The Journal of Chemical Physics **112** (13), 5546–5557 (2000)
- [102] H.-J. Werner: *Third-order multireference perturbation theory The CASPT3 method*. Molecular Physics **89** (2), 645–661 (1996)

BIBLIOGRAPHY

- [103] G. Ghigo, B. O. Roos, and P.-Å. Malmqvist: *A modified definition of the zeroth-order Hamiltonian in multiconfigurational perturbation theory (CASPT2)*. Chem. Phys. Lett. **396** (1-3), 142–149 (2004)
- [104] P. E. M. Siegbahn: *Generalizations of the direct CI method based on the graphical unitary group approach. II. Single and double replacements from any set of reference configurations*. The Journal of Chemical Physics **72** (3), 1647–1656 (1980)
- [105] H.-J. Werner and E.-A. Reinsch: *The self-consistent electron pairs method for multiconfiguration reference state functions*. The Journal of Chemical Physics **76** (6), 3144–3156 (1982)
- [106] V. R. Saunders and J. H. van Lenthe: *The direct CI method*. Molecular Physics **48** (5), 923–954 (1983)
- [107] H.-J. Werner and P. J. Knowles: *An efficient internally contracted multiconfiguration-reference configuration interaction method*. The Journal of Chemical Physics **89** (9), 5803–5814 (1988)
- [108] P. J. Knowles and H.-J. Werner: *An efficient method for the evaluation of coupling coefficients in configuration interaction calculations*. Chemical Physics Letters **145** (6), 514–522 (1988)
- [109] H.-J. Werner and P. J. Knowles: *A comparison of variational and non-variational internally contracted multiconfiguration-reference configuration interaction calculations*. Theoretica chimica acta **78** (3), 175–187 (1990)
- [110] P. J. Knowles and H.-J. Werner: *Internally contracted multiconfiguration-reference configuration interaction calculations for excited states*. Theoretica chimica acta **84** (1), 95–103 (1992)
- [111] P. Celani, H. Stoll, H.-J. Werner, and P. J. Knowles: *The CIPT2 method: Coupling of multi-reference configuration interaction and multi-reference perturbation theory. Application to the chromium dimer*. Molecular Physics **102** (21-22), 2369–2379 (2004)
- [112] K. R. Shamasundar, G. Knizia, and H.-J. Werner: *A new internally contracted multi-reference configuration interaction method*. The Journal of Chemical Physics **135** (5), 054101 (2011)
- [113] P. G. Szalay, T. Müller, G. Gidofalvi, H. Lischka, and R. Shepard: *Multiconfiguration Self-Consistent Field and Multireference Configuration Interaction Methods and Applications*. Chemical Reviews **112** (1), 108–181 (2012)
- [114] B. Jeziorski and H. J. Monkhorst: *Coupled-cluster method for multideterminantal reference states*. Physical Review A **24** (4), 1668–1681 (1981)

BIBLIOGRAPHY

- [115] U. S. Mahapatra, B. Datta, and D. Mukherjee: *A state-specific multi-reference coupled cluster formalism with molecular applications*. *Molecular Physics* **94** (1), 157–171 (1998)
- [116] U. S. Mahapatra, B. Datta, and D. Mukherjee: *A size-consistent state-specific multireference coupled cluster theory: Formal developments and molecular applications*. *The Journal of Chemical Physics* **110** (13), 6171–6188 (1999)
- [117] F. A. Evangelista and J. Gauss: *An orbital-invariant internally contracted multireference coupled cluster approach*. *The Journal of Chemical Physics* **134** (11), 114102 (2011)
- [118] F. A. Evangelista, M. Hanauer, A. Köhn, and J. Gauss: *A sequential transformation approach to the internally contracted multireference coupled cluster method*. *The Journal of Chemical Physics* **136** (20), 204108 (2012)
- [119] M. Hanauer and A. Köhn: *Meaning and magnitude of the reduced density matrix cumulants*. *Chemical Physics* **401**, 50–61 (2012)
- [120] A. Köhn, M. Hanauer, L. A. Mück, T.-C. Jagau, and J. Gauss: *State-specific multireference coupled-cluster theory*. *WIREs Computational Molecular Science* **3** (2), 176–197 (2013)
- [121] M. Page, P. Saxe, G. F. Adams, and B. H. Lengsfeld III: *Multireference CI gradients and MCSCF second derivatives*. *The Journal of Chemical Physics* **81** (1), 434–439 (1984)
- [122] M. R. Hoffmann, D. J. Fox, J. F. Gaw, Y. Osamura, Y. Yamaguchi et al.: *Analytic energy second derivatives for general MCSCF wave functions*. *The Journal of Chemical Physics* **80** (6), 2660–2668 (1984)
- [123] B. H. Lengsfeld III, P. Saxe, and D. R. Yarkony: *On the evaluation of nonadiabatic coupling matrix elements using SA-MCSCF/CI wave functions and analytic gradient methods. I*. *The Journal of Chemical Physics* **81** (10), 4549–4553 (1984)
- [124] P. J. Knowles: *Multiconfiguration Self-Consistent Field Wavefunctions and Properties*. Ph.d. dissertation, University of Cambridge (1984)
- [125] P. Saxe, B. H. Lengsfeld III, and D. R. Yarkony: *On the evaluation of non-adiabatic coupling matrix elements for large scale CI wavefunctions*. *Chemical Physics Letters* **113** (2), 159–164 (1985)
- [126] B. H. Lengsfeld III and D. R. Yarkony: *On the evaluation of nonadiabatic coupling matrix elements for MCSCF/CI wave functions using analytic derivative methods. III: Second derivative terms*. *The Journal of Chemical Physics* **84** (1), 348–353 (1986)

BIBLIOGRAPHY

- [127] T. U. Helgaker, J. Almlöf, H. J. A. Jensen, and P. Jørgensen: *Molecular Hessians for large-scale MCSCF wave functions*. The Journal of Chemical Physics **84** (11), 6266–6279 (1986)
- [128] T. U. Helgaker, H. J. A. Jensen, and P. Jørgensen: *Analytical calculation of MCSCF dipole-moment derivatives*. The Journal of Chemical Physics **84** (11), 6280–6284 (1986)
- [129] P. Saxe and D. R. Yarkony: *On the evaluation of nonadiabatic coupling matrix elements for MCSCF/CI wave functions. IV. Second derivative terms using analytic gradient methods*. The Journal of Chemical Physics **86** (1), 321–328 (1987)
- [130] B. H. Lengsfeld III and D. R. Yarkony: *Nonadiabatic Interactions Between Potential Energy Surfaces: Theory and Applications*. *Advances in Chemical Physics*, volume 82 of *Advances in Chemical Physics*, pp. 1–71 (1992)
- [131] N. Yamamoto, T. Vreven, M. A. Robb, M. J. Frisch, and H. B. Schlegel: *A direct derivative MC-SCF procedure*. Chemical Physics Letters **250** (3-4), 373–378 (1996)
- [132] J. Stårling, A. Bernhardsson, and R. Lindh: *Analytical gradients of a state average MCSCF state and a state average diagnostic*. Molecular Physics **99** (2), 103–114 (2001)
- [133] R. Shepard: *A discussion of some aspects of the MCSCF method*. *Relativistic and Electron Correlation Effects in Molecules and Solids*, edited by G. L. Malli, volume 318, pp. 161–177. Springer US (1994)
- [134] R. Shepard: *On the global convergence of MCSCF wave function optimization: The method of trigonometric interpolation*. Theoretica Chimica Acta **84** (1), 55–83 (1992)
- [135] G. Chaban, M. W. Schmidt, and M. S. Gordon: *Approximate second order method for orbital optimization of SCF and MCSCF wavefunctions*. Theoretical Chemistry Accounts **97** (1), 88–95 (1997)
- [136] M. R. Hoffmann, C. D. Sherrill, M. L. Leininger, and H. F. Schaefer III: *Optimization of MCSCF excited states using directions of negative curvature*. Chemical Physics Letters **355** (1-2), 183–192 (2002)
- [137] J. Ivanic and K. Ruedenberg: *A MCSCF Method for Ground and Excited States Based on Full Optimizations of Successive Jacobi Rotations*. Journal of Computational Chemistry **24** (10), 1250–1262 (2003)
- [138] K. D. Vogiatzis, D. Ma, J. Olsen, L. Gagliardi, and W. A. de Jong: *Pushing configuration-interaction to the limit: Towards massively parallel MCSCF calculations*. The Journal of Chemical Physics **147** (18), 184111 (2017)
- [139] H. Nakano and K. Hirao: *A quasi-complete active space self-consistent field method*. Chemical Physics Letters **317** (1-2), 90–96 (2000)

BIBLIOGRAPHY

- [140] J. Ivanic: *Direct configuration interaction and multiconfigurational self-consistent-field method for multiple active spaces with variable occupations. I. Method.* The Journal of Chemical Physics **119** (18), 9364–9376 (2003)
- [141] J. Ivanic: *Direct configuration interaction and multiconfigurational self-consistent-field method for multiple active spaces with variable occupations. II. Application to oxoMn(salen) and N₂O₄.* The Journal of Chemical Physics **119** (18), 9377–9385 (2003)
- [142] J. Olsen, B. O. Roos, P. Jørgensen, and H. J. A. Jensen: *Determinant based configuration interaction algorithms for complete and restricted configuration interaction spaces.* The Journal of Chemical Physics **89** (4), 2185–2192 (1988)
- [143] D. Ma, G. Li Manni, and L. Gagliardi: *The generalized active space concept in multiconfigurational self-consistent field methods.* The Journal of Chemical Physics **135** (4), 044128 (2011)
- [144] K. D. Vogiatzis, G. Li Manni, S. J. Stoneburner, D. Ma, and L. Gagliardi: *Systematic Expansion of Active Spaces beyond the CASSCF Limit: A GASSCF/SplitGAS Benchmark Study.* Journal of Chemical Theory and Computation **11** (7), 3010–3021 (2015)
- [145] G. H. Booth, A. J. W. Thom, and A. Alavi: *Fermion Monte Carlo without fixed nodes: A game of life, death, and annihilation in Slater determinant space.* The Journal of Chemical Physics **131** (5), 54106 (2009)
- [146] R. E. Thomas, Q. Sun, A. Alavi, and G. H. Booth: *Stochastic Multiconfigurational Self-Consistent Field Theory.* Journal of Chemical Theory and Computation **11** (11), 5316–5325 (2015)
- [147] G. Li Manni, S. D. Smart, and A. Alavi: *Combining the Complete Active Space Self-Consistent Field Method and the Full Configuration Interaction Quantum Monte Carlo within a Super-CI Framework, with Application to Challenging Metal-Porphyrins.* Journal of Chemical Theory and Computation **12** (3), 1245–1258 (2016)
- [148] A. A. Holmes, N. M. Tubman, and C. J. Umrigar: *Heat-Bath Configuration Interaction: An Efficient Selected Configuration Interaction Algorithm Inspired by Heat-Bath Sampling.* Journal of Chemical Theory and Computation **12** (8), 3674–3680 (2016)
- [149] S. Sharma, A. A. Holmes, G. Jeanmairet, A. Alavi, and C. J. Umrigar: *Semistochastic Heat-Bath Configuration Interaction Method: Selected Configuration Interaction with Semistochastic Perturbation Theory.* Journal of Chemical Theory and Computation **13** (4), 1595–1604 (2017)
- [150] J. E. T. Smith, B. Mussard, A. A. Holmes, and S. Sharma: *Cheap and Near Exact CASSCF with Large Active Spaces.* Journal of Chemical Theory and Computation **13** (11), 5468–5478 (2017)

BIBLIOGRAPHY

- [151] D. Zgid and M. Nooijen: *The density matrix renormalization group self-consistent field method: Orbital optimization with the density matrix renormalization group method in the active space*. The Journal of Chemical Physics **128** (14), 144116 (2008)
- [152] D. Ghosh, J. Hachmann, T. Yanai, and G. K.-L. Chan: *Orbital optimization in the density matrix renormalization group, with applications to polyenes and β -carotene*. The Journal of Chemical Physics **128** (14), 144117 (2008)
- [153] G. K.-L. Chan and S. Sharma: *The Density Matrix Renormalization Group in Quantum Chemistry*. Annual Review of Physical Chemistry **62**, 465–481 (2011)
- [154] T. Yanai, Y. Kurashige, D. Ghosh, and G. K.-L. Chan: *Accelerating Convergence in Iterative Solution for Large-Scale Complete Active Space Self-Consistent-Field Calculations*. International Journal of Quantum Chemistry **109** (10), 2178–2190 (2009)
- [155] Y. Ma and H. Ma: *Assessment of various natural orbitals as the basis of large active space density-matrix renormalization group calculations*. The Journal of Chemical Physics **138** (22), 224105 (2013)
- [156] Y. Ma, S. Knecht, S. Keller, and M. Reiher: *Second-Order Self-Consistent-Field Density-Matrix Renormalization Group*. Journal of Chemical Theory and Computation **13** (6), 2533–2549 (2017)
- [157] S. Wouters, V. Van Speybroeck, and D. Van Neck: *DMRG-CASPT2 study of the longitudinal static second hyperpolarizability of all-trans polyenes*. The Journal of Chemical Physics **145** (5), 054120 (2016)
- [158] N. Nakatani and S. Guo: *Density matrix renormalization group (DMRG) method as a common tool for large active-space CASSCF/CASPT2 calculations*. The Journal of Chemical Physics **146** (9), 094102 (2017)
- [159] L. Freitag, S. Knecht, C. Angeli, and M. Reiher: *Multireference Perturbation Theory with Cholesky Decomposition for the Density Matrix Renormalization Group*. Journal of Chemical Theory and Computation **13** (2), 451–459 (2017)
- [160] P. Sharma, V. Bernales, S. Knecht, D. G. Truhlar, and L. Gagliardi: *Density matrix renormalization group pair-density functional theory (DMRG-PDFT): singlet-triplet gaps in polyacenes and polyacetylenes*. Chemical Science **10** (6), 1716–1723 (2019)
- [161] C. Zhou, L. Gagliardi, and D. G. Truhlar: *Multiconfiguration Pair-Density Functional Theory for Iron Porphyrin with CAS, RAS, and DMRG Active Spaces*. Journal of Physical Chemistry A **123** (15), 3389–3394 (2019)
- [162] V. Veryazov, P. Å. Malmqvist, and B. O. Roos: *How to Select Active Space for Multiconfigurational Quantum Chemistry?* International Journal of Quantum Chemistry **111** (13), 3329–3338 (2011)

BIBLIOGRAPHY

- [163] G. Knizia: *Intrinsic Atomic Orbitals: An Unbiased Bridge between Quantum Theory and Chemical Concepts*. *Journal of Chemical Theory and Computation* **9** (11), 4834–4843 (2013)
- [164] E. R. Sayfutyarova, Q. Sun, G. K.-L. Chan, and G. Knizia: *Automated Construction of Molecular Active Spaces from Atomic Valence Orbitals*. *Journal of Chemical Theory and Computation* **13** (9), 4063–4078 (2017)
- [165] J. J. Bao, S. S. Dong, L. Gagliardi, and D. G. Truhlar: *Automatic Selection of an Active Space for Calculating Electronic Excitation Spectra by MS-CASPT2 or MC-PDFT*. *Journal of Chemical Theory and Computation* **14** (4), 2017–2025 (2018)
- [166] J. J. Bao and D. G. Truhlar: *Automatic Active Space Selection for Calculating Electronic Excitation Energies Based on High-Spin Unrestricted Hartree-Fock Orbitals*. *Journal of Chemical Theory and Computation* **15** (10), 5308–5318 (2019)
- [167] A. Khedkar and M. Roemelt: *Active Space Selection Based on Natural Orbital Occupation Numbers from n -Electron Valence Perturbation Theory*. *Journal of Chemical Theory and Computation* **15** (6), 3522–3536 (2019)
- [168] A. Khedkar and M. Roemelt: *Extending the ASSIST Active Space Selection Scheme to Large Molecules and Excited States*. *Journal of Chemical Theory and Computation* **16** (8), 4993–5005 (2020)
- [169] W. Jeong, S. J. Stoneburner, D. King, R. Li, A. Walker et al.: *Automation of Active Space Selection for Multireference Methods via Machine Learning on Chemical Bond Dissociation*. *Journal of Chemical Theory and Computation* **16** (4), 2389–2399 (2020)
- [170] J. Zou, K. Niu, H. Ma, S. Li, and W. Fang: *Automatic Selection of Active Orbitals from Generalized Valence Bond Orbitals*. *The Journal of Physical Chemistry A* **124** (40), 8321–8329 (2020)
- [171] C. J. Stein and M. Reiher: *Automated Selection of Active Orbital Spaces*. *Journal of Chemical Theory and Computation* **12** (4), 1760–1771 (2016)
- [172] C. J. Stein and M. Reiher: *Automated Identification of Relevant Frontier Orbitals for Chemical Compounds and Processes*. *CHIMIA International Journal for Chemistry*, **71** (4), 170–176 (2017)
- [173] C. J. Stein and M. Reiher: *AUTOCAS: A Program for Fully Automated Multiconfigurational Calculations*. *Journal of Computational Chemistry* **40** (25), 2216–2226 (2019)
- [174] S. Ten-No and S. Iwata: *Multiconfiguration self-consistent field procedure employing linear combination of atomic-electron distributions*. *The Journal of Chemical Physics* **105** (9), 3604–3611 (1996)

BIBLIOGRAPHY

- [175] F. Aquilante, P.-Å. Malmqvist, T. B. Pedersen, A. Ghosh, and B. O. Roos: *Cholesky Decomposition-Based Multiconfiguration Second-Order Perturbation Theory (CD-CASPT2): Application to the Spin-State Energetics of Co^{III}(diiminato)(NPh)*. *Journal of Chemical Theory and Computation* **4** (5), 694–702 (2008)
- [176] R. D. Reynolds, T. Yanai, and T. Shiozaki: *Large-scale relativistic complete active space self-consistent field with robust convergence*. *The Journal of Chemical Physics* **149** (1), 014106 (2018)
- [177] W. Gyrrffy, T. Shiozaki, G. Knizia, and H.-J. Werner: *Analytical energy gradients for second-order multireference perturbation theory using density fitting*. *The Journal of Chemical Physics* **138** (10), 104104 (2013)
- [178] E. G. Hohenstein, N. Luehr, I. S. Ufimtsev, and T. J. Martínez: *An atomic orbital-based formulation of the complete active space self-consistent field method on graphical processing units*. *The Journal of Chemical Physics* **142** (22), 224103 (2015)
- [179] Q. Sun, J. Yang, and G. K.-L. Chan: *A general second order complete active space self-consistent-field solver for large-scale systems*. *Chemical Physics Letters* **683**, 291–299 (2017)
- [180] J. W. Snyder, B. F. E. Curchod, and T. J. Martínez: *GPU-Accelerated State-Averaged Complete Active Space Self-Consistent Field Interfaced with Ab Initio Multiple Spawning Unravels the Photodynamics of Provitamin D₃*. *The Journal of Physical Chemistry Letters* **7** (13), 2444–2449 (2016)
- [181] J. W. Snyder, B. S. Fales, E. G. Hohenstein, B. G. Levine, and T. J. Martínez: *A direct-compatible formulation of the coupled perturbed complete active space self-consistent field equations on graphical processing units*. *The Journal of Chemical Physics* **146** (17), 174113 (2017)
- [182] H. J. A. Jensen, K. G. Dyall, T. Saue, and K. Fægri: *Relativistic four-component multiconfigurational self-consistent-field theory for molecules: Formalism*. *The Journal of Chemical Physics* **104** (11), 4083–4097 (1996)
- [183] J. Thyssen, T. Fleig, and H. J. A. Jensen: *A direct relativistic four-component multiconfiguration self-consistent-field method for molecules*. *The Journal of Chemical Physics* **129** (3), 034109 (2008)
- [184] J. E. Bates and T. Shiozaki: *Fully relativistic complete active space self-consistent field for large molecules: Quasi-second-order minimax optimization*. *The Journal of Chemical Physics* **142** (4), 044112 (2015)
- [185] F. Lipparini and J. Gauss: *Cost-Effective Treatment of Scalar Relativistic Effects for Multireference Systems: A CASSCF Implementation Based on the Spin-free Dirac-Coulomb Hamiltonian*. *Journal of Chemical Theory and Computation* **12** (9), 4284–4295 (2016)

BIBLIOGRAPHY

- [186] J. Nocedal: *Updating Quasi-Newton Matrices With Limited Storage*. Mathematics of Computation **35** (151), 773–782 (1980)
- [187] Y. Guo, K. Sivalingam, E. F. Valeev, and F. Neese: *SparseMaps - A systematic infrastructure for reduced-scaling electronic structure methods. III. Linear-scaling multireference domain-based pair natural orbital N-electron valence perturbation theory*. The Journal of Chemical Physics **144** (9), 094111 (2016)
- [188] F. Menezes, D. Kats, and H.-J. Werner: *Local complete active space second-order perturbation theory using pair natural orbitals (PNO-CASPT2)*. The Journal of Chemical Physics **145** (12), 124115 (2016)
- [189] F. Menezes: *A local complete active space 2nd-order perturbation theory method*. Ph.d. dissertation, University Stuttgart (2016)
- [190] H. J. Werner, P. J. Knowles, F. R. Manby, J. A. Black, K. Doll et al.: *The Molpro quantum chemistry package*. The Journal of Chemical Physics **152** (14), 144107 (2020)
- [191] F. Jensen: *Introduction to Computational Chemistry*. John Wiley & Sons, Ltd (2007)
- [192] M. Born and R. Oppenheimer: *Zur Quantentheorie der Molekeln*. Annalen der Physik **389** (20), 457–484 (1927)
- [193] A. W. Jasper, C. Zhu, S. Nangia, and D. G. Truhlar: *Introductory lecture: Nonadiabatic effects in chemical dynamics*. Faraday Discussions **127**, 1–22 (2004)
- [194] G. Rauhut: *Efficient calculation of potential energy surfaces for the generation of vibrational wave functions*. The Journal of Chemical Physics **121** (19), 9313–9322 (2004)
- [195] R. Pauncz: *Spin eigenfunctions*. Plenum Press New York (1979)
- [196] R. McWeeny: *Methods of Molecular Quantum Mechanics*. Academic Press (1992)
- [197] I. Shavitt: *The Method of Configuration Interaction. Methods of Electronic Structure Theory*, edited by H. F. Schaefer III, volume 3, pp. 189–275. Springer Science+Business Media (1977)
- [198] P. J. Knowles and N. C. Handy: *A new determinant-based full configuration interaction method*. Chemical Physics Letters **111** (4-5), 315–321 (1984)
- [199] P. J. Knowles and N. C. Handy: *A determinant based full configuration interaction program*. Computer Physics Communications **54** (1), 75–83 (1989)
- [200] T. Helgaker, P. Jørgensen, and J. Olsen: *Molecular Electronic-Structure Theory*. John Wiley & Sons (2000)
- [201] J. Paldus: *Unitary-group approach to the many-electron correlation problem: Relation of Gelfand and Weyl tableau formulations*. Physical Review A **14** (5), 1620–1625 (1976)

BIBLIOGRAPHY

- [202] J. Paldus: *Unitary Group Approach to Many-Electron Correlation Problem. The Unitary Group for the Evaluation of Electronic Energy Matrix Elements*, edited by J. Hinze, pp. 1–50. Springer-Verlag Berlin Heidelberg New York (1981)
- [203] I. Shavitt: *The utilization of abelian point group symmetry in the graphical unitary group approach to the calculation of correlated electronic wavefunctions*. *Chemical Physics Letters* **63** (3), 421–427 (1979)
- [204] I. Shavitt: *The Graphical Unitary Group Approach and Its Application to Direct Configuration Interaction Calculations. The Unitary Group for the Evaluation of Electronic Energy Matrix Elements*, edited by J. Hinze, pp. 51–99. Springer-Verlag Berlin Heidelberg New York (1981)
- [205] S. F. Boys: *Electronic wave functions - I. A general method of calculation for the stationary states of any molecular system*. *Proceedings of the Royal Society of London. Series A, Mathematical and Physical Sciences* **200** (1063), 542–554 (1950)
- [206] L. E. McMurchie and E. R. Davidson: *One- and Two-Electron Integrals over Cartesian Gaussian Functions*. *Journal of Computational Physics* **26** (2), 218–231 (1978)
- [207] J. A. Pople and W. J. Hehre: *Computation of Electron Repulsion Integrals Involving Contracted Gaussian Basis Functions*. *Journal of Computational Physics* **27** (2), 161–168 (1978)
- [208] S. Obara and A. Saika: *Efficient recursive computation of molecular integrals over Cartesian Gaussian functions*. *The Journal of Chemical Physics* **84** (7), 3963–3974 (1986)
- [209] I. S. Ufimtsev and T. J. Martínez: *Quantum Chemistry on Graphical Processing Units. I. Strategies for Two-Electron Integral Evaluation*. *Journal of Chemical Theory and Computation* **4** (2), 222–231 (2008)
- [210] D. G. Truhlar: *Basis-set extrapolation*. *Chemical Physics Letters* **294** (1-3), 45–48 (1998)
- [211] K. A. Peterson, R. A. Kendall, and T. H. Dunning: *Benchmark calculations with correlated molecular wave functions. II. Configuration interaction calculations on first row diatomic hydrides*. *The Journal of Chemical Physics* **99** (3), 1930–1944 (1993)
- [212] D. E. Woon and T. H. Dunning: *Gaussian basis sets for use in correlated molecular calculations. III. The atoms aluminum through argon*. *The Journal of Chemical Physics* **98** (2), 1358–1371 (1993)
- [213] F. Weigend and R. Ahlrichs: *Balanced basis sets of split valence, triple zeta valence and quadruple zeta valence quality for H to Rn: Design and assessment of accuracy*. *Physical Chemistry Chemical Physics* **7** (18), 3297–3305 (2005)

BIBLIOGRAPHY

- [214] G. Knizia, T. B. Adler, and H.-J. Werner: *Simplified CCSD(T)-F12 methods: Theory and benchmarks*. The Journal of Chemical Physics **130** (5), 054104 (2009)
- [215] L. Kong, F. A. Bischoff, and E. F. Valeev: *Explicitly Correlated R12/F12 Methods for Electronic Structure*. Chemical Reviews **112** (1), 75–107 (2012)
- [216] T. Shiozaki and H.-J. Werner: *Communication: Second-order multireference perturbation theory with explicit correlation: CASPT2-F12*. The Journal of Chemical Physics **133** (14), 141103 (2010)
- [217] T. Shiozaki, W. Gyrfy, P. Celani, and H.-J. Werner: *Communication: Extended multi-state complete active space second-order perturbation theory: Energy and nuclear gradients*. The Journal of Chemical Physics **135** (8), 81106 (2011)
- [218] T. Shiozaki and H.-J. Werner: *Explicitly correlated multireference configuration interaction with multiple reference functions: Avoided crossings and conical intersections*. The Journal of Chemical Physics **134** (18), 184104 (2011)
- [219] T. Shiozaki and H.-J. Werner: *Multireference explicitly correlated F12 theories*. Molecular Physics **111** (5), 607–630 (2013)
- [220] H. J. Werner, F. R. Manby, and P. J. Knowles: *Fast linear scaling second-order Møller-Plesset perturbation theory (MP2) using local and density fitting approximations*. The Journal of Chemical Physics **118** (18), 8149–8160 (2003)
- [221] R. Polly, H.-J. Werner, F. R. Manby, and P. J. Knowles: *Fast Hartree-Fock theory using local density fitting approximations*. Molecular Physics **102** (21-22), 2311–2321 (2004)
- [222] C. Köppl and H.-J. Werner: *Parallel and Low-Order Scaling Implementation of Hartree-Fock Exchange Using Local Density Fitting*. Journal of Chemical Theory and Computation **12** (7), 3122–3134 (2016)
- [223] F. Weigend: *A fully direct RI-HF algorithm: Implementation, optimised auxiliary basis sets, demonstration of accuracy and efficiency*. Physical Chemistry Chemical Physics **4** (18), 4285–4291 (2002)
- [224] F. Weigend, M. Häser, H. Patzelt, and R. Ahlrichs: *RI-MP2: optimized auxiliary basis sets and demonstration of efficiency*. Chemical Physics Letters **294** (1-3), 143–152 (1998)
- [225] F. Weigend, A. Köhn, and C. Hättig: *Efficient use of the correlation consistent basis sets in resolution of the identity MP2 calculations*. The Journal of Chemical Physics **116** (8), 3175–3183 (2002)
- [226] G. J. Atchity and K. Ruedenberg: *Orbital transformations and configurational transformations of electronic wavefunctions*. The Journal of Chemical Physics **111** (7), 2910–2920 (1999)

BIBLIOGRAPHY

- [227] K. Ruedenberg, M. W. Schmidt, M. M. Gilbert, and S. T. Elbert: *Are atoms intrinsic to molecular electronic wavefunctions? I. The FORS model*. *Chemical Physics* **71** (1), 41–49 (1982)
- [228] C. C. J. Roothaan: *Self-Consistent Field Theory for Open Shells of Electronic Systems*. *Reviews of Modern Physics* **32** (2), 179–185 (1960)
- [229] P. P. Hallmen, C. Köppl, G. Rauhut, H. Stoll, and J. van Slageren: *Fast and reliable ab initio calculation of crystal field splittings in lanthanide complexes*. *The Journal of Chemical Physics* **147** (16), 164101 (2017)
- [230] P. Pulay: *Convergence acceleration of iterative sequences. The case of SCF iteration*. *Chemical Physics Letters* **73** (2), 393–398 (1980)
- [231] P. Pulay: *Improved SCF Convergence Acceleration*. *Journal of Computational Chemistry* **3** (4), 556–560 (1982)
- [232] G. Das and A. C. Wahl: *New Techniques for the Computation of Multiconfiguration Self-Consistent Field (MCSCF) Wavefunctions*. *The Journal of Chemical Physics* **56** (4), 1769–1775 (1972)
- [233] G. Das: *Multiconfiguration self-consistent field (MCSCF) theory for excited states*. *The Journal of Chemical Physics* **58** (11), 5104–5110 (1973)
- [234] A. C. Wahl and G. Das: *The Multiconfiguration Self-Consistent Field Method*. *Methods of Electronic Structure Theory*, edited by H. F. Schaefer, volume 3, chapter 3, pp. 51–78. Springer Science+Business Media (1977)
- [235] J. Almlöf, A. V. Nemukhin, and A. Heiberg: *Treatment of Excited States in the CASSCF Method: Application to BO*. *International Journal of Quantum Chemistry* **20** (3), 655–667 (1981)
- [236] M. P. Deskevich, D. J. Nesbitt, and H.-J. Werner: *Dynamically weighted multiconfiguration self-consistent field: Multistate calculations for $F+H_2O \rightarrow HF+OH$ reaction paths*. *The Journal of Chemical Physics* **120** (16), 7281–7289 (2004)
- [237] N. C. Handy and H. F. Schaefer III: *On the evaluation of analytic energy derivatives for correlated wave functions*. *The Journal of Chemical Physics* **81** (11), 5031–5033 (1984)
- [238] J. Gauss: *Molecular Properties. Modern Methods and Algorithms of Quantum Chemistry*, edited by J. Grotendorst, volume 3 of *NIC series*, pp. 541–592. John von Neumann Institute for Computing (NIC) (2000)
- [239] R. D. Amos and J. E. Rice: *CADPAC: The Cambridge Analytic Derivatives Package* (1987)

BIBLIOGRAPHY

- [240] R. Lindh: *The reduced multiplication scheme of the Rys-Gauss quadrature for 1st order integral derivatives*. *Theoretica Chimica Acta* **85** (6), 423–440 (1993)
- [241] P. Celani and H.-J. Werner: *Analytical energy gradients for internally contracted second-order multireference perturbation theory*. *The Journal of Chemical Physics* **119** (10), 5044–5057 (2003)
- [242] J. A. Pople, R. Krishnan, H. B. Schlegel, and J. S. Binkley: *Derivative Studies in Hartree-Fock and Møller-Plesset Theories*. *International Journal of Quantum Chemistry* **16** (S13), 225–241 (1979)
- [243] P. Wormer, F. Visser, and J. Paldus: *Conjugate Gradient Method for the Solution of Linear Equations: Application to Molecular Electronic Structure Calculations*. *Journal of Computational Physics* **48** (1), 23–44 (1982)
- [244] C. Angeli, B. Bories, A. Cavallini, and R. Cimiraglia: *Third-order multireference perturbation theory: The n -electron valence state perturbation-theory approach*. *The Journal of Chemical Physics* **124** (5), 54108 (2006)
- [245] B. O. Roos, P. Linse, P. E. Siegbahn, and M. R. Blomberg: *A simple method for the evaluation of the second-order-perturbation energy from external double-excitations with a CASSCF reference wavefunction*. *Chemical Physics* **66** (1-2), 197–207 (1982)
- [246] K. Hirao: *Multireference Møller-Plesset perturbation theory for high-spin open-shell systems*. *Chemical Physics Letters* **196** (5), 397–403 (1992)
- [247] K. G. Dyall: *The choice of a zeroth-order Hamiltonian for second-order perturbation theory with a complete active space self-consistent-field reference function*. *The Journal of Chemical Physics* **102** (12), 4909–4918 (1995)
- [248] C. Angeli, M. Pastore, and R. Cimiraglia: *New perspectives in multireference perturbation theory: the n -electron valence state approach*. *Theoretical Chemistry Accounts* **117** (5), 743–754 (2007)
- [249] C. Camacho, H. A. Witek, and S. Yamamoto: *Intruder States in Multireference Perturbation Theory: The Ground State of Manganese Dimer*. *Journal of Computational Chemistry* **30** (3), 468–478 (2009)
- [250] K. Andersson, B. O. Roos, P.-Å. Malmqvist, and P.-O.-. Widmark: *The Cr_2 potential energy curve studied with multiconfigurational second-order perturbation theory*. *Chemical Physics Letters* **230** (4-5), 391–397 (1994)
- [251] B. O. Roos and K. Andersson: *Multiconfigurational perturbation theory with level shift - the Cr_2 potential revisited*. *Chemical Physics Letters* **245** (2-3), 215–223 (1995)
- [252] K. Andersson: *The electronic spectrum of Cr_2* . *Chemical Physics Letters* **237** (3-4), 212–221 (1995)

BIBLIOGRAPHY

- [253] J. Finley, P.-Å. Malmqvist, B. O. Roos, and L. Serrano-Andrés: *The multi-state CASPT2 method*. Chemical Physics Letters **288** (2-4), 299–306 (1998)
- [254] S. Ten-no: *A simple F12 geminal correction in multi-reference perturbation theory*. Chemical Physics Letters **447** (1-3), 175–179 (2007)
- [255] Y. Guo, K. Sivalingam, E. F. Valeev, and F. Neese: *Explicitly correlated N-electron valence state perturbation theory (NEVPT2-F12)*. The Journal of Chemical Physics **147** (6), 064110 (2017)
- [256] D. Kats and H.-J. Werner: *Multi-state local complete active space second-order perturbation theory using pair natural orbitals (PNO-MS-CASPT2)*. The Journal of Chemical Physics **150** (21), 214107 (2019)
- [257] S. Epstein: *The variation method in quantum chemistry*. Academic Press Inc. (1974)
- [258] R. Fletcher: *Practical Methods of Optimization*. John Wiley & Sons (2013)
- [259] J. Nocedal and S. Wright: *Numerical optimization*. Springer Series in Operations Research. Springer Science & Business Media (2006)
- [260] D. R. Yarkony: *Comment on the use of the augmented matrix in MCSCF theory*. Chemical Physics Letters **77** (3), 634–635 (1981)
- [261] E. R. Davidson: *The Iterative Calculation of a Few of the Lowest Eigenvalues and Corresponding Eigenvectors of Large Real-Symmetric Matrices*. Journal of Computational Physics **17** (1), 87–94 (1975)
- [262] B. Liu: *The simultaneous expansion method for the iterative solution of several of the lowest eigenvalues and corresponding eigenvectors of large real-symmetric matrices*. *Numerical Algorithms in Chemistry: Algebraic Method*, pp. 49–53 (1978)
- [263] G. L. Sleijpen and H. A. Van Der Vorst: *A Jacobi-Davidson Iteration Method for Linear Eigenvalue Problems*. SIAM Review **42** (2), 267–293 (2000)
- [264] C. Kollmar, K. Sivalingam, B. Helmich-Paris, C. Angeli, and F. Neese: *A Perturbation-Based Super-CI Approach for the Orbital Optimization of a CASSCF Wave Function*. Journal of Computational Chemistry **40** (14), 1463–1470 (2019)
- [265] E. Dalgaard: *A quadratically convergent reference state optimization procedure*. Chemical Physics Letters **65** (3), 559–563 (1979)
- [266] P. Jørgensen, J. Olsen, and D. L. Yeager: *Generalizations of Newton-Raphson and multiplicity independent Newton-Raphson approaches in multiconfigurational Hartree-Fock theory*. The Journal of Chemical Physics **75** (12), 5802–5815 (1981)

BIBLIOGRAPHY

- [267] A. Igawa, D. L. Yeager, and H. Fukutome: *A method to include certain infinite order contributions in a multiconfigurational self-consistent field (MCSCF) calculation*. The Journal of Chemical Physics **76** (11), 5388–5396 (1982)
- [268] D. L. Yeager, D. Lynch, J. Nichols, P. Jørgensen, and J. Olsen: *Newton-Raphson Approaches and Generalizations in Multiconfigurational Self-Consistent Field Calculations*. The Journal of Physical Chemistry **86** (12), 2140–2153 (1982)
- [269] D. Kreplin: *Second-Order MCSCF Optimization with Full Coupling of Higher Order Orbital Rotation Parameters and CI-Coefficients*. Master's thesis, University of Stuttgart (2016)
- [270] H.-J. Zhai, S. Li, D. A. Dixon, and L.-S. Wang: *Probing the Electronic and Structural Properties of Chromium Oxide Clusters $(\text{CrO}_3)_n^-$ and $(\text{CrO}_3)_n$ ($n = 1-5$): Photoelectron Spectroscopy and Density Functional Calculations*. Journal of the American Chemical Society **130** (15), 5167–5177 (2008)
- [271] F. Aquilante, J. Autschbach, A. Baiardi, S. Battaglia, V. A. Borin et al.: *Modern quantum chemistry with [Open]Molcas*. The Journal of Chemical Physics **152** (21), 214117 (2020)
- [272] C. G. Broyden: *The Convergence of a Class of Double-rank Minimization Algorithms I. General Considerations*. IMA Journal of Applied Mathematics **6** (1), 76–90 (1970)
- [273] R. Fletcher: *A new approach to variable metric algorithms*. The Computer Journal **13** (3), 317–322 (1970)
- [274] D. Goldfarb: *A Family of Variable-Metric Methods Derived by Variational Means*. Mathematics of Computation **24** (109), 23–26 (1970)
- [275] D. F. Shanno: *Conditioning of Quasi-Newton Methods for Function Minimization*. Mathematics of Computation **24** (111), 647–656 (1970)
- [276] T. H. Fischer and J. Almlöf: *General Methods for Geometry and Wave Function Optimization*. The Journal of Physical Chemistry **96** (24), 9768–9774 (1992)
- [277] J. D. Head and M. C. Zerner: *An approximate Hessian for molecular geometry optimization*. Chemical Physics Letters **131** (4-5), 359–366 (1986)
- [278] R. Lindh, A. Bernhardsson, G. Karlström, and P.-Å. Malmqvist: *On the use of a Hessian model function in molecular geometry optimizations*. Chemical Physics Letters **241** (4), 423–428 (1995)
- [279] R. H. A. Eade and M. A. Robb: *Direct minimization in MC SCF theory. The quasi-newton method*. Chemical Physics Letters **83** (2), 362–368 (1981)

BIBLIOGRAPHY

- [280] J. Olsen and P. Jørgensen: *Update methods in multiconfigurational self-consistent field calculations*. The Journal of Chemical Physics **77** (12), 6109–6130 (1982)
- [281] R. K. Nesbet: *Algorithm for Diagonalization of Large Matrices*. The Journal of Chemical Physics **43** (1), 311–312 (1965)
- [282] R. A. Kendall, T. H. Dunning, and R. J. Harrison: *Electron affinities of the first-row atoms revisited. Systematic basis sets and wave functions*. The Journal of Chemical Physics **96** (9), 6796–6806 (1992)
- [283] Q. Ma and H.-J. J. Werner: *Scalable Electron Correlation Methods. 7. Local Open-Shell Coupled-Cluster Methods Using Pair Natural Orbitals: PNO-RCCSD and PNO-UCCSD*. Journal of Chemical Theory and Computation **16** (5), 3135–3151 (2020)
- [284] G. E. Scuseria, T. J. Lee, and H. F. Schaefer III: *Accelerating the convergence of the coupled-cluster approach. The use of the DIIS method*. Chemical Physics Letters **130** (3), 236–239 (1986)
- [285] L. Jiang, R. H. Byrd, E. Eskow, and R. B. Schnabel: *A Preconditioned L-BFGS Algorithm with Application to Molecular Energy Minimization*. Technical report, University of Colorado (2004)
- [286] L. Métivier and R. Brossier: *The SEISCOPE optimization toolbox: A large-scale nonlinear optimization library based on reverse communication*. Geophysics **81** (2), F11–F25 (2016)
- [287] H. De Sterck and A. J. Howse: *Nonlinearly preconditioned L-BFGS as an acceleration mechanism for alternating least squares with application to tensor decomposition*. Numerical Linear Algebra with Applications **25** (6), 1–30 (2018)
- [288] C. Angeli, S. Evangelisti, R. Cimiraglia, and D. Maynau: *A novel perturbation-based complete active space-self-consistent-field algorithm: Application to the direct calculation of localized orbitals*. The Journal of Chemical Physics **117** (23), 10525–10533 (2002)
- [289] F. Aquilante, T. B. Pedersen, R. Lindh, B. O. Roos, A. Sánchez de Merás et al.: *Accurate ab initio density fitting for multiconfigurational self-consistent field methods*. The Journal of Chemical Physics **129** (2), 024113 (2008)
- [290] Wolfram Research Inc.: *Mathematica 10.0* (2014)
- [291] C. J. Cramer, M. Włoch, P. Piecuch, C. Puzzarini, and L. Gagliardi: *Theoretical Models on the Cu₂O₂ Torture Track: Mechanistic Implications for Oxytyrosinase and Small-Molecule Analogues*. The Journal of Physical Chemistry A **110** (5), 1991–2004 (2006)

BIBLIOGRAPHY

- [292] L. Roy, M. H. Al-Afyouni, D. E. DeRosh, B. Mondal, I. M. DiMucci et al.: *Reduction of CO₂ by a masked two-coordinate cobalt(I) complex and characterization of a proposed oxodicobalt(II) intermediate*. *Chemical Science* **10** (3), 918–929 (2019)
- [293] A. Zens, F. Bauer, B. Kolb, F. Mannchen, P. Seubert et al.: *Ni(NHC) Catalyzed Rearrangement of 1-Acyl-2-vinylcyclopropanes: Tackling a Mechanistic Puzzle by Combined Experimental and Computational Studies*. *European Journal of Organic Chemistry* **2019** (36), 6285–6295 (2019)
- [294] B. F. Gherman and C. J. Cramer: *Quantum chemical studies of molecules incorporating a Cu₂O₂²⁺ core*. *Coordination Chemistry Reviews* **253** (5-6), 723–753 (2009)
- [295] M. Flock and K. Pierloot: *Theoretical Study of the Interconversion of O₂-Binding Dicopper Complexes*. *The Journal of Physical Chemistry A* **103** (1), 95–102 (1999)
- [296] M. F. Rode and H.-J. Werner: *Ab initio study of the O₂ binding in dicopper complexes*. *Theoretical Chemistry Accounts* **114**, 309–317 (2005)
- [297] P. Å. Malmqvist, K. Pierloot, A. R. M. Shahi, C. J. Cramer, and L. Gagliardi: *The restricted active space followed by second-order perturbation theory method: Theory and application to the study of CuO₂ and Cu₂O₂ systems*. *The Journal of Chemical Physics* **128** (20), 204109 (2008)
- [298] K. H. Marti, I. M. Ondík, G. Moritz, and M. Reiher: *Density matrix renormalization group calculations on relative energies of transition metal complexes and clusters*. *The Journal of Chemical Physics* **128** (1), 14104 (2008)
- [299] T. Yanai, Y. Kurashige, E. Neuscamman, and G. K.-L. Chan: *Multireference quantum chemistry through a joint density matrix renormalization group and canonical transformation theory*. *The Journal of Chemical Physics* **132** (2), 24105 (2010)
- [300] G. Barcza, Ö. Legeza, K. H. Marti, and M. Reiher: *Quantum-information analysis of electronic states of different molecular structures*. *Physical Review A* **83** (1), 12508 (2011)
- [301] Q. M. Phung, S. Wouters, and K. Pierloot: *Cumulant Approximated Second-Order Perturbation Theory Based on the Density Matrix Renormalization Group for Transition Metal Complexes: A Benchmark Study*. *Journal of Chemical Theory and Computation* **12** (9), 4352–4361 (2016)
- [302] B. Helmich-Paris: *CASSCF linear response calculations for large open-shell molecules*. *The Journal of Chemical Physics* **150** (17), 174121 (2019)
- [303] D. E. Woon and T. H. Dunning: *Gaussian basis sets for use in correlated molecular calculations. IV. Calculation of static electrical response properties*. *The Journal of Chemical Physics* **100** (4), 2975–2988 (1994)

BIBLIOGRAPHY

- [304] F. Mata, M. C. Martin, and G. O. Sørensen: *Microwave Spectra of Deuterated Furans. Revised Molecular Structure of Furan*. *Journal of Molecular Structure* **48** (2), 157–163 (1978)
- [305] L. Nygaard, J. T. Nielsen, J. Kirchheiner, G. Maltesen, J. Rastrup-Andersen et al.: *Microwave Spectra of Isotopic Pyrroles. Molecular Structure, Dipole Moment, and ^{14}N Quadrupole Coupling Constants of Pyrrole*. *Journal of Molecular Structure* **3** (6), 491–506 (1969)
- [306] O. Christiansen and P. Jørgensen: *The Electronic Spectrum of Furan*. *Journal of the American Chemical Society* **120** (14), 3423–3430 (1998)
- [307] O. Christiansen, J. Gauss, J. F. Stanton, and P. Jørgensen: *The electronic spectrum of pyrrole*. *The Journal of Chemical Physics* **111** (2), 525–537 (1999)
- [308] S. Grimme: *Semiempirical hybrid density functional with perturbative second-order correlation*. *The Journal of Chemical Physics* **124** (3), 034108 (2006)
- [309] A. Klamt and G. Schüürmann: *COSMO: A new approach to Dielectric Screening in Solvents with Explicit Expressions for the Screening Energy and its Gradient*. *Journal of the Chemical Society, Perkin Transactions 2* (5), 799–805 (1993)
- [310] Q. Ma and H.-J. Werner: *Accurate Intermolecular Interaction Energies Using Explicitly Correlated Local Coupled Cluster Methods [PNO-LCCSD(T)-F12]*. *Journal of Chemical Theory and Computation* **15** (2), 1044–1052 (2019)
- [311] A. N. Schechter: *Hemoglobin research and the origins of molecular medicine*. *Blood* **112** (10), 3927–3938 (2008)
- [312] W. D. Edwards and M. C. Zerner: *Electronic Structure of Model Chlorophyll Systems*. *International Journal of Quantum Chemistry* **23** (4), 1407–1432 (1983)
- [313] G. Li Manni and A. Alavi: *Understanding the Mechanism Stabilizing Intermediate Spin States in Fe(II)-Porphyrin*. *The Journal of Physical Chemistry A* **122** (22), 4935–4947 (2018)
- [314] G. Li Manni, D. Kats, D. P. Tew, and A. Alavi: *Role of Valence and Semicore Electron Correlation on Spin Gaps in Fe(II)-Porphyrins*. *Journal of Chemical Theory and Computation* **15** (3), 1492–1497 (2019)
- [315] R. Olivares-Amaya, W. Hu, N. Nakatani, S. Sharma, J. Yang et al.: *The ab-initio density matrix renormalization group in practice*. *The Journal of Chemical Physics* **142** (3), 34102 (2015)
- [316] Q. M. Phung and K. Pierloot: *The dioxygen adducts of iron and manganese porphyrins: electronic structure and binding energy*. *Physical Chemistry Chemical Physics* **20** (25), 17009–17019 (2018)

BIBLIOGRAPHY

- [317] C. Weiss, H. Kobayashi, and M. Gouterman: *Spectra of Porphyrins. Part III. Self-Consistent Molecular Orbital Calculations of Porphyrin and Related Ring Systems*. Journal of Molecular Spectroscopy **16** (2), 415–450 (1965)
- [318] M. Rubio, B. O. Roos, L. Serrano-Andrés, and M. Merchán: *Theoretical study of the electronic spectrum of magnesium-porphyrin*. The Journal of Chemical Physics **110** (15), 7202–7209 (1999)
- [319] A. Kerridge: *A RASSCF study of free base, magnesium and zinc porphyrins: Accuracy versus efficiency*. Physical Chemistry Chemical Physics **15** (6), 2197–2209 (2013)
- [320] A. Starukhin, A. Shulga, and J. Waluk: *Electronic spectra and symmetry of metalloporphyrins in low-temperature rare gas and nitrogen matrices*. Chemical Physics Letters **272** (5-6), 405–411 (1997)
- [321] M. Gouterman: *Optical Spectra and Electronic Structure of Porphyrins and Related Rings*. *The Porphyrines Volume 3*, edited by D. Dolphin, pp. 1–165. Academic Press Inc. (1978)
- [322] V. Sauri, L. Serrano-Andrés, A. R. M. Shahi, L. Gagliardi, S. Vancoillie et al.: *Multi-configurational Second-Order Perturbation Theory Restricted Active Space (RASPT2) Method for Electronic Excited States: A Benchmark Study*. Journal of Chemical Theory and Computation **7** (1), 153–168 (2011)

Erklärung über die Eigenständigkeit der Dissertation

Ich versichere, dass ich die vorliegende Arbeit mit dem Titel *Multiconfiguration self-consistent field methods for large molecules* selbständig verfasst und keine anderen als die angegebenen Quellen und Hilfsmittel benutzt habe; aus fremden Quellen entnommene Passagen und Gedanken sind als solche kenntlich gemacht.

Declaration of Authorship

I hereby certify that the dissertation entitled *Multiconfiguration self-consistent field methods for large molecules* is entirely my own work except where otherwise indicated. Passages and ideas from other sources have been clearly indicated.

Stuttgart, der 6. April 2021

David Kreplin